Appendix 1

$$40 < P_t^{\gamma} < 50 \ GeV/c$$

Table 1: Selection 1. $\phi_{(\gamma,jet)} = 180^\circ \pm 17^\circ$. UA1 algorithm . $L_{int} = 300 \ pb^{-1}$.

P_{tCUT}^{clust}	30	20	15	10	5
P_t^{jet}	42.646	42.460	42.410	42.564	42.912
$P_t^{Jet} - P_t^{jet}$	0.127	0.127	0.131	0.133	0.105
$P_{t(\nu)}^{Jet}$	0.129	0.128	0.133	0.135	0.106
$R_{event}^{\nu\in Jet}$	0.171	0.170	0.169	0.166	0.152
$P_{t(\mu)}^{Jet}$	0.153	0.153	0.158	0.157	0.113
$R_{event}^{\mu\in Jet}$	0.148	0.146	0.146	0.144	0.126
P_t^{miss}	2.088	2.083	2.096	2.105	2.101
$P_{t\nu\in Jet}^{miss}$	2.366	2.370	2.383	2.403	2.310
$Nevent_{(c)}$	964	926	865	723	348
$Nevent_{(b)}$	100	94	90	70	34
$29sub/all$	0.85	0.85	0.84	0.84	0.83
R_{jet}	0.59	0.59	0.59	0.59	0.59
Entries	10493	10144	9472	7992	4421

Table 2: Selection 1. $\phi_{(\gamma,jet)} = 180^\circ \pm 17^\circ$. UA2 algorithm. $L_{int} = 300 \ pb^{-1}$.

P_{tCUT}^{clust}	30	20	15	10	5
P_t^{jet}	43.135	42.960	42.823	42.805	42.931
$P_t^{Jet} - P_t^{jet}$	0.115	0.108	0.110	0.115	0.099
$P_{t(\nu)}^{Jet}$	0.116	0.110	0.111	0.117	0.101
$R_{event}^{\nu\in Jet}$	0.159	0.158	0.158	0.162	0.160
$P_{t(\mu)}^{Jet}$	0.147	0.144	0.144	0.148	0.141
$R_{event}^{\mu\in Jet}$	0.129	0.127	0.127	0.128	0.127
P_t^{miss}	2.082	2.071	2.072	2.083	2.061
$P_{t\nu\in Jet}^{miss}$	2.412	2.379	2.394	2.418	2.272
$Nevent_{(c)}$	821	788	748	628	377
$Nevent_{(b)}$	81	74	70	55	30
$29sub/all$	0.88	0.88	0.88	0.87	0.86
R_{jet}	0.61	0.61	0.61	0.61	0.61
Entries	8763	8474	7960	6846	4433

Table 3: Selection 1. $\phi_{(\gamma,jet)} = 180^\circ \pm 17^\circ$. LUCELL algorithm. $L_{int} = 300 \ pb^{-1}$.

P_{tCUT}^{clust}	30	20	15	10	5
P_t^{jet}	42.668	42.439	42.351	42.506	42.853
$P_t^{Jet} - P_t^{jet}$	0.130	0.133	0.132	0.136	0.102
$P_{t(\nu)}^{Jet}$	0.133	0.135	0.135	0.138	0.104
$R_{event}^{\nu\in Jet}$	0.170	0.169	0.168	0.166	0.152
$P_{t(\mu)}^{Jet}$	0.146	0.145	0.146	0.143	0.120
$R_{event}^{\mu\in Jet}$	0.150	0.148	0.147	0.145	0.134
P_t^{miss}	2.094	2.095	2.109	2.129	2.082
$P_{t\nu\in Jet}^{miss}$	2.414	2.434	2.439	2.463	2.269
$Nevent_{(c)}$	988	949	889	723	372
$Nevent_{(b)}$	108	103	100	79	41
$29sub/all$	0.85	0.85	0.84	0.84	0.83
R_{jet}	0.60	0.60	0.60	0.60	0.60

$50 < {P_t}^{\gamma} < 70 \ GeV/c$

Table 4: Selection 1. $\phi_{(\gamma,jet)} = 180^{\circ} \pm 17^{\circ}$. UA1 algorithm. $L_{int} = 300\ pb^{-1}$.

P_{tCUT}^{clust}	30	20	15	10	5
${P_t}^{jet}$	53.482	54.013	54.560	55.183	55.798
${P_t}^{Jet}-{P_t}^{jet}$	0.182	0.183	0.179	0.190	0.152
$P_{t(\nu)}^{Jet}$	0.184	0.185	0.181	0.192	0.154
$R_{event}^{\nu\in Jet}$	0.175	0.171	0.169	0.168	0.154
$P_{t(\mu)}^{Jet}$	0.171	0.167	0.163	0.156	0.135
$R_{event}^{\mu\in Jet}$	0.157	0.155	0.153	0.147	0.134
${P_t}^{miss}$	2.148	2.166	2.173	2.187	2.148
$P_{t\nu\in Jet}^{miss}$	2.658	2.710	2.703	2.790	2.617
$Nevent_{(c)}$	714	632	561	441	199
$Nevent_{(b)}$	102	84	71	57	16
$29sub/all$	0.81	0.81	0.81	0.80	0.79
R_{jet}	0.60	0.60	0.60	0.60	0.59
Entries	12973	11712	10320	8179	4162

Table 5: Selection 1. $\phi_{(\gamma,jet)} = 180^{\circ} \pm 17^{\circ}$. UA2 algorithm. $L_{int} = 300\ pb^{-1}$.

P_{tCUT}^{clust}	30	20	15	10	5
${P_t}^{jet}$	55.036	55.364	55.589	55.713	55.802
${P_t}^{Jet}-{P_t}^{jet}$	0.195	0.189	0.185	0.198	0.160
$P_{t(\nu)}^{Jet}$	0.197	0.191	0.187	0.200	0.162
$R_{event}^{\nu\in Jet}$	0.156	0.152	0.151	0.150	0.148
$P_{t(\mu)}^{Jet}$	0.167	0.160	0.163	0.161	0.127
$R_{event}^{\mu\in Jet}$	0.139	0.138	0.137	0.135	0.125
${P_t}^{miss}$	2.166	2.176	2.178	2.196	2.188
$P_{t\nu\in Jet}^{miss}$	2.880	2.906	2.877	2.955	2.766
$Nevent_{(c)}$	549	494	452	383	197
$Nevent_{(b)}$	44	37	35	26	11
$29sub/all$	0.85	0.85	0.85	0.84	0.82
R_{jet}	0.62	0.62	0.62	0.62	0.61
Entries	9699	8857	8035	6607	4085

Table 6: Selection 1. $\phi_{(\gamma,jet)} = 180^{\circ} \pm 17^{\circ}$. LUCELL algorithm. $L_{int} = 300\ pb^{-1}$.

P_{tCUT}^{clust}	30	20	15	10	5
${P_t}^{jet}$	53.757	54.192	54.610	55.231	55.676
${P_t}^{Jet}-{P_t}^{jet}$	0.195	0.194	0.193	0.211	0.174
$P_{t(\nu)}^{Jet}$	0.197	0.196	0.195	0.213	0.176
$R_{event}^{\nu\in Jet}$	0.176	0.171	0.170	0.166	0.157
$P_{t(\mu)}^{Jet}$	0.175	0.169	0.171	0.161	0.148
$R_{event}^{\mu\in Jet}$	0.157	0.155	0.155	0.152	0.139
${P_t}^{miss}$	2.161	2.175	2.185	2.209	2.185
$P_{t\nu\in Jet}^{miss}$	2.713	2.759	2.759	2.890	2.667
$Nevent_{(c)}$	707	624	556	433	223
$Nevent_{(b)}$	98	83	71	57	23
$29sub/all$	0.82	0.81	0.80	0.80	0.79
R_{jet}	0.61	0.61	0.61	0.60	0.60
Entries	12868	11708	10348	8196	4446

$$70 < P_t{}^{\gamma} < 90\ GeV/c$$

Table 7: Selection 1. $\phi_{(\gamma,jet)} = 180^{\circ} \pm 17^{\circ}$. UA1 algorithm. $L_{int} = 300\ pb^{-1}$.

P_{tCUT}^{clust}	30	20	15	10	5
$P_t{}^{jet}$	72.873	74.375	75.239	75.968	76.353
$P_t{}^{Jet}$–$P_t{}^{jet}$	0.257	0.259	0.272	0.250	0.245
$P_{t(\nu)}^{Jet}$	0.259	0.262	0.275	0.253	0.248
$R_{event}^{\nu\in Jet}$	0.182	0.176	0.177	0.175	0.173
$P_{t(\mu)}^{Jet}$	0.184	0.181	0.186	0.168	0.174
$R_{event}^{\mu\in Jet}$	0.172	0.169	0.171	0.172	0.165
$P_t{}^{miss}$	2.178	2.182	2.196	2.168	2.190
$P_{t\nu\in Jet}^{miss}$	3.092	3.123	3.179	3.118	3.089
$Nevent_{(c)}$	129	108	91	64	30
$Nevent_{(b)}$	22	18	13	9	2
$29sub/all$	0.77	0.76	0.76	0.75	0.72
R_{jet}	0.60	0.60	0.60	0.60	0.60
Entries	13641	11613	9892	7495	3845

Table 8: Selection 1. $\phi_{(\gamma,jet)} = 180^{\circ} \pm 17^{\circ}$. UA2 algorithm. $L_{int} = 300\ pb^{-1}$.

P_{tCUT}^{clust}	30	20	15	10	5
$P_t{}^{jet}$	75.350	76.029	76.317	76.507	76.387
$P_t{}^{Jet}$–$P_t{}^{jet}$	0.240	0.239	0.244	0.232	0.219
$P_{t(\nu)}^{Jet}$	0.242	0.241	0.246	0.234	0.222
$R_{event}^{\nu\in Jet}$	0.172	0.170	0.170	0.167	0.170
$P_{t(\mu)}^{Jet}$	0.175	0.178	0.182	0.167	0.140
$R_{event}^{\mu\in Jet}$	0.152	0.153	0.153	0.154	0.157
$P_t{}^{miss}$	2.197	2.199	2.200	2.187	2.187
$P_{t\nu\in Jet}^{miss}$	3.032	3.043	3.078	3.076	2.970
$Nevent_{(c)}$	95	83	73	55	27
$Nevent_{(b)}$	16	12	8	5	2
$29sub/all$	0.82	0.81	0.81	0.79	0.78
R_{jet}	0.64	0.64	0.64	0.64	0.65
Entries	9869	8595	7535	6045	3749

Table 9: Selection 1. $\phi_{(\gamma,jet)} = 180^{\circ} \pm 17^{\circ}$. LUCELL algorithm. $L_{int} = 300\ pb^{-1}$.

P_{tCUT}^{clust}	30	20	15	10	5
$P_t{}^{jet}$	73.400	74.612	75.380	76.028	76.451
$P_t{}^{Jet}$–$P_t{}^{jet}$	0.233	0.229	0.232	0.222	0.243
$P_{t(\nu)}^{Jet}$	0.235	0.231	0.234	0.224	0.246
$R_{event}^{\nu\in Jet}$	0.183	0.178	0.179	0.177	0.173
$P_{t(\mu)}^{Jet}$	0.191	0.183	0.181	0.166	0.175
$R_{event}^{\mu\in Jet}$	0.175	0.175	0.174	0.172	0.169
$P_t{}^{miss}$	2.160	2.153	2.165	2.168	2.176
$P_{t\nu\in Jet}^{miss}$	2.922	2.945	2.960	2.925	2.990
$Nevent_{(c)}$	128	105	89	64	30
$Nevent_{(b)}$	19	16	10	8	2
$29sub/all$	0.76	0.76	0.75	0.74	0.72
R_{jet}	0.61	0.61	0.61	0.61	0.60
Entries	13477	11613	9884	7539	4068

$$90 < P_t^{\gamma} < 140\ GeV/c$$

Table 10: Selection 1. $\phi_{(\gamma,jet)} = 180^\circ \pm 17^\circ$. UA1 algorithm. $L_{int} = 300\ pb^{-1}$.

P_{tCUT}^{clust}	30	20	15	10	5
P_t^{jet}	101.878	103.159	103.988	104.565	104.615
$P_t^{Jet} - P_t^{jet}$	0.331	0.330	0.319	0.312	0.317
$P_{t(\nu)}^{Jet}$	0.334	0.333	0.321	0.315	0.320
$R_{event}^{\nu\in Jet}$	0.190	0.188	0.187	0.185	0.179
$P_{t(\mu)}^{Jet}$	0.272	0.283	0.272	0.280	0.309
$R_{event}^{\mu\in Jet}$	0.181	0.180	0.175	0.170	0.163
P_t^{miss}	2.186	2.197	2.193	2.195	2.201
$P_{t\nu\in Jet}^{miss}$	3.339	3.339	3.276	3.238	3.345
$Nevent_{(c)}$	51	40	32	22	9
$Nevent_{(b)}$	6	5	4	2	1
$29sub/all$	0.70	0.70	0.69	0.68	0.66
R_{jet}	0.60	0.60	0.60	0.60	0.61
Entries	14058	11806	9997	7439	3673

Table 11: Selection 1. $\phi_{(\gamma,jet)} = 180^\circ \pm 17^\circ$. UA2 algorithm. $L_{int} = 300\ pb^{-1}$.

P_{tCUT}^{clust}	30	20	15	10	5
P_t^{jet}	104.753	105.156	105.360	105.451	104.969
$P_t^{Jet} - P_t^{jet}$	0.327	0.315	0.334	0.335	0.322
$P_{t(\nu)}^{Jet}$	0.329	0.318	0.336	0.338	0.325
$R_{event}^{\nu\in Jet}$	0.167	0.165	0.165	0.164	0.166
$P_{t(\mu)}^{Jet}$	0.313	0.335	0.331	0.293	0.338
$R_{event}^{\mu\in Jet}$	0.153	0.153	0.151	0.151	0.152
P_t^{miss}	2.204	2.200	2.227	2.239	2.247
$P_{t\nu\in Jet}^{miss}$	3.573	3.520	3.636	3.621	3.575
$Nevent_{(c)}$	40	35	29	21	13
$Nevent_{(c)}$	35	29	24	20	11
$Nevent_{(b)}$	5	3	2	1	1
$29sub/all$	0.75	0.75	0.74	0.73	0.70
R_{jet}	0.66	0.67	0.67	0.68	0.68
Entries	9745	8454	7401	5940	3671

Table 12: Selection 1. $\phi_{(\gamma,jet)} = 180^\circ \pm 17^\circ$. LUCELL algorithm. $L_{int} = 300\ pb^{-1}$.

P_{tCUT}^{clust}	30	20	15	10	5
P_t^{jet}	102.119	103.240	103.934	104.555	104.643
$P_t^{Jet} - P_t^{jet}$	0.331	0.320	0.334	0.323	0.343
$P_{t(\nu)}^{Jet}$	0.335	0.323	0.336	0.326	0.345
$R_{event}^{\nu\in Jet}$	0.191	0.188	0.187	0.184	0.185
$P_{t(\mu)}^{Jet}$	0.297	0.312	0.302	0.316	0.328
$R_{event}^{\mu\in Jet}$	0.181	0.180	0.176	0.171	0.169
P_t^{miss}	2.187	2.179	2.199	2.200	2.219
$P_{t\nu\in Jet}^{miss}$	3.310	3.259	3.344	3.311	3.388
$Nevent_{(c)}$	50	40	32	23	10
$Nevent_{(b)}$	7	5	3	2	1
$29sub/all$	0.70	0.69	0.69	0.68	0.66
R_{jet}	0.62	0.61	0.61	0.61	0.61
Entries	13958	11704	9947	7472	3856

Appendix 2 $40 < {P_t}^{\gamma} < 50\ GeV/c$

$${P_t}^{isol} < 4\ GeV/c, \quad \epsilon^{\gamma} < 7\%$$

Table 1: Selection 1. $\phi_{(\gamma,jet)} = 180^{\circ} \pm 180^{\circ}$. UA1 algorithm. $L_{int} = 300\ pb^{-1}$.

P_{tCUT}^{clust}	30	20	15	10	5
Nevent*	16342	14538	12834	10260	5490
P_t56	13.2	11.2	9.9	8.3	6.3
$\Delta\phi$	10.8	8.5	7.2	5.8	4.1
${P_t}^{out}$	10.7	9.0	7.8	6.5	4.7
${P_t}^{\lvert\eta\rvert>4.2}$	2.0	2.0	2.0	2.0	2.0
$({P_t}^{\gamma} - {P_t}^{part})/{P_t}^{\gamma}$	0.0260	0.0246	0.0199	0.0135	0.0074
$({P_t}^{J} - {P_t}^{part})/{P_t}^{J}$	-0.0245	-0.0269	-0.0290	-0.0272	-0.0212
$({P_t}^{\gamma} - {P_t}^{J})/{P_t}^{\gamma}$	0.0456	0.0470	0.0444	0.0373	0.0269
$P_t(O{+}\eta{>}4.2)/{P_t}^{\gamma}$	0.0088	0.0259	0.0300	0.0282	0.0223
$1 - cos(\Delta\phi)$	0.0368	0.0211	0.0144	0.0091	0.0046
$\sigma(Db[\gamma,J])^{**}$	0.1632	0.1465	0.1331	0.1157	0.0909
$\sigma(Db[\gamma,part])^{***}$	0.2183	0.1973	0.1755	0.1464	0.1112
Entries	13277	11811	10427	8336	4460

Table 2: Selection 1. $\phi_{(\gamma,jet)} = 180^{\circ} \pm 180^{\circ}$. UA2 algorithm. $L_{int} = 300\ pb^{-1}$.

P_{tCUT}^{clust}	30	20	15	10	5
Nevent	13276	11808	10531	8710	5528
P_t56	12.3	10.4	9.2	7.8	6.4
$\Delta\phi$	9.8	7.7	6.5	5.4	4.2
${P_t}^{out}$	9.9	8.2	7.1	6.0	4.7
${P_t}^{\lvert\eta\rvert>4.2}$	2.0	2.0	2.0	2.0	2.0
$({P_t}^{\gamma} - {P_t}^{part})/{P_t}^{\gamma}$	0.0146	0.0136	0.0103	0.0065	0.0052
$({P_t}^{J} - {P_t}^{part})/{P_t}^{J}$	-0.0193	-0.0226	-0.0261	-0.0271	-0.0240
$({P_t}^{\gamma} - {P_t}^{J})/{P_t}^{\gamma}$	0.0311	0.0331	0.0334	0.0307	0.0271
$P_t(O{+}\eta{>}4.2)/{P_t}^{\gamma}$	0.0011	0.0162	0.0216	0.0228	0.0222
$1 - cos(\Delta\phi)$	0.0301	0.0170	0.0119	0.0080	0.0049
$\sigma(Db[\gamma,J])$	0.1575	0.1405	0.1260	0.1098	0.0909
$\sigma(Db[\gamma,part])$	0.1999	0.1780	0.1575	0.1322	0.1087
Entries	10786	9593	8556	7076	4491

Table 3: Selection 1. $\phi_{(\gamma,jet)} = 180^{\circ} \pm 180^{\circ}$. LUCELL algorithm. $L_{int} = 300\ pb^{-1}$.

P_{tCUT}^{clust}	30	20	15	10	5
Nevent	16514	14707	13034	10302	5775
P_t56	13.1	11.2	9.8	8.1	6.1
$\Delta\phi$	10.7	8.4	7.1	5.6	3.9
${P_t}^{out}$	10.6	8.9	7.8	6.3	4.6
${P_t}^{\lvert\eta\rvert>4.2}$	2.0	2.0	2.0	2.0	2.0
$({P_t}^{\gamma} - {P_t}^{part})/{P_t}^{\gamma}$	0.0254	0.0245	0.0201	0.0128	0.0055
$({P_t}^{J} - {P_t}^{part})/{P_t}^{J}$	-0.0225	-0.0257	-0.0290	-0.0283	-0.0252
$({P_t}^{\gamma} - {P_t}^{J})/{P_t}^{\gamma}$	0.0437	0.0461	0.0450	0.0380	0.0287
$P_t(O{+}\eta{>}4.2)/{P_t}^{\gamma}$	0.0082	0.0255	0.0309	0.0296	0.0247
$1 - cos(\Delta\phi)$	0.0356	0.0206	0.0141	0.0084	0.0040
$\sigma(Db[\gamma,J])$	0.1627	0.1456	0.1313	0.1124	0.0872
$\sigma(Db[\gamma,part])$	0.2176	0.1970	0.1745	0.1438	0.1079
Entries	13417	11949	10589	8370	4692

*Number of events (Nevent) is given in this and in the following tables for integrated luminosity $L_{int} = 300\ pb^{-1}$

Table 4: Selection 1. $\phi_{(\gamma,jet)} = 180^\circ \pm 17^\circ$. UA1 algorithm. $L_{int} = 300\ pb^{-1}$.

P_{tCUT}^{clust}	30	20	15	10	5
Nevent	12915	12486	11659	9837	5442
$P_t 56$	10.1	9.6	8.9	7.9	6.2
$\Delta\phi$	5.9	5.8	5.6	5.1	3.9
${P_t}^{out}$	7.6	7.3	6.8	6.1	4.6
${P_t}^{\lvert\eta\rvert>4.2}$	2.0	2.0	2.0	2.0	2.0
$({P_t}^{\gamma}-{P_t}^{part})/{P_t}^{\gamma}$	0.0120	0.0155	0.0147	0.0116	0.0071
$({P_t}^{J}-{P_t}^{part})/{P_t}^{J}$	-0.0291	-0.0291	-0.0296	-0.0275	-0.0213
$({P_t}^{\gamma}-{P_t}^{J})/{P_t}^{\gamma}$	0.0363	0.0400	0.0400	0.0357	0.0266
$P_t(O{+}\eta{>}4.2)/{P_t}^{\gamma}$	0.0279	0.0319	0.0325	0.0293	0.0226
$1-cos(\Delta\phi)$	0.0084	0.0081	0.0076	0.0064	0.0040
$\sigma(Db[\gamma,J])$	0.1531	0.1414	0.1298	0.1142	0.0904
$\sigma(Db[\gamma,part])$	0.1957	0.1831	0.1667	0.1424	0.1105
Entries	10493	10144	9472	7992	4421

Table 5: Selection 1. $\phi_{(\gamma,jet)} = 180^\circ \pm 17^\circ$. UA2 algorithm. $L_{int} = 300\ pb^{-1}$.

P_{tCUT}^{clust}	30	20	15	10	5
Nevent	10786	10430	9798	8426	5456
$P_t 56$	9.6	9.1	8.5	7.5	6.2
$\Delta\phi$	5.7	5.5	5.3	4.8	3.9
${P_t}^{out}$	7.1	6.8	6.4	5.7	4.6
${P_t}^{\lvert\eta\rvert>4.2}$	2.0	2.0	2.0	2.0	2.0
$({P_t}^{\gamma}-{P_t}^{part})/{P_t}^{\gamma}$	0.0033	0.0065	0.0071	0.0057	0.0046
$({P_t}^{J}-{P_t}^{part})/{P_t}^{J}$	-0.0238	-0.0243	-0.0260	-0.0270	-0.0241
$({P_t}^{\gamma}-{P_t}^{J})/{P_t}^{\gamma}$	0.0242	0.0278	0.0302	0.0298	0.0265
$P_t(O{+}\eta{>}4.2)/{P_t}^{\gamma}$	0.0165	0.0203	0.0233	0.0241	0.0225
$1-cos(\Delta\phi)$	0.0078	0.0075	0.0069	0.0058	0.0040
$\sigma(Db[\gamma,J])$	0.1461	0.1350	0.1232	0.1085	0.0902
$\sigma(Db[\gamma,part])$	0.1793	0.1666	0.1521	0.1298	0.1076
Entries	8763	8474	7960	6846	4433

Table 6: Selection 1. $\phi_{(\gamma,jet)} = 180^\circ \pm 17^\circ$. LUCELL algorithm. $L_{int} = 300\ pb^{-1}$.

P_{tCUT}^{clust}	30	20	15	10	5
Nevent	13111	12684	11888	9958	5754
$P_t 56$	10.1	9.6	8.9	7.8	6.1
$\Delta\phi$	5.9	5.8	5.6	5.1	3.9
${P_t}^{out}$	7.5	7.2	6.8	6.0	4.5
${P_t}^{\lvert\eta\rvert>4.2}$	2.0	2.0	2.0	2.0	2.0
$({P_t}^{\gamma}-{P_t}^{part})/{P_t}^{\gamma}$	0.0120	0.0163	0.0155	0.0109	0.0054
$({P_t}^{J}-{P_t}^{part})/{P_t}^{J}$	-0.0275	-0.0278	-0.0296	-0.0290	-0.0252
$({P_t}^{\gamma}-{P_t}^{J})/{P_t}^{\gamma}$	0.0354	0.0401	0.0412	0.0368	0.0286
$P_t(O{+}\eta{>}4.2)/{P_t}^{\gamma}$	0.0270	0.0320	0.0337	0.0305	0.0248
$1-cos(\Delta\phi)$	0.0084	0.0081	0.0076	0.0063	0.0038
$\sigma(Db[\gamma,J])$	0.1529	0.1400	0.1283	0.1114	0.0870
$\sigma(Db[\gamma,part])$	0.1972	0.1839	0.1664	0.1401	0.1073
Entries	10652	10305	9658	8090	4675

Table 7: Selection 1. $\phi_{(\gamma,jet)} = 180^\circ \pm 11^\circ$. UA1 algorithm. $L_{int} = 300\ pb^{-1}$.

P_{tCUT}^{clust}	30	20	15	10	5
Nevent	10923	10654	10150	8877	5226
P_t56	9.2	8.8	8.3	7.4	5.9
$\Delta\phi$	4.5	4.5	4.4	4.2	3.5
${P_t}^{out}$	6.6	6.4	6.1	5.5	4.3
${P_t}^{\lvert\eta\rvert>4.2}$	2.0	2.0	2.0	2.0	2.0
$({P_t}^{\gamma}-{P_t}^{part})/{P_t}^{\gamma}$	0.0101	0.0133	0.0128	0.0100	0.0066
$({P_t}^{J}-{P_t}^{part})/{P_t}^{J}$	-0.0276	-0.0273	-0.0279	-0.0265	-0.0208
$({P_t}^{\gamma}-{P_t}^{J})/{P_t}^{\gamma}$	0.0332	0.0363	0.0368	0.0332	0.0257
$P_t(O{+}\eta{>}4.2)/{P_t}^{\gamma}$	0.0287	0.0318	0.0324	0.0293	0.0227
$1-cos(\Delta\phi)$	0.0046	0.0045	0.0044	0.0040	0.0030
$\sigma(Db[\gamma,J])$	0.1462	0.1370	0.1272	0.1122	0.0886
$\sigma(Db[\gamma,part])$	0.1850	0.1748	0.1615	0.1396	0.1097
Entries	8874	8656	8246	7212	4246

Table 8: Selection 1. $\phi_{(\gamma,jet)} = 180^\circ \pm 11^\circ$. UA2 algorithm. $L_{int} = 300\ pb^{-1}$.

P_{tCUT}^{clust}	30	20	15	10	5
Nevent	9298	9070	8681	7742	5236
P_t56	8.6	8.3	7.8	7.1	6.0
$\Delta\phi$	4.4	4.3	4.2	4.0	3.6
${P_t}^{out}$	6.2	6.0	5.7	5.2	4.4
${P_t}^{\lvert\eta\rvert>4.2}$	2.0	2.0	2.0	2.0	2.0
$({P_t}^{\gamma}-{P_t}^{part})/{P_t}^{\gamma}$	0.0022	0.0041	0.0050	0.0045	0.0040
$({P_t}^{J}-{P_t}^{part})/{P_t}^{J}$	-0.0235	-0.0243	-0.0255	-0.0261	-0.0238
$({P_t}^{\gamma}-{P_t}^{J})/{P_t}^{\gamma}$	0.0230	0.0255	0.0279	0.0280	0.0257
$P_t(O{+}\eta{>}4.2)/{P_t}^{\gamma}$	0.0187	0.0213	0.0238	0.0242	0.0227
$1-cos(\Delta\phi)$	0.0043	0.0043	0.0041	0.0038	0.0030
$\sigma(Db[\gamma,J])$	0.1393	0.1306	0.1204	0.1070	0.0891
$\sigma(Db[\gamma,part])$	0.1686	0.1584	0.1466	0.1283	0.1071
Entries	7554	7369	7053	6290	4254

Table 9: Selection 1. $\phi_{(\gamma,jet)} = 180^\circ \pm 11^\circ$. LUCELL algorithm. $L_{int} = 300\ pb^{-1}$.

P_{tCUT}^{clust}	30	20	15	10	5
Nevent	11088	10825	10359	9023	5573
P_t56	9.1	8.8	8.2	7.3	5.9
$\Delta\phi$	4.5	4.4	4.4	4.2	3.6
${P_t}^{out}$	6.6	6.3	6.1	5.5	4.4
${P_t}^{\lvert\eta\rvert>4.2}$	2.0	2.0	2.0	2.0	2.0
$({P_t}^{\gamma}-{P_t}^{part})/{P_t}^{\gamma}$	0.0096	0.0133	0.0119	0.0087	0.0047
$({P_t}^{J}-{P_t}^{part})/{P_t}^{J}$	-0.0275	-0.0275	-0.0297	-0.0289	-0.0251
$({P_t}^{\gamma}-{P_t}^{J})/{P_t}^{\gamma}$	0.0333	0.0371	0.0377	0.0344	0.0279
$P_t(O{+}\eta{>}4.2)/{P_t}^{\gamma}$	0.0288	0.0327	0.0334	0.0305	0.0249
$1-cos(\Delta\phi)$	0.0045	0.0045	0.0044	0.0040	0.0031
$\sigma(Db[\gamma,J])$	0.1459	0.1355	0.1258	0.1102	0.0865
$\sigma(Db[\gamma,part])$	0.1855	0.1743	0.1599	0.1369	0.1063
Entries	9008	8795	8416	7331	4528

Table 10: Selection 1. $\phi_{(\gamma,jet)} = 180^{\circ} \pm 6^{\circ}$. UA1 algorithm. $L_{int} = 300\ pb^{-1}$.

P_{tCUT}^{clust}	30	20	15	10	5
Nevent	7114	7001	6751	6169	4085
P_t56	7.9	7.6	7.1	6.5	5.3
$\Delta\phi$	2.5	2.5	2.5	2.5	2.3
${P_t}^{out}$	5.3	5.2	5.0	4.6	3.7
${P_t}^{\|\eta\|>4.2}$	2.0	2.0	2.0	2.0	2.0
$({P_t}^{\gamma}{-}{P_t}^{part})/{P_t}^{\gamma}$	0.0077	0.0099	0.0092	0.0074	0.0051
$({P_t}^{J}{-}{P_t}^{part})/{P_t}^{J}$	-0.0239	-0.0237	-0.0254	-0.0241	-0.0204
$({P_t}^{\gamma} - {P_t}^{J})/{P_t}^{\gamma}$	0.0283	0.0304	0.0315	0.0287	0.0239
$P_t(O{+}\eta{>}4.2)/{P_t}^{\gamma}$	0.0270	0.0291	0.0301	0.0274	0.0227
$1 - cos(\Delta\phi)$	0.0014	0.0014	0.0014	0.0013	0.0012
$\sigma(Db[\gamma, J])$	0.1345	0.1277	0.1197	0.1075	0.0849
$\sigma(Db[\gamma, part])$	0.1701	0.1626	0.1510	0.1335	0.1065
Entries	5780	5688	5485	5012	3319

Table 11: Selection 1. $\phi_{(\gamma,jet)} = 180^{\circ} \pm 6^{\circ}$. UA2 algorithm. $L_{int} = 300\ pb^{-1}$.

P_{tCUT}^{clust}	30	20	15	10	5
Nevent	6237	6140	5962	5512	4073
P_t56	7.4	7.1	6.7	6.2	5.4
$\Delta\phi$	2.5	2.5	2.5	2.4	2.4
${P_t}^{out}$	5.0	4.9	4.7	4.3	3.7
${P_t}^{\|\eta\|>4.2}$	2.0	2.0	2.0	2.0	2.0
$({P_t}^{\gamma}{-}{P_t}^{part})/{P_t}^{\gamma}$	-0.0004	0.0002	0.0006	0.0017	0.0034
$({P_t}^{J}{-}{P_t}^{part})/{P_t}^{J}$	-0.0227	-0.0234	-0.0252	-0.0252	-0.0229
$({P_t}^{\gamma} - {P_t}^{J})/{P_t}^{\gamma}$	0.0200	0.0212	0.0233	0.0244	0.0243
$P_t(O{+}\eta{>}4.2)/{P_t}^{\gamma}$	0.0187	0.0199	0.0220	0.0232	0.0230
$1 - cos(\Delta\phi)$	0.0014	0.0013	0.0013	0.0013	0.0012
$\sigma(Db[\gamma, J])$	0.1276	0.1222	0.1137	0.1021	0.0855
$\sigma(Db[\gamma, part])$	0.1532	0.1470	0.1363	0.1217	0.1050
Entries	5067	4988	4844	4478	3309

Table 12: Selection 1. $\phi_{(\gamma,jet)} = 180^{\circ} \pm 6^{\circ}$. LUCELL algorithm. $L_{int} = 300\ pb^{-1}$.

P_{tCUT}^{clust}	30	20	15	10	5
Nevent	7250	7132	6910	6269	4339
P_t56	7.8	7.5	7.1	6.4	5.3
$\Delta\phi$	2.5	2.5	2.5	2.5	2.4
${P_t}^{out}$	5.4	5.2	5.0	4.5	3.8
${P_t}^{\|\eta\|>4.2}$	2.0	2.0	2.0	2.0	2.0
$({P_t}^{\gamma}{-}{P_t}^{part})/{P_t}^{\gamma}$	0.0075	0.0102	0.0093	0.0073	0.0046
$({P_t}^{J}{-}{P_t}^{part})/{P_t}^{J}$	-0.0256	-0.0258	-0.0278	-0.0265	-0.0233
$({P_t}^{\gamma} - {P_t}^{J})/{P_t}^{\gamma}$	0.0300	0.0329	0.0339	0.0311	0.0262
$P_t(O{+}\eta{>}4.2)/{P_t}^{\gamma}$	0.0287	0.0315	0.0326	0.0298	0.0250
$1 - cos(\Delta\phi)$	0.0014	0.0014	0.0014	0.0013	0.0012
$\sigma(Db[\gamma, J])$	0.1345	0.1259	0.1185	0.1052	0.0842
$\sigma(Db[\gamma, part])$	0.1697	0.1608	0.1493	0.1310	0.1044
Entries	5890	5794	5614	5093	3525

Table 13: Selection 2. $\phi_{(\gamma,jet)} = 180^\circ \pm 17^\circ$. UA1 algorithm. $L_{int} = 300\ pb^{-1}$.

P_{tCUT}^{clust}	30	20	15	10	5
Nevent	5189	5043	4804	4222	2689
P_t56	9.4	8.9	8.4	7.4	5.9
$\Delta\phi$	5.5	5.4	5.3	4.8	3.8
${P_t}^{out}$	7.0	6.7	6.3	5.6	4.3
${P_t}^{\vert\eta\vert>4.2}$	2.0	2.0	2.0	2.0	2.0
$({P_t}^{\gamma} - {P_t}^{part})/{P_t}^{\gamma}$	-0.0237	-0.0179	-0.0143	-0.0126	-0.0085
$({P_t}^{J} - {P_t}^{part})/{P_t}^{J}$	-0.0078	-0.0094	-0.0105	-0.0135	-0.0125
$({P_t}^{\gamma} - {P_t}^{J})/{P_t}^{\gamma}$	-0.0163	-0.0088	-0.0043	0.0001	0.0032
$P_t(O{+}\eta{>}4.2)/{P_t}^{\gamma}$	-0.0238	-0.0161	-0.0111	-0.0058	-0.0005
$1 - cos(\Delta\phi)$	0.0076	0.0074	0.0069	0.0059	0.0038
$\sigma(Db[\gamma, J])$	0.1531	0.1373	0.1253	0.1082	0.0878
$\sigma(Db[\gamma, part])$	0.1814	0.1661	0.1515	0.1251	0.1028
Entries	4216	4097	3903	3430	2185

Table 14: Selection 2. $\phi_{(\gamma,jet)} = 180^\circ \pm 17^\circ$. UA2 algorithm. $L_{int} = 300\ pb^{-1}$.

P_{tCUT}^{clust}	30	20	15	10	5
Nevent	5458	5291	5013	4400	3016
P_t56	9.2	8.7	8.1	7.2	5.9
$\Delta\phi$	5.5	5.4	5.1	4.7	3.9
${P_t}^{out}$	6.8	6.5	6.1	5.4	4.4
${P_t}^{\vert\eta\vert>4.2}$	2.0	2.0	2.0	2.0	2.0
$({P_t}^{\gamma} - {P_t}^{part})/{P_t}^{\gamma}$	-0.0221	-0.0159	-0.0130	-0.0115	-0.0088
$({P_t}^{J} - {P_t}^{part})/{P_t}^{J}$	-0.0172	-0.0178	-0.0197	-0.0230	-0.0226
$({P_t}^{\gamma} - {P_t}^{J})/{P_t}^{\gamma}$	-0.0056	0.0010	0.0058	0.0102	0.0126
$P_t(O{+}\eta{>}4.2)/{P_t}^{\gamma}$	-0.0130	-0.0061	-0.0008	0.0047	0.0086
$1 - cos(\Delta\phi)$	0.0074	0.0071	0.0066	0.0056	0.0040
$\sigma(Db[\gamma, J])$	0.1470	0.1325	0.1202	0.1053	0.0885
$\sigma(Db[\gamma, part])$	0.1725	0.1567	0.1426	0.1191	0.0995
Entries	4434	4299	4073	3575	2450

Table 15: Selection 2. $\phi_{(\gamma,jet)} = 180^\circ \pm 17^\circ$. LUCELL algorithm. $L_{int} = 300\ pb^{-1}$.

P_{tCUT}^{clust}	30	20	15	10	5
Nevent	5369	5216	4968	4329	2784
P_t56	9.5	8.9	8.4	7.3	5.8
$\Delta\phi$	5.6	5.5	5.3	4.8	3.7
${P_t}^{out}$	7.0	6.6	6.2	5.5	4.2
${P_t}^{\vert\eta\vert>4.2}$	2.0	2.0	2.0	2.0	2.1
$({P_t}^{\gamma} - {P_t}^{part})/{P_t}^{\gamma}$	-0.0247	-0.0171	-0.0139	-0.0134	-0.0094
$({P_t}^{J} - {P_t}^{part})/{P_t}^{J}$	-0.0122	-0.0134	-0.0152	-0.0180	-0.0168
$({P_t}^{\gamma} - {P_t}^{J})/{P_t}^{\gamma}$	-0.0130	-0.0042	0.0006	0.0036	0.0065
$P_t(O{+}\eta{>}4.2)/{P_t}^{\gamma}$	-0.0205	-0.0115	-0.0062	-0.0022	0.0029
$1 - cos(\Delta\phi)$	0.0076	0.0074	0.0069	0.0058	0.0036
$\sigma(Db[\gamma, J])$	0.1545	0.1363	0.1241	0.1057	0.0820
$\sigma(Db[\gamma, part])$	0.1827	0.1654	0.1492	0.1220	0.0960
Entries	4362	4238	4036	3517	2262

Table 16: Selection 3. $\phi_{(\gamma,jet)} = 180^{\circ} \pm 17^{\circ}$. UA1 algorithm. $L_{int} = 300\ pb^{-1}$.

P_{tCUT}^{clust}	30	20	15	10	5
Nevent	4137	4005	3771	3229	1935
P_t56	9.1	8.6	7.9	6.9	5.4
$\Delta\phi$	5.4	5.3	5.1	4.5	3.4
P_t^{out}	6.8	6.4	5.9	5.1	3.8
$P_t^{\vert\eta\vert>4.2}$	2.0	2.0	2.0	2.0	2.1
$(P_t^{\gamma}-P_t^{part})/P_t^{\gamma}$	-0.0254	-0.0182	-0.0158	-0.0147	-0.0099
$(P_t^{J}-P_t^{part})/P_t^{J}$	-0.0083	-0.0094	-0.0111	-0.0150	-0.0135
$(P_t^{\gamma}-P_t^{J})/P_t^{\gamma}$	-0.0172	-0.0089	-0.0049	-0.0003	0.0031
$P_t(O+\eta>4.2)/P_t^{\gamma}$	-0.0245	-0.0159	-0.0113	-0.0055	0.0001
$1-cos(\Delta\phi)$	0.0073	0.0071	0.0064	0.0053	0.0031
$\sigma(Db[\gamma,J])$	0.1464	0.1301	0.1173	0.0987	0.0794
$\sigma(Db[\gamma,part])$	0.1745	0.1563	0.1409	0.1129	0.0948
Entries	3361	3254	3064	2623	1572

Table 17: Selection 3. $\phi_{(\gamma,jet)} = 180^{\circ} \pm 17^{\circ}$. UA2 algorithm. $L_{int} = 300\ pb^{-1}$.

P_{tCUT}^{clust}	30	20	15	10	5
Nevent	4137	4005	3771	3229	1935
P_t56	9.1	8.6	7.9	6.9	5.4
$\Delta\phi$	5.5	5.3	5.1	4.6	3.5
P_t^{out}	6.8	6.4	6.0	5.2	3.9
$P_t^{\vert\eta\vert>4.2}$	2.0	2.0	2.0	2.0	2.1
$(P_t^{\gamma}-P_t^{part})/P_t^{\gamma}$	-0.0254	-0.0182	-0.0158	-0.0147	-0.0099
$(P_t^{J}-P_t^{part})/P_t^{J}$	-0.0146	-0.0157	-0.0176	-0.0215	-0.0196
$(P_t^{\gamma}-P_t^{J})/P_t^{\gamma}$	-0.0112	-0.0029	0.0011	0.0058	0.0089
$P_t(O+\eta>4.2)/P_t^{\gamma}$	-0.0185	-0.0099	-0.0053	0.0006	0.0058
$1-cos(\Delta\phi)$	0.0073	0.0071	0.0065	0.0053	0.0031
$\sigma(Db[\gamma,J])$	0.1477	0.1312	0.1186	0.1000	0.0807
$\sigma(Db[\gamma,part])$	0.1745	0.1563	0.1409	0.1129	0.0948
Entries	3361	3254	3064	2623	1572

Table 18: Selection 3. $\phi_{(\gamma,jet)} = 180^{\circ} \pm 17^{\circ}$. LUCELL algorithm. $L_{int} = 300\ pb^{-1}$.

P_{tCUT}^{clust}	30	20	15	10	5
Nevent	4137	4005	3771	3229	1935
P_t56	9.1	8.6	7.9	6.9	5.4
$\Delta\phi$	5.4	5.3	5.1	4.6	3.4
P_t^{out}	6.8	6.4	6.0	5.2	3.8
$P_t^{\vert\eta\vert>4.2}$	2.0	2.0	2.0	2.0	2.1
$(P_t^{\gamma}-P_t^{part})/P_t^{\gamma}$	-0.0254	-0.0182	-0.0158	-0.0147	-0.0099
$(P_t^{J}-P_t^{part})/P_t^{J}$	-0.0112	-0.0123	-0.0140	-0.0180	-0.0159
$(P_t^{\gamma}-P_t^{J})/P_t^{\gamma}$	-0.0144	-0.0061	-0.0022	0.0025	0.0055
$P_t(O+\eta>4.2)/P_t^{\gamma}$	-0.0217	-0.0131	-0.0086	-0.0027	0.0024
$1-cos(\Delta\phi)$	0.0073	0.0071	0.0065	0.0053	0.0031
$\sigma(Db[\gamma,J])$	0.1468	0.1304	0.1177	0.0991	0.0794
$\sigma(Db[\gamma,part])$	0.1745	0.1563	0.1409	0.1129	0.0948
Entries	3361	3254	3064	2623	1572

Appendix 3 $50 < P_t^{\gamma} < 70\ GeV/c$

$P_t^{isol} < 4\ GeV/c, \quad \epsilon^{\gamma} < 7\%$

Table 1: Selection 1. $\phi_{(\gamma,jet)} = 180^{\circ} \pm 180^{\circ}$. UA1 algorithm. $L_{int} = 300\ pb^{-1}$.

P_{tCUT}^{clust}	30	20	15	10	5
Nevent*	11206	9150	7699	5918	2982
P_t56	15.4	12.4	10.8	8.9	6.7
$\Delta\phi$	9.4	7.0	5.7	4.5	3.2
P_t^{out}	13.3	10.4	8.7	6.9	4.9
$P_t^{\|\eta\|>4.2}$	2.0	2.0	2.0	2.0	2.0
$(P_t^{\gamma} - P_t^{part})/P_t^{\gamma}$	0.0540	0.0348	0.0241	0.0134	0.0072
$(P_t^{J} - P_t^{part})/P_t^{J}$	-0.0487	-0.0433	-0.0366	-0.0307	-0.0211
$(P_t^{\gamma} - P_t^{J})/P_t^{\gamma}$	0.0897	0.0691	0.0544	0.0399	0.0261
$P_t(O{+}\eta{>}4.2)/P_t^{\gamma}$	0.0598	0.0520	0.0422	0.0311	0.0206
$1 - cos(\Delta\phi)$	0.0273	0.0144	0.0093	0.0057	0.0029
$\sigma(Db[\gamma, J])^{**}$	0.1771	0.1482	0.1279	0.1047	0.0816
$\sigma(Db[\gamma, part])^{***}$	0.2181	0.1828	0.1590	0.1307	0.1025
Entries	15717	12833	10799	8301	4183

Table 2: Selection 1. $\phi_{(\gamma,jet)} = 180^{\circ} \pm 180^{\circ}$. UA2 algorithm. $L_{int} = 300\ pb^{-1}$.

P_{tCUT}^{clust}	30	20	15	10	5
Nevent	8112	6760	5937	4778	2932
P_t56	14.1	11.2	9.8	8.2	6.7
$\Delta\phi$	8.3	6.2	5.2	4.2	3.2
P_t^{out}	11.6	8.9	7.7	6.3	4.8
$P_t^{\|\eta\|>4.2}$	2.0	2.0	2.0	2.0	2.0
$(P_t^{\gamma} - P_t^{part})/P_t^{\gamma}$	0.0389	0.0181	0.0093	0.0030	0.0032
$(P_t^{J} - P_t^{part})/P_t^{J}$	-0.0251	-0.0265	-0.0282	-0.0288	-0.0247
$(P_t^{\gamma} - P_t^{J})/P_t^{\gamma}$	0.0591	0.0407	0.0334	0.0283	0.0251
$P_t(O{+}\eta{>}4.2)/P_t^{\gamma}$	0.0347	0.0260	0.0222	0.0197	0.0189
$1 - cos(\Delta\phi)$	0.0214	0.0114	0.0078	0.0051	0.0030
$\sigma(Db[\gamma, J])$	0.1662	0.1343	0.1175	0.1001	0.0818
$\sigma(Db[\gamma, part])$	0.2016	0.1644	0.1416	0.1168	0.0982
Entries	11378	9481	8328	6702	4112

Table 3: Selection 1. $\phi_{(\gamma,jet)} = 180^{\circ} \pm 180^{\circ}$. LUCELL algorithm. $L_{int} = 300\ pb^{-1}$.

P_{tCUT}^{clust}	30	20	15	10	5
Nevent	11093	9106	7694	5905	3172
P_t56	15.3	12.3	10.5	8.5	6.4
$\Delta\phi$	9.4	6.8	5.6	4.3	3.1
P_t^{out}	13.1	10.1	8.4	6.6	4.7
$P_t^{\|\eta\|>4.2}$	2.0	2.0	2.0	2.0	2.0
$(P_t^{\gamma} - P_t^{part})/P_t^{\gamma}$	0.0542	0.0341	0.0229	0.0114	0.0060
$(P_t^{J} - P_t^{part})/P_t^{J}$	-0.0411	-0.0380	-0.0351	-0.0305	-0.0239
$(P_t^{\gamma} - P_t^{J})/P_t^{\gamma}$	0.0856	0.0652	0.0524	0.0381	0.0275
$P_t(O{+}\eta{>}4.2)/P_t^{\gamma}$	0.0559	0.0489	0.0410	0.0302	0.0223
$1 - cos(\Delta\phi)$	0.0273	0.0138	0.0087	0.0051	0.0024
$\sigma(Db[\gamma, J])$	0.1740	0.1441	0.1236	0.0995	0.0739
$\sigma(Db[\gamma, part])$	0.2175	0.1818	0.1562	0.1274	0.0966
Entries	15559	12772	10792	8282	4448

*Number of events (Nevent) is given in this and in the following tables for integrated luminosity $L_{int} = 300\ pb^{-1}$.

Table 4: Selection 1. $\phi_{(\gamma,jet)} = 180^\circ \pm 17^\circ$. UA1 algorithm. $L_{int} = 300\ pb^{-1}$.

P_{tCUT}^{clust}	30	20	15	10	5
Nevent	9249	8350	7358	5831	2967
$P_t 56$	12.7	11.3	10.2	8.7	6.6
$\Delta\phi$	5.8	5.4	5.0	4.3	3.1
${P_t}^{out}$	10.3	9.1	8.1	6.7	4.8
${P_t}^{\lvert\eta\rvert>4.2}$	2.0	2.0	2.0	2.0	2.0
$({P_t}^{\gamma} - {P_t}^{part})/{P_t}^{\gamma}$	0.0372	0.0291	0.0215	0.0126	0.0067
$({P_t}^{J} - {P_t}^{part})/{P_t}^{J}$	-0.0467	-0.0403	-0.0359	-0.0303	-0.0211
$({P_t}^{\gamma} - {P_t}^{J})/{P_t}^{\gamma}$	0.0729	0.0616	0.0513	0.0388	0.0255
$P_t(O{+}\eta{>}4.2)/{P_t}^{\gamma}$	0.0620	0.0516	0.0420	0.0309	0.0204
$1 - cos(\Delta\phi)$	0.0081	0.0073	0.0063	0.0047	0.0026
$\sigma(Db[\gamma, J])$	0.1654	0.1431	0.1255	0.1035	0.0802
$\sigma(Db[\gamma, part])$	0.1998	0.1758	0.1553	0.1295	0.1014
Entries	12973	11712	10320	8179	4162

Table 5: Selection 1. $\phi_{(\gamma,jet)} = 180^\circ \pm 17^\circ$. UA2 algorithm. $L_{int} = 300\ pb^{-1}$.

P_{tCUT}^{clust}	30	20	15	10	5
Nevent	6915	6315	5729	4710	2913
$P_t 56$	11.8	10.4	9.4	8.0	6.6
$\Delta\phi$	5.4	5.0	4.6	4.0	3.1
${P_t}^{out}$	9.1	8.0	7.2	6.1	4.7
${P_t}^{\lvert\eta\rvert>4.2}$	2.0	2.0	2.0	2.0	2.0
$({P_t}^{\gamma} - {P_t}^{part})/{P_t}^{\gamma}$	0.0227	0.0140	0.0077	0.0020	0.0027
$({P_t}^{J} - {P_t}^{part})/{P_t}^{J}$	-0.0242	-0.0256	-0.0274	-0.0286	-0.0247
$({P_t}^{\gamma} - {P_t}^{J})/{P_t}^{\gamma}$	0.0436	0.0361	0.0314	0.0271	0.0245
$P_t(O{+}\eta{>}4.2)/{P_t}^{\gamma}$	0.0331	0.0263	0.0224	0.0194	0.0187
$1 - cos(\Delta\phi)$	0.0074	0.0065	0.0056	0.0042	0.0026
$\sigma(Db[\gamma, J])$	0.1542	0.1302	0.1152	0.0986	0.0807
$\sigma(Db[\gamma, part])$	0.1856	0.1586	0.1395	0.1156	0.0972
Entries	9699	8857	8035	6607	4085

Table 6: Selection 1. $\phi_{(\gamma,jet)} = 180^\circ \pm 17^\circ$. LUCELL algorithm. $L_{int} = 300\ pb^{-1}$.

P_{tCUT}^{clust}	30	20	15	10	5
Nevent	9174	8348	7378	5843	3170
$P_t 56$	12.7	11.3	10.1	8.4	6.4
$\Delta\phi$	5.7	5.4	4.9	4.2	3.1
${P_t}^{out}$	10.0	8.9	7.9	6.5	4.7
${P_t}^{\lvert\eta\rvert>4.2}$	2.0	2.0	2.0	2.0	2.0
$({P_t}^{\gamma} - {P_t}^{part})/{P_t}^{\gamma}$	0.0377	0.0292	0.0213	0.0112	0.0060
$({P_t}^{J} - {P_t}^{part})/{P_t}^{J}$	-0.0381	-0.0359	-0.0340	-0.0301	-0.0239
$({P_t}^{\gamma} - {P_t}^{J})/{P_t}^{\gamma}$	0.0681	0.0588	0.0500	0.0376	0.0275
$P_t(O{+}\eta{>}4.2)/{P_t}^{\gamma}$	0.0575	0.0491	0.0411	0.0302	0.0223
$1 - cos(\Delta\phi)$	0.0080	0.0071	0.0062	0.0045	0.0024
$\sigma(Db[\gamma, J])$	0.1620	0.1396	0.1216	0.0991	0.0739
$\sigma(Db[\gamma, part])$	0.2003	0.1753	0.1533	0.1272	0.0966
Entries	12868	11708	10348	8196	4446

Table 7: Selection 1. $\phi_{(\gamma,jet)} = 180° \pm 11°$. UA1 algorithm. $L_{int} = 300\ pb^{-1}$.

P_{tCUT}^{clust}	30	20	15	10	5
Nevent	7833	7279	6610	5503	2916
P_t56	11.5	10.4	9.5	8.3	6.5
$\Delta\phi$	4.3	4.2	4.0	3.8	2.9
${P_t}^{out}$	8.9	8.0	7.2	6.2	4.6
${P_t}^{\lvert\eta\rvert>4.2}$	2.0	2.0	2.0	2.0	2.0
$({P_t}^{\gamma}-{P_t}^{part})/{P_t}^{\gamma}$	0.0305	0.0244	0.0170	0.0104	0.0056
$({P_t}^{J}-{P_t}^{part})/{P_t}^{J}$	-0.0434	-0.0377	-0.0345	-0.0292	-0.0211
$({P_t}^{\gamma}-{P_t}^{J})/{P_t}^{\gamma}$	0.0639	0.0549	0.0458	0.0357	0.0244
$P_t(O{+}\eta{>}4.2)/{P_t}^{\gamma}$	0.0570	0.0481	0.0391	0.0294	0.0199
$1-cos(\Delta\phi)$	0.0042	0.0041	0.0038	0.0034	0.0022
$\sigma(Db[\gamma,J])$	0.1577	0.1374	0.1209	0.1007	0.0786
$\sigma(Db[\gamma,part])$	0.1893	0.1697	0.1499	0.1270	0.0998
Entries	10986	10209	9271	7718	4089

Table 8: Selection 1. $\phi_{(\gamma,jet)} = 180° \pm 11°$. UA2 algorithm. $L_{int} = 300\ pb^{-1}$.

P_{tCUT}^{clust}	30	20	15	10	5
Nevent	5971	5609	5246	4495	2867
P_t56	10.5	9.5	8.8	7.7	6.4
$\Delta\phi$	4.0	4.0	3.8	3.6	2.9
${P_t}^{out}$	7.8	7.0	6.5	5.7	4.5
${P_t}^{\lvert\eta\rvert>4.2}$	2.0	2.0	2.0	2.0	2.0
$({P_t}^{\gamma}-{P_t}^{part})/{P_t}^{\gamma}$	0.0161	0.0102	0.0052	0.0011	0.0020
$({P_t}^{J}-{P_t}^{part})/{P_t}^{J}$	-0.0243	-0.0249	-0.0269	-0.0281	-0.0242
$({P_t}^{\gamma}-{P_t}^{J})/{P_t}^{\gamma}$	0.0372	0.0318	0.0286	0.0257	0.0235
$P_t(O{+}\eta{>}4.2)/{P_t}^{\gamma}$	0.0303	0.0249	0.0218	0.0193	0.0182
$1-cos(\Delta\phi)$	0.0039	0.0037	0.0035	0.0031	0.0022
$\sigma(Db[\gamma,J])$	0.1460	0.1251	0.1117	0.0957	0.0792
$\sigma(Db[\gamma,part])$	0.1749	0.1531	0.1357	0.1128	0.0966
Entries	8375	7867	7357	6305	4021

Table 9: Selection 1. $\phi_{(\gamma,jet)} = 180° \pm 11°$. LUCELL algorithm. $L_{int} = 300\ pb^{-1}$.

P_{tCUT}^{clust}	30	20	15	10	5
Nevent	7783	7296	6659	5553	3135
P_t56	11.3	10.4	9.4	8.1	6.3
$\Delta\phi$	4.2	4.1	4.0	3.7	3.0
${P_t}^{out}$	8.7	7.9	7.1	6.1	4.6
${P_t}^{\lvert\eta\rvert>4.2}$	2.0	2.0	2.0	2.0	2.0
$({P_t}^{\gamma}-{P_t}^{part})/{P_t}^{\gamma}$	0.0304	0.0243	0.0178	0.0097	0.0060
$({P_t}^{J}-{P_t}^{part})/{P_t}^{J}$	-0.0354	-0.0337	-0.0324	-0.0294	-0.0238
$({P_t}^{\gamma}-{P_t}^{J})/{P_t}^{\gamma}$	0.0591	0.0525	0.0454	0.0356	0.0274
$P_t(O{+}\eta{>}4.2)/{P_t}^{\gamma}$	0.0525	0.0460	0.0390	0.0296	0.0224
$1-cos(\Delta\phi)$	0.0042	0.0040	0.0038	0.0033	0.0022
$\sigma(Db[\gamma,J])$	0.1533	0.1345	0.1171	0.0970	0.0738
$\sigma(Db[\gamma,part])$	0.1886	0.1693	0.1487	0.1242	0.0964
Entries	10916	10234	9340	7789	4397

Table 10: Selection 1. $\phi_{(\gamma,jet)} = 180^\circ \pm 6^\circ$. UA1 algorithm. $L_{int} = 300\ pb^{-1}$.

P_{tCUT}^{clust}	30	20	15	10	5
Nevent	5330	5056	4738	4138	2508
$P_t 56$	9.9	9.1	8.4	7.3	5.9
$\Delta\phi$	2.5	2.5	2.5	2.4	2.2
${P_t}^{out}$	7.2	6.5	6.0	5.2	4.1
${P_t}^{\vert\eta\vert>4.2}$	2.0	2.0	2.0	2.0	2.0
$({P_t}^{\gamma}-{P_t}^{part})/{P_t}^{\gamma}$	0.0238	0.0189	0.0133	0.0070	0.0035
$({P_t}^{J}-{P_t}^{part})/{P_t}^{J}$	-0.0367	-0.0324	-0.0308	-0.0282	-0.0211
$({P_t}^{\gamma}-{P_t}^{J})/{P_t}^{\gamma}$	0.0529	0.0459	0.0396	0.0316	0.0225
$P_t(O{+}\eta{>}4.2)/{P_t}^{\gamma}$	0.0489	0.0419	0.0355	0.0276	0.0191
$1-cos(\Delta\phi)$	0.0013	0.0013	0.0013	0.0012	0.0011
$\sigma(Db[\gamma,J])$	0.1449	0.1277	0.1149	0.0964	0.0758
$\sigma(Db[\gamma,part])$	0.1743	0.1586	0.1423	0.1181	0.0967
Entries	7476	7092	6645	5804	3518

Table 11: Selection 1. $\phi_{(\gamma,jet)} = 180^\circ \pm 6^\circ$. UA2 algorithm. $L_{int} = 300\ pb^{-1}$.

P_{tCUT}^{clust}	30	20	15	10	5
Nevent	4241	4051	3884	3494	2462
$P_t 56$	8.9	8.1	7.6	6.8	5.9
$\Delta\phi$	2.4	2.4	2.4	2.3	2.2
${P_t}^{out}$	6.3	5.7	5.3	4.7	4.0
${P_t}^{\vert\eta\vert>4.2}$	1.9	1.9	1.9	1.9	1.9
$({P_t}^{\gamma}-{P_t}^{part})/{P_t}^{\gamma}$	0.0097	0.0047	0.0030	0.0002	0.0012
$({P_t}^{J}-{P_t}^{part})/{P_t}^{J}$	-0.0250	-0.0251	-0.0258	-0.0264	-0.0229
$({P_t}^{\gamma}-{P_t}^{J})/{P_t}^{\gamma}$	0.0313	0.0266	0.0255	0.0235	0.0217
$P_t(O{+}\eta{>}4.2)/{P_t}^{\gamma}$	0.0270	0.0222	0.0210	0.0192	0.0179
$1-cos(\Delta\phi)$	0.0012	0.0012	0.0012	0.0012	0.0011
$\sigma(Db[\gamma,J])$	0.1326	0.1153	0.1057	0.0910	0.0758
$\sigma(Db[\gamma,part])$	0.1549	0.1365	0.1258	0.1060	0.0941
Entries	5948	5682	5447	4901	3453

Table 12: Selection 1. $\phi_{(\gamma,jet)} = 180^\circ \pm 6^\circ$. LUCELL algorithm. $L_{int} = 300\ pb^{-1}$.

P_{tCUT}^{clust}	30	20	15	10	5
Nevent	5337	5097	4798	4205	2677
$P_t 56$	9.7	9.0	8.2	7.2	5.8
$\Delta\phi$	2.5	2.4	2.4	2.4	2.2
${P_t}^{out}$	7.0	6.4	5.8	5.1	4.1
${P_t}^{\vert\eta\vert>4.2}$	2.0	2.0	2.0	2.0	2.0
$({P_t}^{\gamma}-{P_t}^{part})/{P_t}^{\gamma}$	0.0233	0.0178	0.0129	0.0079	0.0050
$({P_t}^{J}-{P_t}^{part})/{P_t}^{J}$	-0.0325	-0.0311	-0.0306	-0.0277	-0.0235
$({P_t}^{\gamma}-{P_t}^{J})/{P_t}^{\gamma}$	0.0503	0.0443	0.0392	0.0325	0.0261
$P_t(O{+}\eta{>}4.2)/{P_t}^{\gamma}$	0.0466	0.0405	0.0353	0.0285	0.0221
$1-cos(\Delta\phi)$	0.0013	0.0013	0.0013	0.0012	0.0011
$\sigma(Db[\gamma,J])$	0.1409	0.1256	0.1112	0.0928	0.0724
$\sigma(Db[\gamma,part])$	0.1730	0.1579	0.1399	0.1180	0.0936
Entries	7485	7149	6729	5898	3755

Table 13: Selection 2. $\phi_{(\gamma,jet)} = 180^\circ \pm 17^\circ$. UA1 algorithm. $L_{int} = 300\ pb^{-1}$.

P_{tCUT}^{clust}	30	20	15	10	5
Nevent	4088	3831	3530	3023	1847
$P_t 56$	11.2	10.1	9.2	8.0	6.3
$\Delta\phi$	5.1	4.8	4.5	4.0	3.0
${P_t}^{out}$	8.5	7.7	6.9	5.9	4.5
${P_t}^{\vert\eta\vert>4.2}$	2.0	2.0	2.0	2.0	2.0
$({P_t}^{\gamma} - {P_t}^{part})/{P_t}^{\gamma}$	-0.0058	-0.0066	-0.0070	-0.0077	-0.0017
$({P_t}^{J} - {P_t}^{part})/{P_t}^{J}$	-0.0121	-0.0135	-0.0151	-0.0165	-0.0146
$({P_t}^{\gamma} - {P_t}^{J})/{P_t}^{\gamma}$	0.0054	0.0057	0.0066	0.0071	0.0113
$P_t(O{+}\eta{>}4.2)/{P_t}^{\gamma}$	-0.0040	-0.0029	-0.0014	0.0004	0.0064
$1 - cos(\Delta\phi)$	0.0068	0.0061	0.0053	0.0041	0.0024
$\sigma(Db[\gamma, J])$	0.1472	0.1268	0.1114	0.0945	0.0778
$\sigma(Db[\gamma, part])$	0.1764	0.1523	0.1351	0.1101	0.0891
Entries	5734	5373	4951	4240	2590

Table 14: Selection 2. $\phi_{(\gamma,jet)} = 180^\circ \pm 17^\circ$. UA2 algorithm. $L_{int} = 300\ pb^{-1}$.

P_{tCUT}^{clust}	30	20	15	10	5
Nevent	4069	3782	3485	2946	1951
$P_t 56$	10.9	9.8	8.9	7.6	6.3
$\Delta\phi$	5.1	4.8	4.4	3.8	3.0
${P_t}^{out}$	8.3	7.4	6.7	5.7	4.5
${P_t}^{\vert\eta\vert>4.2}$	2.0	2.0	2.0	2.0	2.0
$({P_t}^{\gamma} - {P_t}^{part})/{P_t}^{\gamma}$	-0.0075	-0.0079	-0.0095	-0.0100	-0.0041
$({P_t}^{J} - {P_t}^{part})/{P_t}^{J}$	-0.0172	-0.0180	-0.0201	-0.0233	-0.0216
$({P_t}^{\gamma} - {P_t}^{J})/{P_t}^{\gamma}$	0.0088	0.0088	0.0088	0.0110	0.0152
$P_t(O{+}\eta{>}4.2)/{P_t}^{\gamma}$	-0.0004	0.0003	0.0010	0.0045	0.0101
$1 - cos(\Delta\phi)$	0.0067	0.0060	0.0052	0.0039	0.0024
$\sigma(Db[\gamma, J])$	0.1429	0.1206	0.1066	0.0930	0.0775
$\sigma(Db[\gamma, part])$	0.1712	0.1477	0.1306	0.1056	0.0898
Entries	5707	5304	4888	4131	2737

Table 15: Selection 2. $\phi_{(\gamma,jet)} = 180^\circ \pm 17^\circ$. LUCELL algorithm. $L_{int} = 300\ pb^{-1}$.

P_{tCUT}^{clust}	30	20	15	10	5
Nevent	4196	3941	3622	3069	1901
$P_t 56$	11.0	10.0	9.0	7.7	6.0
$\Delta\phi$	5.1	4.8	4.5	3.9	2.9
${P_t}^{out}$	8.5	7.6	6.8	5.8	4.3
${P_t}^{\vert\eta\vert>4.2}$	2.0	2.0	2.0	2.0	2.1
$({P_t}^{\gamma} - {P_t}^{part})/{P_t}^{\gamma}$	-0.0075	-0.0072	-0.0064	-0.0087	-0.0042
$({P_t}^{J} - {P_t}^{part})/{P_t}^{J}$	-0.0167	-0.0173	-0.0187	-0.0203	-0.0177
$({P_t}^{\gamma} - {P_t}^{J})/{P_t}^{\gamma}$	0.0081	0.0088	0.0108	0.0098	0.0119
$P_t(O{+}\eta{>}4.2)/{P_t}^{\gamma}$	-0.0010	0.0004	0.0031	0.0034	0.0075
$1 - cos(\Delta\phi)$	0.0069	0.0061	0.0053	0.0039	0.0021
$\sigma(Db[\gamma, J])$	0.1461	0.1241	0.1072	0.0893	0.0664
$\sigma(Db[\gamma, part])$	0.1723	0.1482	0.1290	0.1051	0.0803
Entries	5885	5528	5081	4305	2666

Table 16: Selection 3. $\phi_{(\gamma,jet)} = 180^\circ \pm 17^\circ$. UA1 algorithm. $L_{int} = 300\ pb^{-1}$.

P_{tCUT}^{clust}	30	20	15	10	5
Nevent	3117	2884	2636	2190	1262
$P_t 56$	10.7	9.6	8.6	7.2	5.5
$\Delta\phi$	5.0	4.7	4.3	3.6	2.6
${P_t}^{out}$	8.2	7.3	6.5	5.3	3.7
${P_t}^{\vert\eta\vert>4.2}$	2.0	2.0	2.0	2.0	2.0
$({P_t}^{\gamma}-{P_t}^{part})/{P_t}^{\gamma}$	-0.0052	-0.0078	-0.0092	-0.0102	-0.0038
$({P_t}^{J}-{P_t}^{part})/{P_t}^{J}$	-0.0123	-0.0138	-0.0162	-0.0185	-0.0162
$({P_t}^{\gamma}-{P_t}^{J})/{P_t}^{\gamma}$	0.0068	0.0051	0.0056	0.0065	0.0106
$P_t(O{+}\eta{>}4.2)/{P_t}^{\gamma}$	-0.0024	-0.0032	-0.0022	0.0003	0.0061
$1-cos(\Delta\phi)$	0.0065	0.0057	0.0049	0.0034	0.0017
$\sigma(Db[\gamma,J])$	0.1417	0.1186	0.1037	0.0857	0.0631
$\sigma(Db[\gamma,part])$	0.1682	0.1423	0.1237	0.0957	0.0707
Entries	4372	4045	3698	3071	1771

Table 17: Selection 3. $\phi_{(\gamma,jet)} = 180^\circ \pm 17^\circ$. UA2 algorithm. $L_{int} = 300\ pb^{-1}$.

P_{tCUT}^{clust}	30	20	15	10	5
Nevent	3117	2884	2636	2190	1262
$P_t 56$	10.7	9.6	8.6	7.2	5.5
$\Delta\phi$	5.0	4.7	4.3	3.6	2.6
${P_t}^{out}$	8.2	7.3	6.5	5.3	3.8
${P_t}^{\vert\eta\vert>4.2}$	2.0	2.0	2.0	2.0	2.0
$({P_t}^{\gamma}-{P_t}^{part})/{P_t}^{\gamma}$	-0.0052	-0.0078	-0.0092	-0.0102	-0.0038
$({P_t}^{J}-{P_t}^{part})/{P_t}^{J}$	-0.0163	-0.0176	-0.0201	-0.0219	-0.0196
$({P_t}^{\gamma}-{P_t}^{J})/{P_t}^{\gamma}$	0.0104	0.0086	0.0092	0.0096	0.0138
$P_t(O{+}\eta{>}4.2)/{P_t}^{\gamma}$	0.0012	0.0002	0.0014	0.0034	0.0093
$1-cos(\Delta\phi)$	0.0065	0.0057	0.0049	0.0034	0.0017
$\sigma(Db[\gamma,J])$	0.1425	0.1194	0.1045	0.0862	0.0639
$\sigma(Db[\gamma,part])$	0.1682	0.1423	0.1237	0.0957	0.0707
Entries	4372	4045	3698	3071	1771

Table 18: Selection 3. $\phi_{(\gamma,jet)} = 180^\circ \pm 17^\circ$. LUCELL algorithm. $L_{int} = 300\ pb^{-1}$.

P_{tCUT}^{clust}	30	20	15	10	5
Nevent	3117	2884	2636	2190	1262
$P_t 56$	10.7	9.6	8.6	7.2	5.5
$\Delta\phi$	5.0	4.7	4.3	3.6	2.6
${P_t}^{out}$	8.2	7.3	6.5	5.4	3.8
${P_t}^{\vert\eta\vert>4.2}$	2.0	2.0	2.0	2.0	2.0
$({P_t}^{\gamma}-{P_t}^{part})/{P_t}^{\gamma}$	-0.0052	-0.0078	-0.0092	-0.0102	-0.0038
$({P_t}^{J}-{P_t}^{part})/{P_t}^{J}$	-0.0146	-0.0163	-0.0186	-0.0209	-0.0183
$({P_t}^{\gamma}-{P_t}^{J})/{P_t}^{\gamma}$	0.0090	0.0075	0.0079	0.0088	0.0126
$P_t(O{+}\eta{>}4.2)/{P_t}^{\gamma}$	-0.0002	-0.0009	0.0001	0.0025	0.0081
$1-cos(\Delta\phi)$	0.0066	0.0057	0.0049	0.0034	0.0017
$\sigma(Db[\gamma,J])$	0.1418	0.1189	0.1040	0.0864	0.0635
$\sigma(Db[\gamma,part])$	0.1682	0.1423	0.1237	0.0957	0.0707
Entries	4372	4045	3698	3071	1771

Appendix 4 $70 < P_t^{\gamma} < 90\ GeV/c$

$P_t^{isol} < 4\ GeV/c, \quad \epsilon^{\gamma} < 7\%$

Table 1: Selection 1. $\phi_{(\gamma,jet)} = 180^\circ \pm 180^\circ$. UA1 algorithm. $L_{int} = 300\ pb^{-1}$.

P_{tCUT}^{clust}	30	20	15	10	5
Nevent*	2708	2138	1780	1331	682
P_t56	16.7	13.2	11.3	9.2	6.8
$\Delta\phi$	7.4	5.4	4.5	3.4	2.3
P_t^{out}	14.9	11.1	9.2	7.1	4.9
$P_t^{\lvert\eta\rvert>4.2}$	1.9	1.9	1.9	2.0	2.0
$(P_t^{\gamma}-P_t^{part})/P_t^{\gamma}$	0.0434	0.0205	0.0125	0.0068	0.0036
$(P_t^{J}-P_t^{part})/P_t^{J}$	-0.0460	-0.0334	-0.0251	-0.0192	-0.0151
$(P_t^{\gamma}-P_t^{J})/P_t^{\gamma}$	0.0775	0.0477	0.0337	0.0234	0.0169
$P_t(O{+}\eta{>}4.2)/P_t^{\gamma}$	0.0605	0.0393	0.0281	0.0202	0.0153
$1-cos(\Delta\phi)$	0.0170	0.0084	0.0056	0.0031	0.0015
$\sigma(Db[\gamma,J])^{**}$	0.1619	0.1245	0.1029	0.0815	0.0628
$\sigma(Db[\gamma,part])^{***}$	0.1917	0.1503	0.1278	0.1049	0.0845
Entries	15301	12081	10056	7520	3851

Table 2: Selection 1. $\phi_{(\gamma,jet)} = 180^\circ \pm 180^\circ$. UA2 algorithm. $L_{int} = 300\ pb^{-1}$.

P_{tCUT}^{clust}	30	20	15	10	5
Nevent	1877	1557	1348	1073	665
P_t56	14.7	11.7	10.1	8.7	7.1
$\Delta\phi$	6.1	4.7	3.9	3.1	2.4
P_t^{out}	12.1	9.3	7.9	6.4	5.0
$P_t^{\lvert\eta\rvert>4.2}$	2.0	2.0	2.0	2.0	2.0
$(P_t^{\gamma}-P_t^{part})/P_t^{\gamma}$	0.0203	0.0066	0.0023	0.0022	0.0028
$(P_t^{J}-P_t^{part})/P_t^{J}$	-0.0214	-0.0205	-0.0193	-0.0157	-0.0142
$(P_t^{\gamma}-P_t^{J})/P_t^{\gamma}$	0.0374	0.0236	0.0188	0.0157	0.0155
$P_t(O{+}\eta{>}4.2)/P_t^{\gamma}$	0.0258	0.0173	0.0145	0.0130	0.0138
$1-cos(\Delta\phi)$	0.0116	0.0063	0.0043	0.0027	0.0017
$\sigma(Db[\gamma,J])$	0.1365	0.1066	0.0911	0.0767	0.0629
$\sigma(Db[\gamma,part])$	0.1654	0.1276	0.1075	0.0979	0.0869
Entries	10602	8796	7615	6064	3759

Table 3: Selection 1. $\phi_{(\gamma,jet)} = 180^\circ \pm 180^\circ$. LUCELL algorithm. $L_{int} = 300\ pb^{-1}$.

P_{tCUT}^{clust}	30	20	15	10	5
Nevent	2665	2126	1769	1336	720
P_t56	16.5	12.9	10.9	9.0	6.6
$\Delta\phi$	7.3	5.3	4.3	3.3	2.3
P_t^{out}	14.4	10.8	8.8	6.9	4.8
$P_t^{\lvert\eta\rvert>4.2}$	1.9	1.9	1.9	2.0	2.0
$(P_t^{\gamma}-P_t^{part})/P_t^{\gamma}$	0.0401	0.0184	0.0097	0.0050	0.0016
$(P_t^{J}-P_t^{part})/P_t^{J}$	-0.0394	-0.0308	-0.0248	-0.0200	-0.0166
$(P_t^{\gamma}-P_t^{J})/P_t^{\gamma}$	0.0703	0.0442	0.0313	0.0225	0.0164
$P_t(O{+}\eta{>}4.2)/P_t^{\gamma}$	0.0541	0.0362	0.0262	0.0196	0.0150
$1-cos(\Delta\phi)$	0.0162	0.0081	0.0051	0.0029	0.0013
$\sigma(Db[\gamma,J])$	0.1563	0.1197	0.0975	0.0786	0.0583
$\sigma(Db[\gamma,part])$	0.1897	0.1483	0.1232	0.1020	0.0795
Entries	15055	12012	9997	7546	4068

*Number of events (Nevent) is given in this and in the following tables for integrated luminosity $L_{int} = 300\ pb^{-1}$

Table 4: Selection 1. $\phi_{(\gamma,jet)} = 180^\circ \pm 17^\circ$. UA1 algorithm. $L_{int} = 300\ pb^{-1}$.

P_{tCUT}^{clust}	30	20	15	10	5
Nevent	2414	2055	1751	1327	681
P_t56	14.7	12.5	11.0	9.1	6.8
$\Delta\phi$	5.4	4.7	4.2	3.4	2.3
${P_t}^{out}$	12.5	10.4	8.9	7.0	4.9
${P_t}^{\lvert\eta\rvert>4.2}$	1.9	1.9	2.0	2.0	2.0
$({P_t}^{\gamma}{-}{P_t}^{part})/{P_t}^{\gamma}$	0.0328	0.0184	0.0118	0.0067	0.0038
$({P_t}^{J}{-}{P_t}^{part})/{P_t}^{J}$	-0.0411	-0.0310	-0.0244	-0.0192	-0.0151
$({P_t}^{\gamma} - {P_t}^{J})/{P_t}^{\gamma}$	0.0642	0.0440	0.0325	0.0233	0.0171
$P_t(O{+}\eta{>}4.2)/{P_t}^{\gamma}$	0.0570	0.0382	0.0279	0.0203	0.0156
$1 - cos(\Delta\phi)$	0.0073	0.0058	0.0046	0.0030	0.0014
$\sigma(Db[\gamma, J])$	0.1518	0.1207	0.1015	0.0812	0.0624
$\sigma(Db[\gamma, part])$	0.1789	0.1467	0.1268	0.1048	0.0843
Entries	13641	11613	9892	7495	3845

Table 5: Selection 1. $\phi_{(\gamma,jet)} = 180^\circ \pm 17^\circ$. UA2 algorithm. $L_{int} = 300\ pb^{-1}$.

P_{tCUT}^{clust}	30	20	15	10	5
Nevent	1747	1521	1334	1070	664
P_t56	13.4	11.3	10.0	8.6	7.1
$\Delta\phi$	4.9	4.3	3.7	3.0	2.4
${P_t}^{out}$	10.6	8.9	7.7	6.4	5.0
${P_t}^{\lvert\eta\rvert>4.2}$	2.0	2.0	2.0	2.0	2.0
$({P_t}^{\gamma}{-}{P_t}^{part})/{P_t}^{\gamma}$	0.0143	0.0055	0.0023	0.0021	0.0030
$({P_t}^{J}{-}{P_t}^{part})/{P_t}^{J}$	-0.0203	-0.0193	-0.0186	-0.0157	-0.0142
$({P_t}^{\gamma} - {P_t}^{J})/{P_t}^{\gamma}$	0.0308	0.0217	0.0182	0.0156	0.0157
$P_t(O{+}\eta{>}4.2)/{P_t}^{\gamma}$	0.0244	0.0168	0.0145	0.0130	0.0140
$1 - cos(\Delta\phi)$	0.0063	0.0049	0.0037	0.0025	0.0016
$\sigma(Db[\gamma, J])$	0.1302	0.1044	0.0901	0.0763	0.0625
$\sigma(Db[\gamma, part])$	0.1573	0.1261	0.1071	0.0977	0.0867
Entries	9869	8595	7535	6045	3749

Table 6: Selection 1. $\phi_{(\gamma,jet)} = 180^\circ \pm 17^\circ$. LUCELL algorithm. $L_{int} = 300\ pb^{-1}$.

P_{tCUT}^{clust}	30	20	15	10	5
Nevent	2385	2055	1749	1334	720
P_t56	14.5	12.3	10.8	9.0	6.6
$\Delta\phi$	5.3	4.7	4.1	3.3	2.3
${P_t}^{out}$	12.1	10.1	8.6	6.9	4.8
${P_t}^{\lvert\eta\rvert>4.2}$	1.9	1.9	2.0	2.0	2.0
$({P_t}^{\gamma}{-}{P_t}^{part})/{P_t}^{\gamma}$	0.0285	0.0157	0.0091	0.0049	0.0016
$({P_t}^{J}{-}{P_t}^{part})/{P_t}^{J}$	-0.0361	-0.0297	-0.0246	-0.0200	-0.0166
$({P_t}^{\gamma} - {P_t}^{J})/{P_t}^{\gamma}$	0.0573	0.0408	0.0305	0.0224	0.0164
$P_t(O{+}\eta{>}4.2)/{P_t}^{\gamma}$	0.0502	0.0350	0.0260	0.0196	0.0150
$1 - cos(\Delta\phi)$	0.0072	0.0058	0.0045	0.0029	0.0013
$\sigma(Db[\gamma, J])$	0.1456	0.1158	0.0968	0.0785	0.0583
$\sigma(Db[\gamma, part])$	0.1761	0.1438	0.1224	0.1019	0.0795
Entries	13477	11613	9884	7539	4068

Table 7: Selection 1. $\phi_{(\gamma,jet)} = 180^\circ \pm 11^\circ$. UA1 algorithm. $L_{int} = 300\ pb^{-1}$.

P_{tCUT}^{clust}	30	20	15	10	5
Nevent	2102	1874	1649	1301	678
P_t56	13.4	11.7	10.5	9.0	6.8
$\Delta\phi$	4.1	3.9	3.6	3.2	2.3
${P_t}^{out}$	10.9	9.3	8.2	6.8	4.9
${P_t}^{\lvert\eta\rvert>4.2}$	1.9	1.9	1.9	2.0	2.0
$({P_t}^{\gamma}-{P_t}^{part})/{P_t}^{\gamma}$	0.0264	0.0155	0.0101	0.0065	0.0034
$({P_t}^{J}-{P_t}^{part})/{P_t}^{J}$	-0.0377	-0.0295	-0.0231	-0.0184	-0.0150
$({P_t}^{\gamma}-{P_t}^{J})/{P_t}^{\gamma}$	0.0554	0.0399	0.0298	0.0223	0.0166
$P_t(O{+}\eta{>}4.2)/{P_t}^{\gamma}$	0.0514	0.0363	0.0266	0.0198	0.0152
$1-cos(\Delta\phi)$	0.0040	0.0036	0.0032	0.0025	0.0013
$\sigma(Db[\gamma,J])$	0.1446	0.1174	0.0991	0.0805	0.0621
$\sigma(Db[\gamma,part])$	0.1674	0.1403	0.1234	0.1047	0.0841
Entries	11874	10587	9319	7352	3830

Table 8: Selection 1. $\phi_{(\gamma,jet)} = 180^\circ \pm 11^\circ$. UA2 algorithm. $L_{int} = 300\ pb^{-1}$.

P_{tCUT}^{clust}	30	20	15	10	5
Nevent	1556	1416	1287	1054	660
P_t56	12.1	10.7	9.7	8.5	7.0
$\Delta\phi$	3.8	3.6	3.4	2.9	2.3
${P_t}^{out}$	9.2	8.1	7.3	6.2	4.9
${P_t}^{\lvert\eta\rvert>4.2}$	2.0	2.0	2.0	2.0	2.0
$({P_t}^{\gamma}-{P_t}^{part})/{P_t}^{\gamma}$	0.0092	0.0038	0.0021	0.0017	0.0022
$({P_t}^{J}-{P_t}^{part})/{P_t}^{J}$	-0.0197	-0.0181	-0.0176	-0.0157	-0.0144
$({P_t}^{\gamma}-{P_t}^{J})/{P_t}^{\gamma}$	0.0252	0.0190	0.0172	0.0151	0.0151
$P_t(O{+}\eta{>}4.2)/{P_t}^{\gamma}$	0.0216	0.0158	0.0144	0.0129	0.0136
$1-cos(\Delta\phi)$	0.0035	0.0032	0.0028	0.0021	0.0014
$\sigma(Db[\gamma,J])$	0.1249	0.1019	0.0893	0.0759	0.0620
$\sigma(Db[\gamma,part])$	0.1467	0.1221	0.1069	0.0972	0.0858
Entries	8794	8003	7271	5955	3728

Table 9: Selection 1. $\phi_{(\gamma,jet)} = 180^\circ \pm 11^\circ$. LUCELL algorithm. $L_{int} = 300\ pb^{-1}$.

P_{tCUT}^{clust}	30	20	15	10	5
Nevent	2081	1876	1657	1311	719
P_t56	13.2	11.5	10.3	8.8	6.6
$\Delta\phi$	4.1	3.9	3.6	3.1	2.3
${P_t}^{out}$	10.5	9.1	8.0	6.7	4.8
${P_t}^{\lvert\eta\rvert>4.2}$	1.9	1.9	1.9	2.0	2.0
$({P_t}^{\gamma}-{P_t}^{part})/{P_t}^{\gamma}$	0.0224	0.0131	0.0077	0.0048	0.0015
$({P_t}^{J}-{P_t}^{part})/{P_t}^{J}$	-0.0329	-0.0281	-0.0235	-0.0194	-0.0166
$({P_t}^{\gamma}-{P_t}^{J})/{P_t}^{\gamma}$	0.0489	0.0370	0.0283	0.0218	0.0163
$P_t(O{+}\eta{>}4.2)/{P_t}^{\gamma}$	0.0449	0.0334	0.0251	0.0193	0.0149
$1-cos(\Delta\phi)$	0.0040	0.0036	0.0032	0.0024	0.0013
$\sigma(Db[\gamma,J])$	0.1377	0.1118	0.0951	0.0780	0.0582
$\sigma(Db[\gamma,part])$	0.1646	0.1371	0.1192	0.1016	0.0794
Entries	11760	10597	9359	7407	4064

Table 10: Selection 1. $\phi_{(\gamma,jet)} = 180^\circ \pm 6^\circ$. UA1 algorithm. $L_{int} = 300\ pb^{-1}$.

P_{tCUT}^{clust}	30	20	15	10	5
Nevent	1478	1371	1263	1077	637
P_t56	11.1	10.0	9.1	8.0	6.4
$\Delta\phi$	2.4	2.4	2.3	2.2	1.9
P_t^{out}	8.6	7.5	6.7	5.8	4.5
$P_t^{\|\eta\|>4.2}$	1.9	1.9	1.9	2.0	2.0
$(P_t^\gamma - P_t^{part})/P_t^\gamma$	0.0180	0.0109	0.0069	0.0043	0.0021
$(P_t^J - P_t^{part})/P_t^J$	-0.0333	-0.0264	-0.0217	-0.0184	-0.0156
$(P_t^\gamma - P_t^J)/P_t^\gamma$	0.0440	0.0328	0.0254	0.0202	0.0159
$P_t(O{+}\eta{>}4.2)/P_t^\gamma$	0.0427	0.0315	0.0242	0.0190	0.0150
$1 - cos(\Delta\phi)$	0.0012	0.0012	0.0012	0.0011	0.0009
$\sigma(Db[\gamma, J])$	0.1325	0.1092	0.0927	0.0777	0.0611
$\sigma(Db[\gamma, part])$	0.1504	0.1294	0.1139	0.0989	0.0810
Entries	8351	7745	7134	6085	3598

Table 11: Selection 1. $\phi_{(\gamma,jet)} = 180^\circ \pm 6^\circ$. UA2 algorithm. $L_{int} = 300\ pb^{-1}$.

P_{tCUT}^{clust}	30	20	15	10	5
Nevent	1152	1087	1027	904	610
P_t56	10.1	9.1	8.5	7.7	6.5
$\Delta\phi$	2.3	2.3	2.2	2.1	1.9
P_t^{out}	7.3	6.5	6.0	5.4	4.5
$P_t^{\|\eta\|>4.2}$	2.0	2.0	2.0	2.0	2.0
$(P_t^\gamma - P_t^{part})/P_t^\gamma$	0.0050	0.0007	0.0006	0.0009	0.0014
$(P_t^J - P_t^{part})/P_t^J$	-0.0194	-0.0181	-0.0170	-0.0156	-0.0147
$(P_t^\gamma - P_t^J)/P_t^\gamma$	0.0208	0.0160	0.0152	0.0144	0.0146
$P_t(O{+}\eta{>}4.2)/P_t^\gamma$	0.0196	0.0148	0.0141	0.0134	0.0137
$1 - cos(\Delta\phi)$	0.0012	0.0012	0.0011	0.0010	0.0009
$\sigma(Db[\gamma, J])$	0.1131	0.0949	0.0837	0.0732	0.0604
$\sigma(Db[\gamma, part])$	0.1318	0.1127	0.1017	0.0928	0.0807
Entries	6507	6143	5804	5109	3448

Table 12: Selection 1. $\phi_{(\gamma,jet)} = 180^\circ \pm 6^\circ$. LUCELL algorithm. $L_{int} = 300\ pb^{-1}$.

P_{tCUT}^{clust}	30	20	15	10	5
Nevent	1468	1375	1275	1094	676
P_t56	10.9	9.8	8.9	7.9	6.3
$\Delta\phi$	2.4	2.4	2.3	2.2	2.0
P_t^{out}	8.2	7.2	6.5	5.7	4.5
$P_t^{\|\eta\|>4.2}$	1.9	1.9	1.9	1.9	1.9
$(P_t^\gamma - P_t^{part})/P_t^\gamma$	0.0150	0.0095	0.0057	0.0031	0.0009
$(P_t^J - P_t^{part})/P_t^J$	-0.0293	-0.0248	-0.0218	-0.0188	-0.0167
$(P_t^\gamma - P_t^J)/P_t^\gamma$	0.0390	0.0306	0.0247	0.0195	0.0157
$P_t(O{+}\eta{>}4.2)/P_t^\gamma$	0.0378	0.0294	0.0235	0.0184	0.0148
$1 - cos(\Delta\phi)$	0.0012	0.0012	0.0012	0.0011	0.0009
$\sigma(Db[\gamma, J])$	0.1250	0.1041	0.0890	0.0747	0.0577
$\sigma(Db[\gamma, part])$	0.1468	0.1267	0.1115	0.0959	0.0798
Entries	8295	7766	7201	6181	3822

Table 13: Selection 2. $\phi_{(\gamma,jet)} = 180^\circ \pm 17^\circ$. UA1 algorithm. $L_{int} = 300\ pb^{-1}$.

P_{tCUT}^{clust}	30	20	15	10	5
Nevent	1262	1152	1038	849	505
P_t56	12.7	11.3	10.1	8.7	6.7
$\Delta\phi$	4.7	4.3	3.9	3.2	2.3
${P_t}^{out}$	10.0	8.8	7.8	6.4	4.7
${P_t}^{\vert\eta\vert>4.2}$	2.0	2.0	2.0	2.0	2.0
$({P_t}^{\gamma}-{P_t}^{part})/{P_t}^{\gamma}$	-0.0056	-0.0074	-0.0080	-0.0055	-0.0007
$({P_t}^{J}-{P_t}^{part})/{P_t}^{J}$	-0.0126	-0.0135	-0.0137	-0.0120	-0.0124
$({P_t}^{\gamma}-{P_t}^{J})/{P_t}^{\gamma}$	0.0054	0.0042	0.0039	0.0049	0.0098
$P_t(O{+}\eta{>}4.2)/{P_t}^{\gamma}$	-0.0006	-0.0007	-0.0001	0.0022	0.0083
$1-cos(\Delta\phi)$	0.0060	0.0050	0.0040	0.0027	0.0014
$\sigma(Db[\gamma,J])$	0.1207	0.1012	0.0897	0.0743	0.0620
$\sigma(Db[\gamma,part])$	0.1442	0.1212	0.1083	0.0937	0.0806
Entries	7128	6507	5866	4794	2852

Table 14: Selection 2. $\phi_{(\gamma,jet)} = 180^\circ \pm 17^\circ$. UA2 algorithm. $L_{int} = 300\ pb^{-1}$.

P_{tCUT}^{clust}	30	20	15	10	5
Nevent	1208	1089	967	794	513
P_t56	12.4	10.8	9.5	8.3	6.8
$\Delta\phi$	4.7	4.1	3.6	3.0	2.4
${P_t}^{out}$	9.7	8.4	7.3	6.2	4.9
${P_t}^{\vert\eta\vert>4.2}$	2.0	2.0	2.0	2.0	2.0
$({P_t}^{\gamma}-{P_t}^{part})/{P_t}^{\gamma}$	-0.0069	-0.0072	-0.0079	-0.0053	-0.0007
$({P_t}^{J}-{P_t}^{part})/{P_t}^{J}$	-0.0155	-0.0168	-0.0170	-0.0153	-0.0141
$({P_t}^{\gamma}-{P_t}^{J})/{P_t}^{\gamma}$	0.0067	0.0073	0.0072	0.0081	0.0119
$P_t(O{+}\eta{>}4.2)/{P_t}^{\gamma}$	0.0008	0.0027	0.0037	0.0057	0.0102
$1-cos(\Delta\phi)$	0.0058	0.0046	0.0035	0.0024	0.0016
$\sigma(Db[\gamma,J])$	0.1173	0.0976	0.0854	0.0738	0.0620
$\sigma(Db[\gamma,part])$	0.1383	0.1124	0.0978	0.0885	0.0800
Entries	6826	6152	5463	4487	2899

Table 15: Selection 2. $\phi_{(\gamma,jet)} = 180^\circ \pm 17^\circ$. LUCELL algorithm. $L_{int} = 300\ pb^{-1}$.

P_{tCUT}^{clust}	30	20	15	10	5
Nevent	1301	1187	1058	855	513
P_t56	12.7	11.1	9.9	8.4	6.3
$\Delta\phi$	4.8	4.3	3.8	3.1	2.2
${P_t}^{out}$	10.1	8.8	7.8	6.3	4.6
${P_t}^{\vert\eta\vert>4.2}$	2.0	2.0	2.0	2.0	2.0
$({P_t}^{\gamma}-{P_t}^{part})/{P_t}^{\gamma}$	-0.0079	-0.0089	-0.0092	-0.0068	-0.0029
$({P_t}^{J}-{P_t}^{part})/{P_t}^{J}$	-0.0168	-0.0182	-0.0177	-0.0158	-0.0144
$({P_t}^{\gamma}-{P_t}^{J})/{P_t}^{\gamma}$	0.0071	0.0071	0.0066	0.0071	0.0095
$P_t(O{+}\eta{>}4.2)/{P_t}^{\gamma}$	0.0010	0.0021	0.0026	0.0045	0.0081
$1-cos(\Delta\phi)$	0.0061	0.0050	0.0040	0.0026	0.0013
$\sigma(Db[\gamma,J])$	0.1213	0.1015	0.0883	0.0736	0.0582
$\sigma(Db[\gamma,part])$	0.1431	0.1183	0.1039	0.0882	0.0755
Entries	7350	6708	5980	4832	2896

Table 16: Selection 3. $\phi_{(\gamma,jet)} = 180^\circ \pm 17^\circ$. UA1 algorithm. $L_{int} = 300\ pb^{-1}$.

P_{tCUT}^{clust}	30	20	15	10	5
Nevent	925	829	729	588	326
$P_t 56$	12.2	10.5	9.2	7.9	5.8
$\Delta\phi$	4.6	4.1	3.5	2.8	2.0
${P_t}^{out}$	9.6	8.3	7.1	5.8	4.2
${P_t}^{\vert\eta\vert>4.2}$	2.0	2.0	2.0	2.0	2.0
$({P_t}^{\gamma}-{P_t}^{part})/{P_t}^{\gamma}$	-0.0110	-0.0093	-0.0104	-0.0086	-0.0034
$({P_t}^{J}-{P_t}^{part})/{P_t}^{J}$	-0.0139	-0.0150	-0.0152	-0.0134	-0.0131
$({P_t}^{\gamma} - {P_t}^{J})/{P_t}^{\gamma}$	0.0012	0.0037	0.0028	0.0030	0.0078
$P_t(O{+}\eta{>}4.2)/{P_t}^{\gamma}$	-0.0047	-0.0009	-0.0005	0.0008	0.0067
$1 - cos(\Delta\phi)$	0.0058	0.0046	0.0033	0.0022	0.0011
$\sigma(Db[\gamma, J])$	0.1158	0.0951	0.0826	0.0700	0.0563
$\sigma(Db[\gamma, part])$	0.1341	0.1085	0.0932	0.0825	0.0689
Entries	5226	4683	4118	3323	1841

Table 17: Selection 3. $\phi_{(\gamma,jet)} = 180^\circ \pm 17^\circ$. UA2 algorithm. $L_{int} = 300\ pb^{-1}$.

P_{tCUT}^{clust}	30	20	15	10	5
Nevent	925	829	729	588	326
$P_t 56$	12.2	10.5	9.2	7.9	5.8
$\Delta\phi$	4.6	4.1	3.5	2.8	2.0
${P_t}^{out}$	9.6	8.3	7.1	5.8	4.2
${P_t}^{\vert\eta\vert>4.2}$	2.0	2.0	2.0	2.0	2.0
$({P_t}^{\gamma}-{P_t}^{part})/{P_t}^{\gamma}$	-0.0110	-0.0093	-0.0104	-0.0086	-0.0034
$({P_t}^{J}-{P_t}^{part})/{P_t}^{J}$	-0.0162	-0.0172	-0.0173	-0.0155	-0.0158
$({P_t}^{\gamma} - {P_t}^{J})/{P_t}^{\gamma}$	0.0033	0.0057	0.0048	0.0050	0.0103
$P_t(O{+}\eta{>}4.2)/{P_t}^{\gamma}$	-0.0025	0.0011	0.0015	0.0028	0.0091
$1 - cos(\Delta\phi)$	0.0058	0.0046	0.0033	0.0021	0.0011
$\sigma(Db[\gamma, J])$	0.1163	0.0955	0.0830	0.0704	0.0572
$\sigma(Db[\gamma, part])$	0.1341	0.1085	0.0932	0.0825	0.0689
Entries	5226	4683	4118	3323	1841

Table 18: Selection 3. $\phi_{(\gamma,jet)} = 180^\circ \pm 17^\circ$. LUCELL algorithm. $L_{int} = 300\ pb^{-1}$.

P_{tCUT}^{clust}	30	20	15	10	5
Nevent	925	829	729	588	326
$P_t 56$	12.2	10.5	9.2	7.9	5.8
$\Delta\phi$	4.6	4.1	3.5	2.8	2.0
${P_t}^{out}$	9.7	8.3	7.2	5.9	4.2
${P_t}^{\vert\eta\vert>4.2}$	2.0	2.0	2.0	2.0	2.0
$({P_t}^{\gamma}-{P_t}^{part})/{P_t}^{\gamma}$	-0.0110	-0.0093	-0.0104	-0.0086	-0.0034
$({P_t}^{J}-{P_t}^{part})/{P_t}^{J}$	-0.0160	-0.0172	-0.0173	-0.0152	-0.0147
$({P_t}^{\gamma} - {P_t}^{J})/{P_t}^{\gamma}$	0.0031	0.0057	0.0048	0.0047	0.0092
$P_t(O{+}\eta{>}4.2)/{P_t}^{\gamma}$	-0.0027	0.0010	0.0014	0.0025	0.0081
$1 - cos(\Delta\phi)$	0.0058	0.0046	0.0034	0.0022	0.0011
$\sigma(Db[\gamma, J])$	0.1162	0.0956	0.0832	0.0707	0.0568
$\sigma(Db[\gamma, part])$	0.1341	0.1085	0.0932	0.0825	0.0689
Entries	5226	4683	4118	3323	1841

Appendix 5 $90 < P_t^{\gamma} < 140\ GeV/c$

$P_t^{isol} < 4\ GeV/c, \quad \epsilon^{\gamma} < 7\%$

Table 1: Selection 1. $\phi_{(\gamma,jet)} = 180° \pm 180°$. UA1 algorithm. $L_{int} = 300\ pb^{-1}$.

P_{tCUT}^{clust}	30	20	15	10	5
Nevent*	1290	1052	887	669	333
P_t56	15.9	12.9	11.2	9.4	7.0
$\Delta\phi$	5.1	3.8	3.2	2.5	1.8
P_t^{out}	14.2	10.8	9.0	7.1	5.0
$P_t^{\|\eta\|>4.2}$	1.9	1.9	1.9	1.9	1.9
$(P_t^{\gamma}-P_t^{part})/P_t^{\gamma}$	0.0132	0.0049	0.0015	0.0007	0.0003
$(P_t^{J}-P_t^{part})/P_t^{J}$	-0.0405	-0.0279	-0.0221	-0.0160	-0.0121
$(P_t^{\gamma}-P_t^{J})/P_t^{\gamma}$	0.0461	0.0292	0.0214	0.0153	0.0112
$P_t(O{+}\eta{>}4.2)/P_t^{\gamma}$	0.0381	0.0249	0.0185	0.0135	0.0103
$1-cos(\Delta\phi)$	0.0080	0.0043	0.0029	0.0018	0.0009
$\sigma(Db[\gamma,J])^{**}$	0.1212	0.0904	0.0756	0.0605	0.0479
$\sigma(Db[\gamma,part])^{***}$	0.1425	0.1118	0.0984	0.0861	0.0677
Entries	27785	22651	19106	14415	7163

Table 2: Selection 1. $\phi_{(\gamma,jet)} = 180° \pm 180°$. UA2 algorithm. $L_{int} = 300\ pb^{-1}$.

P_{tCUT}^{clust}	30	20	15	10	5
Nevent	870	744	652	526	326
P_t56	13.9	11.5	10.2	8.9	7.4
$\Delta\phi$	4.2	3.3	2.8	2.3	1.8
P_t^{out}	11.4	9.1	7.7	6.4	5.0
$P_t^{\|\eta\|>4.2}$	1.9	1.9	1.9	1.9	1.9
$(P_t^{\gamma}-P_t^{part})/P_t^{\gamma}$	-0.0008	-0.0054	-0.0054	-0.0038	-0.0004
$(P_t^{J}-P_t^{part})/P_t^{J}$	-0.0202	-0.0177	-0.0155	-0.0127	-0.0110
$(P_t^{\gamma}-P_t^{J})/P_t^{\gamma}$	0.0169	0.0105	0.0086	0.0078	0.0093
$P_t(O{+}\eta{>}4.2)/P_t^{\gamma}$	0.0116	0.0073	0.0064	0.0063	0.0084
$1-cos(\Delta\phi)$	0.0054	0.0032	0.0022	0.0015	0.0009
$\sigma(Db[\gamma,J])$	0.0988	0.0776	0.0662	0.0558	0.0482
$\sigma(Db[\gamma,part])$	0.1192	0.0946	0.0838	0.0759	0.0694
Entries	18745	16027	14039	11326	7012

Table 3: Selection 1. $\phi_{(\gamma,jet)} = 180° \pm 180°$. LUCELL algorithm. $L_{int} = 300\ pb^{-1}$.

P_{tCUT}^{clust}	30	20	15	10	5
Nevent	1276	1047	886	672	351
P_t56	15.7	12.7	11.1	9.2	6.8
$\Delta\phi$	5.0	3.8	3.2	2.5	1.7
P_t^{out}	13.8	10.6	8.8	7.0	4.9
$P_t^{\|\eta\|>4.2}$	1.9	1.9	1.9	1.9	1.9
$(P_t^{\gamma}-P_t^{part})/P_t^{\gamma}$	0.0120	0.0037	0.0015	0.0002	-0.0001
$(P_t^{J}-P_t^{part})/P_t^{J}$	-0.0360	-0.0264	-0.0213	-0.0163	-0.0137
$(P_t^{\gamma}-P_t^{J})/P_t^{\gamma}$	0.0421	0.0270	0.0208	0.0153	0.0127
$P_t(O{+}\eta{>}4.2)/P_t^{\gamma}$	0.0346	0.0229	0.0181	0.0137	0.0119
$1-cos(\Delta\phi)$	0.0076	0.0042	0.0028	0.0017	0.0008
$\sigma(Db[\gamma,J])$	0.1160	0.0871	0.0729	0.0581	0.0441
$\sigma(Db[\gamma,part])$	0.1407	0.1101	0.0975	0.0832	0.0643
Entries	27477	22549	19087	14466	7552

*Number of events (Nevent) is given in this and in the following tables for integrated luminosity $L_{int} = 300\ pb^{-1}$.

Table 4: Selection 1. $\phi_{(\gamma,jet)} = 180^{\circ} \pm 17^{\circ}$. UA1 algorithm. $L_{int} = 300\ pb^{-1}$.

P_{tCUT}^{clust}	30	20	15	10	5
Nevent	1242	1043	885	669	333
P_t56	15.0	12.7	11.2	9.4	7.0
$\Delta\phi$	4.5	3.7	3.2	2.5	1.8
${P_t}^{out}$	13.2	10.6	9.0	7.1	5.0
${P_t}^{\|\eta\|>4.2}$	1.9	1.9	1.9	1.9	1.9
$({P_t}^{\gamma}{-}{P_t}^{part})/{P_t}^{\gamma}$	0.0102	0.0045	0.0014	0.0007	0.0003
$({P_t}^{J}{-}{P_t}^{part})/{P_t}^{J}$	-0.0382	-0.0276	-0.0221	-0.0160	-0.0121
$({P_t}^{\gamma} - {P_t}^{J})/{P_t}^{\gamma}$	0.0417	0.0286	0.0213	0.0153	0.0112
$P_t(O{+}\eta{>}4.2)/{P_t}^{\gamma}$	0.0363	0.0248	0.0185	0.0136	0.0103
$1 - cos(\Delta\phi)$	0.0054	0.0038	0.0028	0.0018	0.0009
$\sigma(Db[\gamma, J])$	0.1154	0.0896	0.0753	0.0605	0.0479
$\sigma(Db[\gamma, part])$	0.1359	0.1111	0.0981	0.0861	0.0677
Entries	26759	22471	19068	14411	7163

Table 5: Selection 1. $\phi_{(\gamma,jet)} = 180^{\circ} \pm 17^{\circ}$. UA2 algorithm. $L_{int} = 300\ pb^{-1}$.

P_{tCUT}^{clust}	30	20	15	10	5
Nevent	855	742	651	526	325
P_t56	13.5	11.4	10.2	8.8	7.3
$\Delta\phi$	3.9	3.3	2.8	2.3	1.8
${P_t}^{out}$	11.0	9.0	7.7	6.4	5.0
${P_t}^{\|\eta\|>4.2}$	1.9	1.9	1.9	1.9	1.9
$({P_t}^{\gamma}{-}{P_t}^{part})/{P_t}^{\gamma}$	-0.0018	-0.0056	-0.0054	-0.0038	-0.0005
$({P_t}^{J}{-}{P_t}^{part})/{P_t}^{J}$	-0.0194	-0.0176	-0.0154	-0.0127	-0.0110
$({P_t}^{\gamma} - {P_t}^{J})/{P_t}^{\gamma}$	0.0153	0.0102	0.0085	0.0077	0.0092
$P_t(O{+}\eta{>}4.2)/{P_t}^{\gamma}$	0.0110	0.0072	0.0064	0.0062	0.0083
$1 - cos(\Delta\phi)$	0.0043	0.0030	0.0022	0.0015	0.0009
$\sigma(Db[\gamma, J])$	0.0969	0.0772	0.0661	0.0556	0.0478
$\sigma(Db[\gamma, part])$	0.1169	0.0943	0.0837	0.0758	0.0691
Entries	18409	15973	14025	11321	7010

Table 6: Selection 1. $\phi_{(\gamma,jet)} = 180^{\circ} \pm 17^{\circ}$. LUCELL algorithm. $L_{int} = 300\ pb^{-1}$.

P_{tCUT}^{clust}	30	20	15	10	5
Nevent	1233	1039	885	671	351
P_t56	15.0	12.6	11.1	9.2	6.8
$\Delta\phi$	4.4	3.7	3.1	2.5	1.7
${P_t}^{out}$	12.9	10.4	8.8	7.0	4.9
${P_t}^{\|\eta\|>4.2}$	1.9	1.9	1.9	1.9	1.9
$({P_t}^{\gamma}{-}{P_t}^{part})/{P_t}^{\gamma}$	0.0097	0.0034	0.0014	0.0002	-0.0001
$({P_t}^{J}{-}{P_t}^{part})/{P_t}^{J}$	-0.0345	-0.0263	-0.0212	-0.0163	-0.0137
$({P_t}^{\gamma} - {P_t}^{J})/{P_t}^{\gamma}$	0.0388	0.0266	0.0207	0.0153	0.0127
$P_t(O{+}\eta{>}4.2)/{P_t}^{\gamma}$	0.0335	0.0229	0.0181	0.0137	0.0119
$1 - cos(\Delta\phi)$	0.0053	0.0038	0.0027	0.0017	0.0008
$\sigma(Db[\gamma, J])$	0.1120	0.0866	0.0727	0.0581	0.0441
$\sigma(Db[\gamma, part])$	0.1353	0.1095	0.0975	0.0832	0.0643
Entries	26568	22389	19060	14464	7552

Table 7: Selection 1. $\phi_{(\gamma,jet)} = 180^{\circ} \pm 11^{\circ}$. UA1 algorithm. $L_{int} = 300\ pb^{-1}$.

P_{tCUT}^{clust}	30	20	15	10	5
Nevent	1137	998	868	666	332
P_t56	13.9	12.2	11.0	9.3	7.0
$\Delta\phi$	3.6	3.3	3.0	2.5	1.8
${P_t}^{out}$	11.7	9.9	8.7	7.0	4.9
${P_t}^{\|\eta\|>4.2}$	1.9	1.9	1.9	1.9	1.9
$({P_t}^{\gamma} - {P_t}^{part})/{P_t}^{\gamma}$	0.0084	0.0040	0.0012	0.0006	0.0002
$({P_t}^{J} - {P_t}^{part})/{P_t}^{J}$	-0.0349	-0.0262	-0.0213	-0.0159	-0.0119
$({P_t}^{\gamma} - {P_t}^{J})/{P_t}^{\gamma}$	0.0375	0.0269	0.0205	0.0152	0.0110
$P_t(O{+}\eta{>}4.2)/{P_t}^{\gamma}$	0.0343	0.0242	0.0182	0.0135	0.0102
$1 - cos(\Delta\phi)$	0.0033	0.0027	0.0023	0.0016	0.0008
$\sigma(Db[\gamma, J])$	0.1098	0.0878	0.0744	0.0600	0.0469
$\sigma(Db[\gamma, part])$	0.1291	0.1083	0.0967	0.0855	0.0676
Entries	24490	21499	18687	14340	7153

Table 8: Selection 1. $\phi_{(\gamma,jet)} = 180^{\circ} \pm 11^{\circ}$. UA2 algorithm. $L_{int} = 300\ pb^{-1}$.

P_{tCUT}^{clust}	30	20	15	10	5
Nevent	804	723	644	524	325
P_t56	12.7	11.1	10.1	8.8	7.3
$\Delta\phi$	3.3	3.0	2.7	2.3	1.8
${P_t}^{out}$	10.0	8.6	7.5	6.3	4.9
${P_t}^{\|\eta\|>4.2}$	1.9	1.9	1.9	1.9	1.9
$({P_t}^{\gamma} - {P_t}^{part})/{P_t}^{\gamma}$	-0.0027	-0.0060	-0.0056	-0.0039	-0.0007
$({P_t}^{J} - {P_t}^{part})/{P_t}^{J}$	-0.0184	-0.0171	-0.0152	-0.0126	-0.0108
$({P_t}^{\gamma} - {P_t}^{J})/{P_t}^{\gamma}$	0.0136	0.0094	0.0081	0.0076	0.0090
$P_t(O{+}\eta{>}4.2)/{P_t}^{\gamma}$	0.0108	0.0070	0.0062	0.0062	0.0082
$1 - cos(\Delta\phi)$	0.0028	0.0024	0.0019	0.0014	0.0009
$\sigma(Db[\gamma, J])$	0.0941	0.0759	0.0654	0.0550	0.0469
$\sigma(Db[\gamma, part])$	0.1132	0.0921	0.0829	0.0757	0.0690
Entries	17310	15572	13870	11288	7002

Table 9: Selection 1. $\phi_{(\gamma,jet)} = 180^{\circ} \pm 11^{\circ}$. LUCELL algorithm. $L_{int} = 300\ pb^{-1}$.

P_{tCUT}^{clust}	30	20	15	10	5
Nevent	1130	996	867	668	351
P_t56	13.9	12.1	10.8	9.1	6.8
$\Delta\phi$	3.6	3.3	2.9	2.4	1.7
${P_t}^{out}$	11.5	9.8	8.5	6.9	4.9
${P_t}^{\|\eta\|>4.2}$	1.9	1.9	1.9	1.9	1.9
$({P_t}^{\gamma} - {P_t}^{part})/{P_t}^{\gamma}$	0.0085	0.0028	0.0011	0.0002	-0.0001
$({P_t}^{J} - {P_t}^{part})/{P_t}^{J}$	-0.0316	-0.0253	-0.0209	-0.0162	-0.0137
$({P_t}^{\gamma} - {P_t}^{J})/{P_t}^{\gamma}$	0.0353	0.0252	0.0201	0.0152	0.0127
$P_t(O{+}\eta{>}4.2)/{P_t}^{\gamma}$	0.0322	0.0226	0.0179	0.0137	0.0119
$1 - cos(\Delta\phi)$	0.0032	0.0027	0.0022	0.0016	0.0008
$\sigma(Db[\gamma, J])$	0.1072	0.0850	0.0721	0.0580	0.0441
$\sigma(Db[\gamma, part])$	0.1297	0.1065	0.0956	0.0826	0.0643
Entries	24339	21461	18682	14386	7552

Table 10: Selection 1. $\phi_{(\gamma,jet)} = 180^\circ \pm 6^\circ$. UA1 algorithm. $L_{int} = 300\ pb^{-1}$.

P_{tCUT}^{clust}	30	20	15	10	5
Nevent	866	803	734	603	323
P_t56	11.9	10.8	9.9	8.7	6.8
$\Delta\phi$	2.2	2.2	2.1	2.0	1.6
${P_t}^{out}$	9.3	8.2	7.3	6.3	4.7
${P_t}^{\vert\eta\vert>4.2}$	1.9	1.9	1.9	1.9	1.9
$({P_t}^{\gamma}-{P_t}^{part})/{P_t}^{\gamma}$	0.0055	0.0020	0.0000	-0.0002	-0.0002
$({P_t}^{J}-{P_t}^{part})/{P_t}^{J}$	-0.0287	-0.0235	-0.0198	-0.0155	-0.0117
$({P_t}^{\gamma}-{P_t}^{J})/{P_t}^{\gamma}$	0.0298	0.0226	0.0178	0.0140	0.0104
$P_t(O{+}\eta{>}4.2)/{P_t}^{\gamma}$	0.0287	0.0215	0.0168	0.0131	0.0098
$1-cos(\Delta\phi)$	0.0011	0.0011	0.0010	0.0009	0.0006
$\sigma(Db[\gamma,J])$	0.1000	0.0826	0.0710	0.0585	0.0460
$\sigma(Db[\gamma,part])$	0.1175	0.1013	0.0921	0.0815	0.0673
Entries	18665	17291	15805	12980	6962

Table 11: Selection 1. $\phi_{(\gamma,jet)} = 180^\circ \pm 6^\circ$. UA2 algorithm. $L_{int} = 300\ pb^{-1}$.

P_{tCUT}^{clust}	30	20	15	10	5
Nevent	645	605	565	485	315
P_t56	10.9	9.9	9.2	8.3	7.1
$\Delta\phi$	2.2	2.1	2.0	1.9	1.6
${P_t}^{out}$	8.0	7.1	6.5	5.7	4.7
${P_t}^{\vert\eta\vert>4.2}$	1.9	1.9	1.9	1.9	1.9
$({P_t}^{\gamma}-{P_t}^{part})/{P_t}^{\gamma}$	-0.0039	-0.0056	-0.0053	-0.0042	-0.0012
$({P_t}^{J}-{P_t}^{part})/{P_t}^{J}$	-0.0160	-0.0152	-0.0138	-0.0125	-0.0108
$({P_t}^{\gamma}-{P_t}^{J})/{P_t}^{\gamma}$	0.0102	0.0080	0.0072	0.0071	0.0085
$P_t(O{+}\eta{>}4.2)/{P_t}^{\gamma}$	0.0091	0.0070	0.0062	0.0062	0.0078
$1-cos(\Delta\phi)$	0.0011	0.0010	0.0010	0.0009	0.0007
$\sigma(Db[\gamma,J])$	0.0863	0.0717	0.0628	0.0535	0.0461
$\sigma(Db[\gamma,part])$	0.1027	0.0880	0.0805	0.0731	0.0688
Entries	13899	13030	12174	10453	6796

Table 12: Selection 1. $\phi_{(\gamma,jet)} = 180^\circ \pm 6^\circ$. LUCELL algorithm. $L_{int} = 300\ pb^{-1}$.

P_{tCUT}^{clust}	30	20	15	10	5
Nevent	865	804	737	610	343
P_t56	11.9	10.7	9.8	8.6	6.7
$\Delta\phi$	2.2	2.2	2.1	2.0	1.6
${P_t}^{out}$	9.1	8.0	7.2	6.2	4.7
${P_t}^{\vert\eta\vert>4.2}$	1.9	1.9	1.9	1.9	1.9
$({P_t}^{\gamma}-{P_t}^{part})/{P_t}^{\gamma}$	0.0051	0.0012	-0.0001	-0.0004	-0.0003
$({P_t}^{J}-{P_t}^{part})/{P_t}^{J}$	-0.0270	-0.0232	-0.0197	-0.0161	-0.0138
$({P_t}^{\gamma}-{P_t}^{J})/{P_t}^{\gamma}$	0.0285	0.0219	0.0179	0.0145	0.0125
$P_t(O{+}\eta{>}4.2)/{P_t}^{\gamma}$	0.0274	0.0208	0.0169	0.0137	0.0119
$1-cos(\Delta\phi)$	0.0011	0.0011	0.0010	0.0009	0.0006
$\sigma(Db[\gamma,J])$	0.0971	0.0804	0.0694	0.0570	0.0436
$\sigma(Db[\gamma,part])$	0.1166	0.0998	0.0912	0.0792	0.0631
Entries	18638	17312	15884	13147	7380

Table 13: Selection 2. $\phi_{(\gamma,jet)} = 180^\circ \pm 17^\circ$. UA1 algorithm. $L_{int} = 300\ pb^{-1}$.

P_{tCUT}^{clust}	30	20	15	10	5
Nevent	797	711	632	511	288
P_t56	13.4	11.6	10.4	8.9	6.9
$\Delta\phi$	4.0	3.4	2.9	2.4	1.8
${P_t}^{out}$	10.9	9.2	8.0	6.6	4.8
${P_t}^{\lvert\eta\rvert>4.2}$	1.9	1.9	1.9	1.9	1.9
$({P_t}^{\gamma}{-}{P_t}^{part})/{P_t}^{\gamma}$	-0.0100	-0.0101	-0.0092	-0.0062	-0.0018
$({P_t}^{J}{-}{P_t}^{part})/{P_t}^{J}$	-0.0160	-0.0149	-0.0137	-0.0118	-0.0105
$({P_t}^{\gamma} - {P_t}^{J})/{P_t}^{\gamma}$	0.0045	0.0036	0.0034	0.0047	0.0077
$P_t(O{+}\eta{>}4.2)/{P_t}^{\gamma}$	0.0000	0.0004	0.0010	0.0031	0.0069
$1 - cos(\Delta\phi)$	0.0045	0.0033	0.0024	0.0016	0.0008
$\sigma(Db[\gamma, J])$	0.0934	0.0764	0.0668	0.0552	0.0456
$\sigma(Db[\gamma, part])$	0.1145	0.0956	0.0872	0.0763	0.0624
Entries	17161	15309	13613	11009	6200

Table 14: Selection 2. $\phi_{(\gamma,jet)} = 180^\circ \pm 17^\circ$. UA2 algorithm. $L_{int} = 300\ pb^{-1}$.

P_{tCUT}^{clust}	30	20	15	10	5
Nevent	685	605	537	439	278
P_t56	12.8	11.0	9.8	8.4	7.0
$\Delta\phi$	3.8	3.2	2.8	2.3	1.8
${P_t}^{out}$	10.4	8.7	7.5	6.2	4.9
${P_t}^{\lvert\eta\rvert>4.2}$	1.9	1.9	1.9	1.9	1.9
$({P_t}^{\gamma}{-}{P_t}^{part})/{P_t}^{\gamma}$	-0.0106	-0.0115	-0.0102	-0.0077	-0.0030
$({P_t}^{J}{-}{P_t}^{part})/{P_t}^{J}$	-0.0170	-0.0163	-0.0152	-0.0133	-0.0118
$({P_t}^{\gamma} - {P_t}^{J})/{P_t}^{\gamma}$	0.0048	0.0035	0.0039	0.0046	0.0078
$P_t(O{+}\eta{>}4.2)/{P_t}^{\gamma}$	0.0008	0.0006	0.0018	0.0031	0.0069
$1 - cos(\Delta\phi)$	0.0041	0.0029	0.0021	0.0014	0.0009
$\sigma(Db[\gamma, J])$	0.0903	0.0736	0.0639	0.0535	0.0458
$\sigma(Db[\gamma, part])$	0.1065	0.0870	0.0772	0.0679	0.0612
Entries	14745	13038	11563	9455	5994

Table 15: Selection 2. $\phi_{(\gamma,jet)} = 180^\circ \pm 17^\circ$. LUCELL algorithm. $L_{int} = 300\ pb^{-1}$.

P_{tCUT}^{clust}	30	20	15	10	5
Nevent	815	723	640	517	299
P_t56	13.4	11.5	10.3	8.6	6.6
$\Delta\phi$	4.0	3.4	2.9	2.4	1.7
${P_t}^{out}$	11.0	9.2	8.0	6.5	4.7
${P_t}^{\lvert\eta\rvert>4.2}$	1.9	1.9	1.9	1.9	1.9
$({P_t}^{\gamma}{-}{P_t}^{part})/{P_t}^{\gamma}$	-0.0102	-0.0101	-0.0089	-0.0071	-0.0033
$({P_t}^{J}{-}{P_t}^{part})/{P_t}^{J}$	-0.0187	-0.0173	-0.0158	-0.0145	-0.0129
$({P_t}^{\gamma} - {P_t}^{J})/{P_t}^{\gamma}$	0.0069	0.0058	0.0057	0.0065	0.0087
$P_t(O{+}\eta{>}4.2)/{P_t}^{\gamma}$	0.0024	0.0026	0.0034	0.0049	0.0079
$1 - cos(\Delta\phi)$	0.0045	0.0032	0.0024	0.0016	0.0008
$\sigma(Db[\gamma, J])$	0.0936	0.0764	0.0663	0.0547	0.0426
$\sigma(Db[\gamma, part])$	0.1124	0.0939	0.0852	0.0729	0.0587
Entries	17549	15576	13794	11135	6435

Table 16: Selection 3. $\phi_{(\gamma,jet)} = 180^\circ \pm 17^\circ$. UA1 algorithm. $L_{int} = 300\ pb^{-1}$.

P_{tCUT}^{clust}	30	20	15	10	5
Nevent	553	486	427	338	183
P_t56	12.6	10.7	9.4	7.9	6.0
$\Delta\phi$	3.8	3.2	2.7	2.2	1.5
${P_t}^{out}$	10.3	8.5	7.3	5.9	4.1
${P_t}^{\vert\eta\vert>4.2}$	1.9	1.9	1.9	1.9	1.9
$({P_t}^{\gamma} - {P_t}^{part})/{P_t}^{\gamma}$	-0.0130	-0.0134	-0.0121	-0.0088	-0.0042
$({P_t}^{J} - {P_t}^{part})/{P_t}^{J}$	-0.0165	-0.0160	-0.0146	-0.0128	-0.0111
$({P_t}^{\gamma} - {P_t}^{J})/{P_t}^{\gamma}$	0.0023	0.0015	0.0016	0.0033	0.0062
$P_t(O{+}\eta{>}4.2)/{P_t}^{\gamma}$	-0.0018	-0.0013	-0.0004	0.0020	0.0056
$1 - cos(\Delta\phi)$	0.0041	0.0028	0.0020	0.0013	0.0006
$\sigma(Db[\gamma, J])$	0.0875	0.0715	0.0617	0.0502	0.0386
$\sigma(Db[\gamma, part])$	0.1029	0.0815	0.0715	0.0607	0.0479
Entries	11922	10474	9200	7290	3938

Table 17: Selection 3. $\phi_{(\gamma,jet)} = 180^\circ \pm 17^\circ$. UA2 algorithm. $L_{int} = 300\ pb^{-1}$.

P_{tCUT}^{clust}	30	20	15	10	5
Nevent	553	486	427	338	183
P_t56	12.6	10.7	9.4	7.9	6.0
$\Delta\phi$	3.7	3.1	2.7	2.2	1.5
${P_t}^{out}$	10.3	8.5	7.3	5.9	4.2
${P_t}^{\vert\eta\vert>4.2}$	1.9	1.9	1.9	1.9	1.9
$({P_t}^{\gamma} - {P_t}^{part})/{P_t}^{\gamma}$	-0.0130	-0.0134	-0.0121	-0.0088	-0.0042
$({P_t}^{J} - {P_t}^{part})/{P_t}^{J}$	-0.0170	-0.0165	-0.0151	-0.0132	-0.0119
$({P_t}^{\gamma} - {P_t}^{J})/{P_t}^{\gamma}$	0.0027	0.0019	0.0020	0.0036	0.0069
$P_t(O{+}\eta{>}4.2)/{P_t}^{\gamma}$	-0.0013	-0.0009	0.0000	0.0023	0.0063
$1 - cos(\Delta\phi)$	0.0041	0.0028	0.0020	0.0013	0.0006
$\sigma(Db[\gamma, J])$	0.0881	0.0719	0.0621	0.0504	0.0389
$\sigma(Db[\gamma, part])$	0.1029	0.0815	0.0715	0.0607	0.0479
Entries	11922	10474	9200	7290	3938

Table 18: Selection 3. $\phi_{(\gamma,jet)} = 180^\circ \pm 17^\circ$. LUCELL algorithm. $L_{int} = 300\ pb^{-1}$.

P_{tCUT}^{clust}	30	20	15	10	5
Nevent	553	486	427	338	183
P_t56	12.6	10.7	9.4	7.9	6.0
$\Delta\phi$	3.8	3.2	2.7	2.2	1.5
${P_t}^{out}$	10.3	8.6	7.3	5.9	4.2
${P_t}^{\vert\eta\vert>4.2}$	1.9	1.9	1.9	1.9	1.9
$({P_t}^{\gamma} - {P_t}^{part})/{P_t}^{\gamma}$	-0.0130	-0.0134	-0.0121	-0.0088	-0.0042
$({P_t}^{J} - {P_t}^{part})/{P_t}^{J}$	-0.0184	-0.0176	-0.0162	-0.0143	-0.0125
$({P_t}^{\gamma} - {P_t}^{J})/{P_t}^{\gamma}$	0.0040	0.0030	0.0031	0.0047	0.0075
$P_t(O{+}\eta{>}4.2)/{P_t}^{\gamma}$	0.0000	0.0002	0.0011	0.0034	0.0068
$1 - cos(\Delta\phi)$	0.0041	0.0028	0.0020	0.0013	0.0006
$\sigma(Db[\gamma, J])$	0.0880	0.0717	0.0620	0.0505	0.0389
$\sigma(Db[\gamma, part])$	0.1029	0.0815	0.0715	0.0607	0.0479
Entries	11922	10474	9200	7290	3938

Appendix 6

$$\hat{p}_{\perp}^{\,min} = 40\ GeV/c$$
$$P_t^{\,isol} < 2\ GeV/c, \quad \epsilon^{\tilde{\gamma}} < 5\%, \quad \Delta\phi = 17^{\circ} \quad \text{(Selection 1)}$$

Table 1: Number of signal and background events (per $L_{int} = 300\ pb^{-1}$) selected with cuts 1–10 of Table 13.

$P_{t\ cut}^{\,clust}$ (GeV/c)	$P_{t\ cut}^{\,out}$ (GeV/c) 5	10	15	20	30	1000
5	40000	59000	62000	62000	62000	62000
10	50000	96000	112000	115000	115000	115000
15	52000	105000	132000	141000	143000	143000
20	53000	107000	139000	153000	158000	159000
30	53000	109000	143000	159000	170000	173000

Table 2: S/B.

$P_{t\ cut}^{\,clust}$ (GeV/c)	$P_{t\ cut}^{\,out}$ (GeV/c) 5	10	15	20	30	1000
5	4.3± 0.3	4.1± 0.3	4.1± 0.3	4.0± 0.3	4.0± 0.3	4.0± 0.3
10	3.9± 0.3	3.5± 0.2	3.3± 0.2	3.3± 0.1	3.2± 0.1	3.2± 0.1
15	3.8± 0.3	3.2± 0.2	2.9± 0.1	2.8± 0.1	2.8± 0.1	2.8± 0.1
20	3.7± 0.3	3.1± 0.1	2.7± 0.1	2.7± 0.1	2.6± 0.1	2.6± 0.1
30	3.7± 0.2	3.0± 0.1	2.6± 0.1	2.5± 0.1	2.5± 0.1	2.5± 0.1

Table 3: $\langle F \rangle,\ F = (P_t^{\,\tilde{\gamma}} - P_t^{\,Jet})/P_t^{\,\tilde{\gamma}}$.

$P_{t\ cut}^{\,clust}$ (GeV/c)	$P_{t\ cut}^{\,out}$ (GeV/c) 5	10	15	20	30	1000
5	0.012	0.020	0.023	0.023	0.023	0.023
10	0.011	0.024	0.032	0.034	0.035	0.035
15	0.011	0.025	0.035	0.040	0.042	0.043
20	0.011	0.025	0.036	0.041	0.046	0.046
30	0.011	0.025	0.035	0.042	0.047	0.049

Table 4: $\sigma(F),\ F = (P_t^{\,\tilde{\gamma}} - P_t^{\,Jet})/P_t^{\,\tilde{\gamma}}$.

$P_{t\ cut}^{\,clust}$ (GeV/c)	$P_{t\ cut}^{\,out}$ (GeV/c) 5	10	15	20	30	1000
5	0.053	0.070	0.074	0.074	0.075	0.076
10	0.054	0.080	0.095	0.099	0.101	0.102
15	0.055	0.082	0.104	0.115	0.121	0.121
20	0.055	0.083	0.108	0.123	0.135	0.137
30	0.055	0.083	0.109	0.127	0.150	0.159

$$\hat{p}_{\perp}^{\,min} = 70\ GeV/c$$
$$P_t^{\,isol} < 2\ GeV/c, \quad \epsilon^{\tilde{\gamma}} < 5\%, \quad \Delta\phi = 17^{\circ} \quad \text{(Selection 1)}$$

Table 5: Number of signal and background events (per $L_{int} = 300\ pb^{-1}$) selected with cuts 1–10 of Table 13.

$P_{t\ cut}^{\,clust}$ (GeV/c)	$P_{t\ cut}^{\,out}$ (GeV/c): 5	10	15	20	30	1000
5	2900	4500	4700	4700	4700	4700
10	3600	7100	8500	8900	9000	9000
15	3800	7700	10100	11200	11800	11800
20	3800	7900	10600	12300	13600	13700
30	3800	8000	10900	12900	15400	16000

Table 6: S/B.

$P_{t\ cut}^{\,clust}$ (GeV/c)	$P_{t\ cut}^{\,out}$ (GeV/c): 5	10	15	20	30	1000
5	12.6± 1.3	12.1± 1.0	12.1± 1.0	12.0± 1.0	12.0± 1.0	12.0± 1.0
10	11.1± 1.0	9.8± 0.6	9.3± 0.5	9.0± 0.5	9.0± 0.5	8.9± 0.5
15	11.0± 1.0	9.1± 0.5	8.2± 0.4	7.8± 0.4	7.5± 0.3	7.5± 0.3
20	10.4± 0.9	8.7± 0.5	7.6± 0.4	7.2± 0.3	6.6± 0.3	6.6± 0.3
30	10.4± 0.9	8.4± 0.5	7.1± 0.3	6.6± 0.3	5.8± 0.2	5.6± 0.2

Table 7: $\langle F \rangle,\ F = (P_t^{\tilde{\gamma}} - P_t^{\,Jet})/P_t^{\tilde{\gamma}}$.

$P_{t\ cut}^{\,clust}$ (GeV/c)	$P_{t\ cut}^{\,out}$ (GeV/c): 5	10	15	20	30	1000
5	0.008	0.014	0.016	0.016	0.016	0.016
10	0.008	0.015	0.020	0.023	0.024	0.024
15	0.008	0.015	0.022	0.027	0.031	0.031
20	0.007	0.014	0.022	0.028	0.037	0.039
30	0.007	0.014	0.022	0.029	0.043	0.052

Table 8: $\sigma(F),\ F = (P_t^{\tilde{\gamma}} - P_t^{\,Jet})/P_t^{\tilde{\gamma}}$.

$P_{t\ cut}^{\,clust}$ (GeV/c)	$P_{t\ cut}^{\,out}$ (GeV/c): 5	10	15	20	30	1000
5	0.031	0.042	0.045	0.046	0.046	0.046
10	0.032	0.048	0.058	0.062	0.064	0.064
15	0.032	0.049	0.063	0.072	0.078	0.078
20	0.032	0.050	0.065	0.078	0.089	0.090
30	0.032	0.050	0.066	0.080	0.099	0.102

$$\hat{p}_{\perp}^{\,min} = 100\ GeV/c$$

$$P_t^{\,isol} < 2\ GeV/c, \quad \epsilon^{\tilde{\gamma}} < 5\%, \quad \Delta\phi = 17^{\circ} \quad \text{(Selection 1)}$$

Table 9: Number of signal and background events (per $L_{int} = 300\ pb^{-1}$) selected with cuts 1–10 of Table 13.

$P_{t\ cut}^{\ clust}$	$P_{t\ cut}^{\ out}$ (GeV/c)					
(GeV/c)	5	10	15	20	30	1000
5	510	820	870	870	870	870
10	630	1270	1560	1630	1650	1650
15	650	1380	1830	2050	2150	2150
20	660	1410	1930	2260	2520	2560
30	670	1430	1970	2370	2870	3060

Table 10: S/B.

$P_{t\ cut}^{\ clust}$	$P_{t\ cut}^{\ out}$ (GeV/c)					
(GeV/c)	5	10	15	20	30	1000
5	24.5± 3.1	23.7± 2.3	23.1± 2.2	23.0± 2.2	23.0± 2.2	23.0± 2.2
10	25.3± 2.9	20.6± 1.5	18.9± 1.2	18.3± 1.2	17.9± 1.1	17.9± 1.1
15	23.3± 2.6	18.4± 1.3	16.2± 0.9	15.4± 0.8	14.5± 0.7	14.4± 0.7
20	22.3± 2.4	17.1± 1.1	14.8± 0.8	13.5± 0.6	12.2± 0.5	11.9± 0.5
30	22.1± 2.3	16.8± 1.1	14.2± 0.7	12.5± 0.6	10.6± 0.4	9.8± 0.4

Table 11: $\langle F\rangle,\ F = (P_t^{\,\tilde{\gamma}} – P_t^{\,Jet})/P_t^{\,\tilde{\gamma}}$.

(GeV/c)	5	10	15	20	30	1000
5	0.007	0.012	0.013	0.013	0.013	0.013
10	0.007	0.012	0.017	0.018	0.019	0.019
15	0.007	0.012	0.017	0.021	0.024	0.024
20	0.007	0.012	0.017	0.022	0.027	0.029
30	0.007	0.012	0.017	0.022	0.030	0.038

Table 12: $\sigma(F),\ F = (P_t^{\,\tilde{\gamma}} – P_t^{\,Jet})/P_t^{\,\tilde{\gamma}}$.

$P_{t\ cut}^{\ clust}$	$P_{t\ cut}^{\ out}$ (GeV/c)					
(GeV/c)	5	10	15	20	30	1000
5	0.022	0.031	0.034	0.034	0.034	0.034
10	0.023	0.035	0.042	0.044	0.045	0.045
15	0.023	0.035	0.045	0.052	0.055	0.055
20	0.023	0.036	0.046	0.055	0.061	0.061
30	0.023	0.036	0.047	0.057	0.066	0.067

$$\hat{p}_{\perp}^{min} = 40 \ GeV/c$$

$$P_t^{isol} < 2 \ GeV/c, \quad \epsilon^{\tilde{\gamma}} < 5\%, \quad \Delta\phi = 17^{\circ}, \quad \epsilon^{jet} < 3\% \quad \text{(Selection 2)}$$

Table 13: Number of signal and background events (per $L_{int} = 300 \ pb^{-1}$) selected with cuts 1–10 of Table 13.

$P_{t\ cut}^{clust}$ (GeV/c)	$P_{t\ cut}^{out}$ (GeV/c) 5	10	15	20	30	1000
5	23000	33000	34000	34000	34000	34000
10	27000	47000	53000	54000	54000	54000
15	28000	50000	60000	63000	63000	63000
20	28000	51000	62000	66000	68000	68000
30	28000	51000	63000	68000	72000	73000

Table 14: S/B.

$P_{t\ cut}^{clust}$ (GeV/c)	$P_{t\ cut}^{out}$ (GeV/c) 5	10	15	20	30	1000
5	4.4± 0.5	4.6± 0.4	4.6± 0.4	4.6± 0.4	4.6± 0.4	4.6± 0.4
10	4.5± 0.4	4.5± 0.3	4.4± 0.3	4.3± 0.3	4.3± 0.3	4.3± 0.3
15	4.4± 0.4	4.2± 0.3	3.8± 0.2	3.7± 0.2	3.7± 0.2	3.7± 0.2
20	4.3± 0.4	4.2± 0.3	3.7± 0.2	3.6± 0.2	3.5± 0.2	3.5± 0.2
30	4.3± 0.4	4.0± 0.3	3.6± 0.2	3.5± 0.2	3.3± 0.2	3.3± 0.2

Table 15: $\langle F \rangle, \ F = (P_t^{\tilde{\gamma}} – P_t^{Jet})/P_t^{\tilde{\gamma}}$.

$P_{t\ cut}^{clust}$ (GeV/c)	$P_{t\ cut}^{out}$ (GeV/c) 5	10	15	20	30	1000
5	0.006	0.008	0.008	0.008	0.008	0.008
10	0.006	0.005	0.004	0.003	0.003	0.003
15	0.006	0.006	0.003	0.003	0.001	0.001
20	0.006	0.006	0.003	0.000	-0.002	-0.003
30	0.006	0.006	0.003	0.001	-0.005	-0.006

Table 16: $\sigma(F), \ F = (P_t^{\tilde{\gamma}} – P_t^{Jet})/P_t^{\tilde{\gamma}}$.

$P_{t\ cut}^{clust}$ (GeV/c)	$P_{t\ cut}^{out}$ (GeV/c) 5	10	15	20	30	1000
5	0.050	0.066	0.069	0.069	0.069	0.069
10	0.052	0.074	0.086	0.089	0.090	0.090
15	0.051	0.075	0.095	0.102	0.107	0.107
20	0.052	0.075	0.097	0.109	0.120	0.123
30	0.052	0.075	0.098	0.113	0.136	0.147

$$\hat{p}_{\perp}^{\,min} = 70\ GeV/c$$

$$P_t^{\,isol} < 2\ GeV/c, \quad \epsilon^{\tilde{\gamma}} < 5\%, \quad \Delta\phi = 17^{\circ}, \quad \epsilon^{jet} < 3\% \ \ \text{(Selection 2)}$$

Table 17: Number of signal and background events (per $L_{int} = 300\ pb^{-1}$) selected with cuts 1–10 of Table 13.

$P_{t\ cut}^{\ clust}$ (GeV/c)	$P_{t\ cut}^{\ out}$ (GeV/c) 5	10	15	20	30	1000
5	2300	3400	3600	3600	3600	3600
10	2800	5000	5800	6000	6000	6000
15	2900	5300	6700	7200	7400	7400
20	2900	5400	6900	7700	8200	8300
30	2900	5500	7000	8000	9000	9200

Table 18: S/B.

$P_{t\ cut}^{\ clust}$ (GeV/c)	$P_{t\ cut}^{\ out}$ (GeV/c) 5	10	15	20	30	1000
5	13.7± 1.7	13.7± 1.4	13.9± 1.4	13.9± 1.4	13.9± 1.4	13.9± 1.4
10	12.5± 1.3	11.4± 0.9	10.7± 0.8	10.4± 0.7	10.4± 0.7	10.4± 0.7
15	12.6± 1.3	10.7± 0.8	9.7± 0.6	9.2± 0.6	8.9± 0.5	8.9± 0.5
20	12.2± 1.3	10.4± 0.8	9.2± 0.6	8.6± 0.5	8.1± 0.4	8.0± 0.4
30	12.2± 1.3	10.3± 0.7	8.9± 0.5	8.2± 0.4	7.3± 0.4	7.1± 0.3

Table 19: $\langle F\rangle,\ F = (P_t^{\tilde{\gamma}} - P_t^{\,Jet})/P_t^{\tilde{\gamma}}$.

$P_{t\ cut}^{\ clust}$ (GeV/c)	$P_{t\ cut}^{\ out}$ (GeV/c) 5	10	15	20	30	1000
5	0.006	0.009	0.009	0.009	0.009	0.009
10	0.006	0.007	0.008	0.009	0.009	0.009
15	0.005	0.007	0.009	0.009	0.009	0.009
20	0.005	0.006	0.008	0.009	0.010	0.010
30	0.005	0.006	0.008	0.009	0.010	0.010

Table 20: $\sigma(F),\ F = (P_t^{\tilde{\gamma}} - P_t^{\,Jet})/P_t^{\tilde{\gamma}}$.

$P_{t\ cut}^{\ clust}$ (GeV/c)	$P_{t\ cut}^{\ out}$ (GeV/c) 5	10	15	20	30	1000
5	0.031	0.040	0.043	0.043	0.043	0.043
10	0.031	0.046	0.054	0.057	0.058	0.058
15	0.031	0.047	0.059	0.066	0.069	0.069
20	0.031	0.047	0.060	0.071	0.078	0.078
30	0.032	0.047	0.061	0.073	0.086	0.088

$$\hat{p}_{\perp}^{min} = 100\ GeV/c$$

$$P_t^{isol} < 2\ GeV/c,\quad \epsilon^{\tilde{\gamma}} < 5\%,\quad \Delta\phi = 17^{\circ},\ \epsilon^{jet} < 3\%\ \ \text{(Selection 2)}$$

Table 21: Number of signal and background events (per $L_{int} = 300\ pb^{-1}$) selected with cuts 1–10 of Table 13.

$P_{t\ cut}^{clust}$ (GeV/c)	$P_{t\ cut}^{out}$ (GeV/c)					
	5	10	15	20	30	1000
5	460	720	760	760	760	760
10	560	1060	1250	1300	1300	1300
15	580	1130	1440	1570	1620	1620
20	580	1150	1490	1700	1830	1840
30	580	1160	1520	1750	2020	2090

Table 22: S/B.

$P_{t\ cut}^{clust}$ (GeV/c)	$P_{t\ cut}^{out}$ (GeV/c)					
	5	10	15	20	30	1000
5	27.7± 3.9	25.3± 2.7	24.9± 2.6	25.0± 2.6	25.0± 2.6	25.0± 2.6
10	29.9± 3.9	22.9± 1.9	20.8± 1.6	20.4± 1.5	20.3± 1.5	20.2± 1.5
15	28.4± 3.6	21.0± 1.7	17.7± 1.2	17.2± 1.1	16.5± 1.0	16.4± 1.0
20	27.6± 3.4	20.0± 1.6	16.6± 1.1	15.5± 0.9	14.3± 0.8	14.1± 0.8
30	27.1± 3.3	19.5± 1.5	16.0± 1.0	14.6± 0.8	12.5± 0.6	12.0± 0.6

Table 23: $\langle F \rangle,\ F = (P_t^{\tilde{\gamma}} - P_t^{Jet})/P_t^{\tilde{\gamma}}$.

(GeV/c)	5	10	15	20	30	1000
5	0.006	0.009	0.010	0.010	0.010	0.010
10	0.006	0.009	0.010	0.011	0.011	0.011
15	0.006	0.008	0.010	0.011	0.011	0.011
20	0.006	0.008	0.010	0.010	0.011	0.011
30	0.006	0.008	0.009	0.010	0.011	0.011

Table 24: $\sigma(F),\ F = (P_t^{\tilde{\gamma}} - P_t^{Jet})/P_t^{\tilde{\gamma}}$.

$P_{t\ cut}^{clust}$ (GeV/c)	$P_{t\ cut}^{out}$ (GeV/c)					
	5	10	15	20	30	1000
5	0.022	0.030	0.032	0.032	0.033	0.033
10	0.023	0.033	0.040	0.042	0.042	0.042
15	0.023	0.034	0.043	0.048	0.050	0.050
20	0.023	0.035	0.044	0.051	0.056	0.056
30	0.023	0.035	0.044	0.053	0.060	0.060

“$\gamma + Jet$” process application for setting the absolute scale of jet energy and determining the gluon distribution at the Tevatron Run II.

D.V. Bandurin, N.B. Skachkov

Laboratory of Nuclear Problems
Joint Institute for Nuclear Research, Dubna, Russia

D0 Note 3948

Abstract

We study the effect of application of new set of cuts, proposed in our previous works, on the improvement of accuracy of the jet energy calibration with “$p\bar{p} \to \gamma + Jet + X$” process at Tevatron. Monte Carlo events produced by the PYTHIA 5.7 generator are used for this aim. The selection criteria for “$\gamma + Jet$” event samples that would provide a good balance of ${P_t}^{\gamma}$ with ${P_t}^{Jet}$ and would allow to reduce the background are described. The distributions of these events over ${P_t}^{\gamma}$ and η^{Jet} are presented. The features of “$\gamma + Jet$” events in the central calorimeter region of the D0 detector ($|\eta| < 0.7$) are exposed. The efficiency of the cuts used for background suppression is demonstrated.

It is shown that the samples of “$\gamma + Jet$” events, gained with the cuts for the jet energy calibration, may have enough statistics for determining the gluon distribution inside a proton in the region of $x \geq 10^{-3}$ and of Q^2 by one order higher than that studied at HERA.

Contents

1. INTRODUCTION.

Setting an absolute energy scale for a jet, detected mostly by hadronic and electromagnetic calorimeters (HCAL and ECAL), is an important task for any of $p\bar{p}$ and pp collider experiments (see e.g. [1–8]).

The main goal of this work is to find out the selection criteria for "$p\bar{p} \to \gamma + Jet + X$" events (we shall use in what follows the abreviation "$\gamma + Jet$" for them) that would lead to the most precise determination of the transverse momentum of a jet (i.e. ${P_t}^{Jet}$) via assigning a photon ${P_t}^{\gamma}$ to a signal produced by a jet. Our study is based on the "$\gamma + Jet$" events generated by using PYTHIA 5.7 [9]. Their analysis was done on the "particle level" (in the terminology of [1]), i.e. without inclusion of the detector effects. The information provided by this generator is analyzed to track starting from the parton level (where parton-photon balance is supposed to take place in a case of initial state radiation absence) all possible sources that may lead to the ${P_t}^{\gamma} - {P_t}^{Jet}$ disbalance in a final state. We use here the methods applied in [10]–[18] (see also [19]) and [20], [21] for analogous task at LHC energy. The corresponding cuts on physical variables, introduced in [10]–[17], are applied here. Their efficiency is estimated at the particle level of simulation at Tevatron energy with account of D0 geometry. The results of further analysis of "$\gamma + Jet$" events planned to be done at the level of the full event reconstruction after the detector responce simulation with GEANT-3 [22] based package D0GSTAR [23] will be presented in our following publications.

We consider here the case of the Tevatron Run II luminosity $L = 10^{32}\ cm^{-2}s^{-1}$. It will be shown below that its value is quite sufficient for selecting the event samples of large enough volume for application of much more restrictive cuts as well as of new physical variables introduced in [10]–[17]. Our aim is to select the samples of topologically clean "$\gamma + Jet$" events with a good balance of ${P_t}^{\gamma}$ and ${P_t}^{Jet}$ and to use them for further modeling of the jet energy calibration procedure within D0GSTAR. In this way one can estimate a jet energy calibration accuracy that can be achieved with the proposed cuts in the experiment.

Section 2 is a short introduction into the physics connected with the discussed problem. General features of "$\gamma + Jet$" processes at Tevatron energy are presented here. We review the possible sources of the ${P_t}^{\gamma}$ and ${P_t}^{Jet}$ disbalance and the ways of selecting those events where this disbalance has a minimal value on the particle level.

In Section 3.1 the definitions are given for the transverse momenta of different physical objects that we have introduced as a part of "$\gamma + Jet$" production event and that we suppose to be important for studying the physics connected with a jet calibration procedure. These values of transverse momenta enter into the P_t-balance equation that reflects the total P_t conservation law for the $p\bar{p}$-collision event as a whole.

Section 3.2 describes the criteria we have chosen to select "$\gamma + Jet$" events for the jet energy calibration procedure. The "cluster" (or mini–jet) suppression criterion (P_{tCUT}^{clust}) which was formulated in an evident form in our previous publications [10]–[18] is used here [1]. (Its important role for selection of events with a good balance of ${P_t}^{\gamma}$ and ${P_t}^{Jet}$ will be illustrated in Sections 5–8.) [2] These clusters have a physical meaning of a part of another new experimentally measurable quantity, introduced in [10]–[18] for the first time, namely, the sum of $\vec{P}_t$ of those particles that are *out* of the "$\gamma + Jet$" system (denoted as ${P_t}^{out}$) and are detectable in the whole

[1] We use here, as in [13]–[18], the LUCELL subroutine from PYTHIA as well as two jetfinders UA1 and UA2 from the CMS program of fast simulation CMSJET [24] for defining jets in an event.

[2] The analogous third jet cut thresholds E_T^3 (varying from 20 to 8 GeV) for improving a single jet energy resolution in di-jet events were used in [28].

pseudorapidity η region covered by the detector ($|\eta| < 4.2$ for D0). The vector and scalar forms of the total P_t balance equation, used for the $p\bar{p}-$event as a whole, are given in Sections 3.1 and 3.2 respectively.

Another new thing is a use of a new physical object, proposed also in [10]–[18] and named an "isolated jet". This jet is contained in the cone of radius $R = 0.7$ in the $\eta - \phi$ space and it does not have any noticeable P_t activity in some ring around. The width of this ring is taken to be of $\Delta R = 0.3$ (or approximately of the width of 3 calorimeter towers). In other words, we will select a class of events having a total P_t activity inside the ring around this "isolated jet" within $3 - 5\%$ of jet P_t. (It will be shown in Sections 6, 7 and Appendices 2–5 that the number of events with such a clean topological structure would not be small at Tevatron energy.)

Section 4 is devoted to the estimation of the size of the non-detectable neutrino contribution to ${P_t}^{Jet}$. The correlation of the upper cut value, imposed onto ${P_t}^{miss}$, with the mean value of P_t of neutrinos belonging to the jet P_t, i.e. $\langle P_{t(\nu)}^{Jet} \rangle$, is considered. The detailed results of this section are presented in the tables of Appendix 1. They also include the ratios of the gluonic events $qg \to q + \gamma$ containing the information about the gluon distribution inside a proton. In the same tables the expected number of events (at $L_{int} = 300\, pb^{-1}$) having charm (c) and beauty (b) quarks in the initial state of the gluonic subprocess are also given.

Since the jet energy calibration is rather a practical than an academic task, in all the following sections we present the rates obtained with the cuts varying from strict to weak because their choice would be a matter of step-by-step statistics collection during the data taking.

Section 5 includes the results of studying the dependence of the initial state radiation (ISR) P_t-spectrum on the cut imposed on the clusters P_t (P_{tCUT}^{clust}) and on the angle between the transverse momenta vectors of a jet and a photon. We also present the rates for four different types of "$\gamma + Jet$" events, in which jet fits completely in one definite region of the calorimeter: in Central Calorimeter (CC) with $|\eta| < 0.7$ or in Intercryostat Calorimeter (IC) with $0.7 < |\eta| < 1.8$ or in End Calorimeter (EC) with $1.8 < |\eta| < 2.5$ or, finally, in Forward Calorimeter (FC) with $2.5 < |\eta| < 4.2$.

Starting with Section 6 our analysis is concentrated on the "$\gamma + 1\ jet$" events having a jet entirely contained within the central calorimeter region. The dependence of spectra of different physical variables [3] (and among them those appearing in the P_t balance equation of event as a whole) on P_{tCUT}^{clust}, as well as the dependence on it of the spatial distribution of P_t activity inside a jet as well as outside it is shown in Figs. 8–11.

The dependence of the number of events (for $L_{int} = 300\ pb^{-1}$) on P_{tCUT}^{clust} as well as the dependence on it of the fractional $({P_t}^{\gamma} - {P_t}^{Jet})/{P_t}^{\gamma}$ disbalance is studied in Section 7. The details of this study are presented in the tables of Appendices 2–5 that together with the corresponding Figs. 12–18 can serve to justify the variables and cuts introduced in Section 3. Figs. 15–18 as well as Tables 13–18 of Appendices 2 – 5 demonstrate the influence of the jet isolation criterion. The impact of P_{tCUT}^{out} on the fractional $({P_t}^{\gamma} - {P_t}^{Jet})/{P_t}^{\gamma}$ disbalance is shown in Figs. 19 and 20.

In Section 8 we present the estimation of the efficiency of background suppression (that was one of the main guidelines to establish the selection rules proposed in Section 3) for different numerical values of cuts.

The importance of the simultaneous use of the above-mentioned new parameters P_{tCUT}^{clust} and P_{tCUT}^{out} and also of the "isolated jet" criterion for background suppression (as well as for improving the value of the ${P_t}^{\gamma}$ and ${P_t}^{Jet}$ balance) is demonstrated in Tables 14–17 of Section 8 as well as in the tables of Appendix 6 that show the dependence of selected events on P_{tCUT}^{clust}

[3] mostly those that have a strong influence on the ${P_t}^{\gamma} - {P_t}^{Jet}$ balance in an event.

and P_{tCUT}^{out} for various P_t^{γ} intervals. The tables of Appendix 6 include the fractional disbalance values $(P_t^{\gamma} - P_t^{Jet})/P_t^{\gamma}$ that are found with an additional (as compared with tables of Appendix 2–5) account of the P_t^{out} cut. In this sense the tables of Appendix 6 contain the final (and *first main*) result (as they include the background contribution) of our study of setting the absolute scale of the jet energy at the particle level defined by generation with PYTHIA.

In Section 9 we show the tables and some plots that demonstrate a possible influence of the intrinsic transverse parton momentum k_t parameter variation (including, as an illustration, some extreme k_t values) on the $P_t^{\gamma} - P_t^{Jet}$ disbalance.

Section 10 contains the *second main* result of our study of "$\gamma + Jet$" events at the Tevatron energy. Here we investigate the possibility of using the same sample of the topologically clean "$\gamma + Jet$" events, obtained with the described cuts, for determining the gluon distribution in a proton (as it was done earlier for LHC energy in [18], [19]). The kinematic plot presented here shows what a region of x and Q^2 variables (namely: $10^{-3} \leq x \leq 1.0$ and $1.6 \cdot 10^3 \leq Q^2 \leq 2 \cdot 10^4\ (GeV/c)^2$) can be covered at Tevatron energies, with a sufficient number of events for this aim. The comparison with the kinematic regions covered by other experiments where parton distributions were studied is also shown in the same plot (see Fig. 29).

About the Summary. We tried to write it in a way allowing a dedicated reader, who is interested in result rather than in method, to pass directly to it after this sentence.

Since the results presented here were obtained with the PYTHIA simulation, we are planning to carry out analogous estimations with another event generator like HERWIG, for example, in subsequent papers.

2. GENERALITIES OF THE "$\gamma + Jet$" PROCESS.

The useful variables are introduced for studying the effects of its on initial and final state radiation basing on the simulation in the framework of PYTHIA. Other effects of non-perturbative nature like primordial parton k_t effect, parton-to-jet hadronization that may lead to $P_t^{\gamma} - P_t^{Jet}$ disbalance within the physical models used in PYTHIA are also discussed.

2.1 Leading order picture.

The idea of absolute jet energy scale setting (and hadronic calorimeter (HCAL) calibration) by means of the physical process "$p\bar{p} \to \gamma + Jet + X$" was realized many times in different experiments (see [1–8] and references therein). It is based on the parton picture where two partons ($q\bar{q}$ or qg), supposed to be moving in different colliding nucleons with zero transverse momenta (with respect to the beam line), produce a photon called the "direct photon". This process is described by the leading order (LO) Feynman diagrams shown in Fig. 1 (for the explanation of the numeration of lines see Section 2.2) for the "Compton-like" subprocess (ISUB=29 in PYTHIA)

$$qg \to q + \gamma \qquad (1a)$$

and for the "annihilation" subprocess (ISUB=14)

$$q\overline{q} \to g + \gamma. \qquad (1b)$$

As the initial partons were supposed to have zero transverse momenta, P_t of the "γ+parton" system produced in the final state should be also equal to zero, i.e. one can write the following P_t balance equation for photon and final parton

$$\vec{P}_t^{\gamma+part} = \vec{P}_t^{\gamma} + \vec{P}_t^{part} = 0. \qquad (2)$$

Thus, one could expect that the transverse momentum of the jet produced by the final state parton (q or g), having $\vec{P_t}^{part} = -\vec{P_t}^{\gamma}$, will be close in magnitude, with a reasonable precision, to the transverse momentum of the final state photon, i.e. $\vec{P_t}^{Jet} \approx -\vec{P_t}^{\gamma}$.

It allows the absolute jet energy scale to be determined (and the HCAL to be calibrated) in the experiments with a well-calibrated electromagnetic calorimeter (ECAL). To put it simpler, one can assign to the part of the jet transverse energy E_t^{Jet} deposited in the HCAL the value of the difference between the values of the transverse energy deposited in the ECAL in the photon direction (i.e. E_t^{γ}) and the transverse energy deposited in the ECAL in the jet direction.

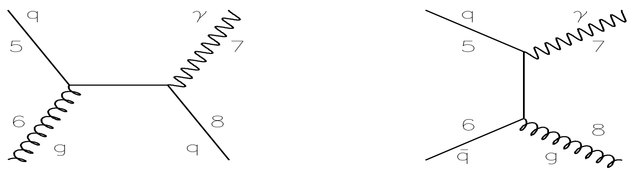

(a) (b)

Fig. 1: Some of the leading order Feynman diagrams for direct photon production.

2.2 Initial state radiation.

Since we believe in the perturbation theory, the leading order (LO) picture described above is expected to be dominant and to determine the main contribution to the cross section. The Next-to-Leading Order (NLO) approximation (see some of the NLO diagrams in Figs. 2 and 4) introduces some deviations from a rather straightforward LO-motivated idea of jet energy calibration. A gluon radiated in the initial state (ISR), as it is seen from Fig. 2, can have its own non-zero transverse momentum $P_t^{gluon} \equiv P_t^{ISR} \neq 0$. Apart of a problem of appearance of extra jets (or mini-jets and clusters), that will be discussed in what follows, it leads to the non-zero transverse momenta of partons that appear in the initial state of fundamental $2 \to 2$ QCD subprocesses (1a) and (1b). As a result of the transverse momentum conservation there arises a disbalance between the transverse momenta of a photon P_t^{γ} and of a parton P_t^{part} produced in the fundamental $2 \to 2$ process $5 + 6 \to 7 + 8$ shown in Fig. 2 (and in Fig. 3) and thus, finally, the disbalance between P_t^{γ} and P_t of a jet produced by this parton.

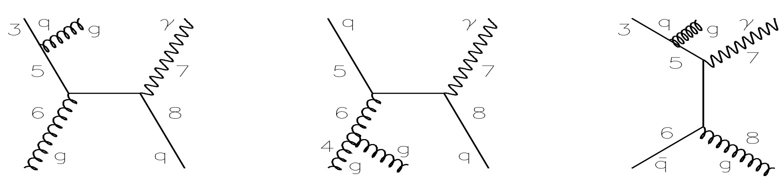

Fig. 2: Some of Feynman diagrams of direct photon production including gluon radiation in the initial state.

Following [13]–[17] and [25] we choose the modulus of the vector sum of the transverse momentum vectors $\vec{P_t}^5$ and $\vec{P_t}^6$ of the incoming into $2 \to 2$ fundamental QCD subprocesses $5 + 6 \to 7 + 8$ partons (lines 5 and 6 in Fig. 2) and the sum of their modulus as two quantitative measures

$$P_t^{5+6} = |\vec{P_t}^5 + \vec{P_t}^6|, \qquad P_t 56 = |P_t^5| + |P_t^6| \tag{3}$$

to estimate the P_t disbalance caused by ISR [4]. The modulus of the vector sum

$$P_t^{\gamma+Jet} = |\vec{P_t}^{\gamma} + \vec{P_t}^{Jet}| \tag{4}$$

[4]The variable P_t^{5+6} was used in analysis in [10]–[13].

was also used as an estimator of the final state P_t disbalance in the "$\gamma + Jet$" system in [13]–[17].

The numerical notations in the Feynman diagrams (shown in Figs. 1 and 2) and in formula (3) are chosen to be in correspondence with those used in the PYTHIA event listing for description of the parton–parton subprocess displayed schematically in Fig. 3. The "ISR" block describes the initial state radiation process that can take place before the fundamental hard $2 \to 2$ process.

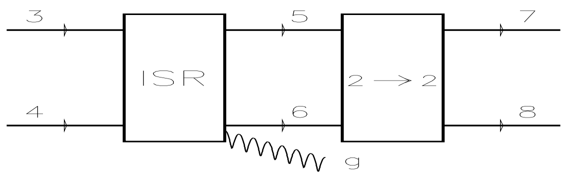

Fig. 3: PYTHIA "diagram" of $2 \to 2$ process (5+6→7+8) following the block (3+4→5+6) of initial state radiation (ISR), drawn here to illustrate the PYTHIA event listing information.

2.3 Final state radiation.

Let us consider fundamental subprocesses in which there is no initial state radiation but instead final state radiation (FSR) takes place. These subprocesses are described in the quantum field theory by the NLO diagrams like those shown in Fig. 4. It is clear that appearance of an extra gluon leg in the final state may lead to appearance of two (or more) jets or an intense jet and a weaker jet (mini-jet or cluster) in an event as it happens in the case of ISR described above. So, to suppress FSR (manifesting itself as some extra jets or clusters) the same tools as for reducing ISR should be used. But due to the string model of fragmentation used in PYTHIA it is much more difficult to deduce basing on the PYTHIA event listing information the variables (analogous to (3) and (4)) to describe the disbalance between P_t of a jet parent parton and P_t^{γ}. That is why, keeping in mind a close analogy of the physical pictures of ISR and FSR (see Figs. 2 and 4), we shall concentrate in the following sections on the initial state radiation supposing it to serve in some sense as a quantum field theory perturbative model of the final state radiation mechanism.

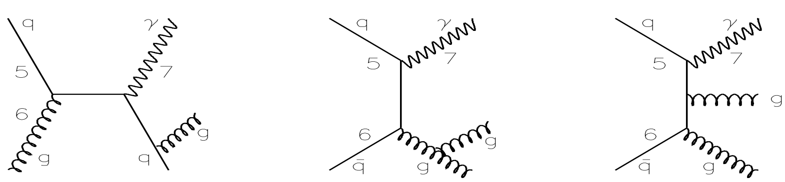

Fig. 4: Some of Feynman diagrams of direct photon production including gluon radiation in the final state.

2.4 Primordial parton k_t effect.

Now after considering the disbalance sources connected with the perturbative corrections to the leading order diagrams let us mention the physical effects of the non-perturbative nature. Thus, a possible non-zero value of the intrinsic transverse parton velocity inside a colliding proton may be another source of the P_t^{γ} and P_t^{part} disbalance in the final state. Nowadays this effect can be described mainly in the phenomenological way. Its reasonable value is supposed to lead to the value $k_t \leq 1.0\ GeV/c$. Sometimes in the literature the total effect of ISR and of the intrinsic parton transverse momentum is denoted by a common symbol "k_t". Here we follow the approach and the phenomenological model used in PYTHIA where these two sources of the P_t^{γ} and P_t^{Jet} disbalance, having different nature, perturbative and non-perturbative, can be switched on separately by different keys (MSTP(61) for ISR and PARP(91), PARP(93), MSTP(91) for

intrinsic parton transverse momentum k_t). In what follows we shall keep the value of k_t mainly to be fixed by the PYTHIA default value $\langle k_t \rangle = 0.44\ GeV/c$. The dependence of the disbalance between ${P_t}^{\gamma}$ and ${P_t}^{Jet}$ on possible variation of k_t will be discussed in detail in Section 9. The general conclusion from here is that any variation of k_t within reasonable boundaries (as well as slightly beyond them) does not produce a large effect in the case when the initial state radiation is switched on. The latter makes a dominant contribution.

2.5 Parton-to-jet hadronization.

Another non-perturbative effect that leads to the ${P_t}^{\gamma} - {P_t}^{Jet}$ disbalance is connected with hadronization (or fragmentation into hadrons) of the parton produced in the fundamental $2 \to 2$ subprocess into a jet. The hadronization of the parton into a jet is described in PYTHIA within the Lund string fragmentation model. The mean values of the fractional ${P_t}^{Jet} - {P_t}^{parton}$ disbalance will be presented in the tables of Appendices 2 – 5 for three different jetfinders. As it will be shown in Section 7 (see also tables of Appendices 2–5) the hadronization effect has approximately the contribution into ${P_t}^{\gamma} - {P_t}^{Jet}$ disbalance of the same size as that of ISR.

3. CHOICE OF MEASURABLE PHYSICAL VARIABLES FOR THE "$\gamma + Jet$" PROCESS AND THE CUTS FOR BACKGROUND REDUCTION.

The classification of different physical objects that participate in "$\gamma + Jet$" events and that may give a noticeable contribution into the total P_t-balance in the event as a whole is done.

Two new physical observables, namely, P_t of a cluster and P_t of all detectable particles beyond "$\gamma + Jet$" system, as well as the definion of isolated jet, proposed for studying ${P_t}^{\gamma} - {P_t}^{Jet}$ disbalance in [10]–[17], are discussed.

The selection cuts for physical observables of "$\gamma + Jet$" events are given.

The P_t-balance equation for the event as a whole is written in scalar form that allow to express the ${P_t}^{\gamma} - {P_t}^{Jet}$ disbalance in terms of the considered physical variables.

Apart from (1a) and (1b), other QCD subprocesses with large cross sections, by orders of magnitude larger than the cross sections of (1a) and (1b), can also lead to high P_t photons and jets in final state. So, we face the problem of selecting signal "$\gamma + Jet$" events from a large QCD background. Here we shall discuss the choice of physical variables that would be useful, under some cuts on their values, for separation of the desirable processes with direct photon ("γ^{dir}") from the background events. The possible "$\gamma^{dir}-$candidate" may originate from the $\pi^0,\ \eta,\ \omega$ and K_s^0 meson decays [20], [21] or may be caused by a bremsstrahlung photon or by an electron (see Section 8).

We take the D0 ECAL size to be limited by $|\eta| \leq 2.5$ and the calorimeter to be limited by $|\eta| \leq 4.2$ and to consist of CC, IC, EC, FC parts, where $\eta = -ln\ (tan\ (\theta/2))$ is a pseudorapidity defined in terms of a polar angle θ counted from the beam line. In the plane transverse to the beam line the azimuthal angle ϕ defines the directions of $\vec{P_t}^{Jet}$ and $\vec{P_t}^{\gamma}$.

3.1 Measurable physical observables and the P_t vector balance equation.

In $p\bar{p} \to \gamma + Jet + X$ events we are going to study the main physical object will be a high P_t jet to be detected in the $|\eta| < 4.2$ region and a direct photon registered by the ECAL up to $|\eta| < 2.5$. In these events there will be a set of particles mainly caused by beam remnants, i.e. by spectator parton fragments, that are flying mostly in the direction of a non-instrumented volume ($|\eta| > 4.2$)

in the detector. Let us denote the total transverse momentum of these non-observable particles (i) as

$$\sum_{i\in|\eta|>4.2} \vec{P_t}^{\,i} \equiv \vec{P_t}^{\,|\eta|>4.2}. \tag{5}$$

Among the particles with $|\eta|<4.2$ there may also be neutrinos. We shall denote their total momentum as

$$\sum_{i\in|\eta|<4.2} \vec{P}^{\,i}_{t(\nu)} \equiv \vec{P}_{t(\nu)}. \tag{6}$$

The sum of the transverse momenta of these two kinds of non-detectable particles will be denoted as P_t^{miss} [5]:

$$\vec{P_t}^{\,miss} = \vec{P}_{t(\nu)} + \vec{P_t}^{\,|\eta|>4.2}. \tag{7}$$

A high-energy jet may also contain neutrinos that may carry part of the total jet energy and of P_t^{Jet}. The average values of these neutrino parts can be estimated from simulation.

From the total jet transverse momentum $\vec{P_t}^{\,Jet}$ we shall separate the part that can be measured in the detector, i.e. in the ECAL+HCAL calorimeter system and in the muon system. Let us denote this detectable part as $\vec{P_t}^{\,jet}$ (small "j"!). So, we shall present the total jet transverse momentum $\vec{P_t}^{\,Jet}$ as a sum of three parts:

1. $\vec{P}^{\,Jet}_{t(\nu)}$, containing the contribution of neutrinos that belong to the jet, i.e. a non-detectable part of jet P_t (i - neutrino):

$$\vec{P}^{\,Jet}_{t(\nu)} = \sum_{i\in Jet} \vec{P}^{\,i}_{t(\nu)}. \tag{8}$$

2. $\vec{P}^{\,Jet}_{t(\mu)}$, containing the contribution of jet muons to $\vec{P_t}^{\,Jet}$ (i - muon):

$$\vec{P}^{\,Jet}_{t(\mu)} = \sum_{i\in Jet} \vec{P}^{\,i}_{t(\mu)}. \tag{9}$$

These muons make a weak signal in the calorimeter but their energy can be measured, in principle, in the muon system (in the region of $|\eta|<2.5$ in the case of D0 geometry). Due to the absence of the muon system and the tracker beyond the $|\eta|<2.5$ region, there exists a part of P_t^{Jet} caused by muons with $|\eta|>2.5$. We denote this part as $P^{Jet}_{t(\mu,|\eta|>2.5)}$. It can be considered, in some sense, as the analogue of $P^{Jet}_{t(\nu)}$ since the only trace of its presence would be weak MIP signals in calorimeter towers.

As for both points 1 and 2, let us say in advance that the estimation of the average values of neutrino and muon contributions to P_t^{Jet} (see Section 4 and Tables 1–12 of Appendix 1) have shown that they are quite small: about 0.30% of $\langle P_t^{Jet}\rangle_{all}$ is due to neutrinos and about 0.33% of $\langle P_t^{Jet}\rangle_{all}$ is due to muons, where "all" means averaging over all events including those without neutrinos and/or muons in jets. So, they together may cause approximately about 0.63% of the P_t^{γ} and P_t^{Jet} disbalance if muon signal is lost.

3. And finally, as we have mentioned before, we use $\vec{P_t}^{\,jet}$ to denote the part of $\vec{P_t}^{\,Jet}$ which includes all detectable particles of the jet [6], i.e. the sum of P_t of jet particles that may produce a signal in the calorimeter and muon system (calo=ECAL+HCAL signal)

[5] This value is a part of true missing P_t in an experiment that includes the detector effects (see [1, 2]).

[6] We shall consider the issue of charged particles contribution with small P_t into the total jet P_t while discussing the results of the full GEANT simulation (with account of the magnetic field effect) in our forthcoming papers.

$$\vec{P}_t^{\,jet} = \vec{P}_{t(calo)}^{\,Jet} + \vec{P}_{t(\mu)}^{\,Jet}, \quad |\eta^\mu| < 2.5. \tag{10}$$

Thus, in the general case we can write for any η values:

$$\vec{P}_t^{\,Jet} = \vec{P}_t^{\,jet} + \vec{P}_{t(\nu)}^{\,Jet} + \vec{P}_{t(\mu,|\eta^\mu|>2.5)}^{\,Jet}. \tag{11}$$

In the case of $p\bar{p} \to \gamma + Jet + X$ events the particles detected in the $|\eta| < 4.2$ region may originate from the fundamental subprocesses (1a) and (1b) corresponding to LO diagrams shown in Fig. 1, as well as from the processes corresponding to NLO diagrams (like those in Figs. 2, 4 that include ISR and FSR), and also from the "underlying" event [1], of course.

As was already mentioned in Section 2, the final states of fundamental subprocesses (1a) and (1b) may contain additional jets due to the ISR and final state radiation (FSR) caused by the higher order QCD corrections to the LO Feynman diagrams given in Fig. 1. To understand and then to realize the jet energy calibration procedure, we need to use the event generator to find the criteria for selection of events with a good balance of $\vec{P}_t^{\,\gamma}$ with the $\vec{P}_t^{\,jet}$ part measurable in the detector. It means that to make a reasonable simulation of the calibration procedure, we need to have a selected sample of generated events having a small P_t^{miss} (see Section 4) contribution and use as a model. We also have to find a way to select events without additional jets or with jets suppressed down to the level of mini-jets or clusters having very small P_t.

So, for any event we separate the particles in the $|\eta| < 4.2$ region into two subsystems. The first one consists of the particles belonging to the "$\gamma + Jet$" system (here "Jet" denotes the jet with the highest $P_t \geq 30\ GeV/c$) having the total transverse momentum $\vec{P}_t^{\,\gamma+Jet}$ (large "Jet", see (4)). The second subsystem involves all other (O) particles beyond the "$\gamma + Jet$" system in the region, covered by the detector, i.e. $|\eta| < 4.2$. Let us mention that the value of $\vec{P}_t^{\,\gamma+Jet}$ may be different from the value of observable:

$$\vec{P}_t^{\,\gamma+jet} = \vec{P}_t^{\,\gamma} + \vec{P}_t^{\,jet} \quad (\text{small``jet''}), \tag{12}$$

in the case of non-detectable particles presence in a jet. The total transverse momentum of this O-system are denoted as $P_t^{\,O}$ and it is a sum of P_t of additional mini-jets (or clusters) and P_t of single hadrons, photons and leptons in the $|\eta| < 4.2$ region. Since a part of neutrinos are also present among these leptons, the difference of $\vec{P}_{t(\nu)}$ and $\vec{P}_{t(\nu)}^{\,Jet}$ gives us the transverse momentum

$$\vec{P}_{t(\nu)}^{\,O} = \vec{P}_{t(\nu)} - \vec{P}_{t(\nu)}^{\,Jet} \quad |\eta^\nu| < 4.2, \tag{13}$$

carried out by the neutrinos that do not belong to the jet but are contained in the $|\eta| < 4.2$ region.

We denote by $\vec{P}_t^{\,out}$ a part of $\vec{P}_t^{\,O}$ that can be measured, in principle, in the detector. Thus, $\vec{P}_t^{\,out}$ is a sum of P_t of other mini-jets or, generally, clusters (with P_t^{clust} smaller than P_t^{Jet}) and P_t of single hadrons (h), photons (γ) and electrons (e) with $|\eta| < 4.2$ and muons (μ) with $|\eta^\mu| < 2.5$ that are out of the "$\gamma + Jet$" system. For simplicity these mini-jets and clusters will be called "clusters" [7]. So, for our "$\gamma + Jet$" events $\vec{P}_t^{\,out}$ is the following sum (all $\{h,\ \gamma,\ e,\ \mu\} \notin$ Jet):

$$\vec{P}_t^{\,out} = \vec{P}_t^{\,clust} + \vec{P}_{t(h)}^{\,sing} + \vec{P}_{t(\gamma)}^{\,nondir} + \vec{P}_{t(e)} + \vec{P}_{t(\mu,|\eta^\mu|<2.5)}^{\,O}; \quad |\eta| < 4.2. \tag{14}$$

And thus, finally, we have:

[7] As was already mentioned in Introduction, these clusters are found by the LUCELL jetfinder with the same value of the cone radius as for jets: $R^{clust} = R^{jet} = 0.7$.

$$\vec{P_t}^{O} = \vec{P_t}^{out} + \vec{P}^{O}_{t(\nu)} + \vec{P}^{O}_{t(\mu,|\eta^\mu|>2.5)}. \tag{15}$$

With these notations we come to the following vector form [13] of the P_t- conservation law for the "$\gamma + Jet$" event (where γ is a direct photon) as a whole (supposing that the jet and the photon are contained in the corresponding detectable regions):

$$\vec{P_t}^{\gamma} + \vec{P_t}^{Jet} + \vec{P_t}^{O} + \vec{P_t}^{|\eta|>4.2} = 0 \tag{16}$$

with last three terms defined correspondingly by (11), (15) and (5) respectively.

3.2 Definition of selection cuts for physical variables and the scalar form of the P_t balance equation.

1. We shall select the events with one jet and one "γ^{dir}-candidate" (in what follows we shall designate it as γ and call the "photon" for brevity and only in Section 8, devoted to the backgrounds, we shall denote γ^{dir}-candidate by $\tilde{\gamma}$) with

$$P_t^{\gamma} \geq 40\ GeV/c \quad \text{and} \quad P_t^{Jet} \geq 30\ GeV/c. \tag{17}$$

The ECAL signal can be considered as a candidate for a direct photon if it fits inside one D0 calorimeter tower having size 0.1×0.1 in the $\eta - \phi$ space.

For most of our applications in Sections 4, 5 and 6 mainly the PYTHIA jetfinding algorithm LUCELL will be used. The jet cone radius R in the $\eta - \phi$ space counted from the jet initiator cell (ic) is taken to be $R_{ic} = ((\Delta\eta)^2 + (\Delta\phi)^2)^{1/2} = 0.7$. Below in Section 6 we shall also consider the jet radius counted from the center of gravity (gc) of the jet, i.e. R_{gc}. Comparison with the UA1 and UA2 jetfinding algorithms (taken from the CMSJET program of fast simulation [24]) is presented in Sections 6 and 7.

2. To suppress the contribution of background processes, i.e. to select mostly the events with "isolated" direct photons and to discard the events with fake "photons" (that may originate as γ^{dir}-candidates from meson decays, for instance), we restrict

a) the value of the scalar sum of P_t of hadrons and other particles surrounding a "photon" within a cone of $R^{\gamma}_{isol} = ((\Delta\eta)^2 + (\Delta\phi)^2)^{1/2} = 0.7$ ("absolute isolation cut") [8]

$$\sum_{i \in R} {P_t}^i \equiv {P_t}^{isol} \leq P^{isol}_{tCUT}; \tag{18}$$

b) the value of a fraction ("fractional isolation cut")

$$\sum_{i \in R} {P_t}^i / {P_t}^{\gamma} \equiv \epsilon^{\gamma} \leq \epsilon^{\gamma}_{CUT}. \tag{19}$$

3. To be consistent with the application condition of the NLO formulae, one should avoid an infrared dangerous region and take care of P_t population in the region close to a γ^{dir}-candidate (see [29], [30]). In accordance with [29] and [30], we also restrict the scalar sum of P_t of particles around a "photon" within a cone of a smaller radius $R^{\gamma}_{singl} = 0.2$.

Due to this cut,

$$\sum_{i \in R^{\gamma}_{singl}} {P_t}^i \equiv {P_t}^{singl} \leq 2\ GeV/c \quad (i \neq \gamma^{dir}), \tag{20}$$

[8] We have found that S/B ratio with $R^{\gamma}_{isol} = 0.7$ is in about 1.5 times better than with $R^{\gamma}_{isol} = 0.4$ what is accompanied by only 10% of additional loss of the number of signal events.

an "isolated" photon with high P_t also becomes a "single" one within an area of 8 calorimeter towers (of size 0.1×0.1 according to D0 geometry) which surround the tower fired by it, i.e. a tower with the highest P_t.

4. We accept only the events having no charged tracks (particles) with $P_t > 5\ GeV/c$ within the $R = 0.4$ cone around the γ^{dir}-candidate.

5. To suppress the background events with photons resulting from π^0, η, ω and K_S^0 meson decays, we require the absence of a high P_t hadron in the tower containing the γ^{dir}-candidate:

$$P_t^{hadr} \leq 7\ GeV/c. \tag{21}$$

At the PYTHIA level of simulation this cut may effectively take into account the imposing of an upper cut on the HCAL signal in the towers behind the ECAL tower fired by the direct photon.

6. We select the events with the vector $\vec{P_t}^{Jet}$ being "back-to-back" to the vector $\vec{P_t}^{\gamma}$ (in the plane transverse to the beam line) within $\Delta\phi$ defined by the equation:

$$\phi_{(\gamma,\ jet)} = 180^\circ \pm \Delta\phi, \tag{22}$$

where $\phi_{(\gamma,\ jet)}$ is the angle between the ${P_t}^{\gamma}$ and ${P_t}^{Jet}$ vectors: $\vec{P_t}^{\gamma}\vec{P_t}^{Jet} = {P_t}^{\gamma}{P_t}^{Jet} \cdot cos(\phi_{(\gamma,\ jet)})$, ${P_t}^{\gamma} = |\vec{P_t}^{\gamma}|$, ${P_t}^{Jet} = |\vec{P_t}^{Jet}|$. The cases $\Delta\phi \leq 17^\circ, 11^\circ, 6^\circ$ are considered in this paper (6° is approximately one D0 calorimeter tower size in ϕ).

7. The initial and final state radiations (ISR and FSR) manifest themselves most clearly as some final state mini-jets or clusters activity. To suppress it, we impose a new cut condition that was not formulated in an evident form in previous experiments: we choose the "$\gamma + Jet$" events that do not have any other jet-like or cluster high P_t activity by selecting the events with the values of P_t^{clust} (the cluster cone $R_{clust}(\eta,\phi) = 0.7$), being lower than some threshold P_{tCUT}^{clust} value, i.e. we select the events with

$$P_t^{clust} \leq P_{tCUT}^{clust} \tag{23}$$

($P_{tCUT}^{clust} = 15, 10, 5\ GeV/c$ are most effective as will be shown in Sections 6–8). Here, in contrast to [13]–[17], the clusters are found by one and the same jetfinder LUCELL while three different jetfinders UA1, UA2 and LUCELL are used to find the jet (${P_t}^{Jet} \geq 30\ GeV/c$) in the event.

8. Now we pass to another new quantity (proposed also for the first time in [13]–[17]) that can be measured at the experiment. We limit the value of the modulus of the vector sum of $\vec{P_t}$ of all particles, except those of the "$\gamma + Jet$" system, that fit into the region $|\eta| < 4.2$ covered by the ECAL and HCAL, i.e., we limit the signal in the cells "beyond the jet and photon" region by the following cut:

$$\left|\sum_{i \notin Jet, \gamma-dir} \vec{P_t}^{i}\right| \equiv P_t^{out} \leq P_{tCUT}^{out}, \quad |\eta^i| < 4.2. \tag{24}$$

The importance of P_{tCUT}^{out} and P_{tCUT}^{clust} for selection of events with a good balance of ${P_t}^{\gamma}$ and ${P_t}^{Jet}$ and for the background reduction will be demonstrated in Sections 7 and 8.

Below the set of selection cuts 1 – 8 will be referred to as "Selection 1". The last two of them, 7 and 8, are new criteria [13] not used in previous experiments.

9. In addition to them one more new object, introduced in [13] – [17] and named an "isolated jet", will be used in our analysis. i.e. we shall require the presence of a "clean enough" (in the sense of limited P_t activity) region inside the ring of $\Delta R = 0.3$ width (or approximately of a size of three calorimeter towers) around the jet. Following this picture, we restrict the ratio of the scalar sum of transverse momenta of particles belonging to this ring, i.e.

$$P_t^{ring}/P_t^{jet} \equiv \epsilon^{jet} \leq \epsilon_0^{jet}, \quad \text{where} \quad P_t^{ring} = \sum_{i \in 0.7<R<1.0} |\vec{P}_t^{\,i}|. \tag{25}$$

(ϵ_0^{jet} is chosen to be $3-5\%$, see Sections 7 and 8).

The set of cuts 1 – 9 will be called in what follows "Selection 2".

10. In the following we shall consider also "Selection 3" where we shall keep only those events in which one and the same jet is found simultaneously by every of three jetfinders used here: UA1, UA2 and LUCELL (i.e. up to good accuracy having the same values of P_t^{Jet}, R^{jet} and $\Delta\phi$). For these jets (and also clusters in the same event) we require the following conditions:

$$P_t^{Jet} > 30\ GeV/c, \qquad P_t^{clust} < P_{tCUT}^{clust}, \qquad \Delta\phi < 17^\circ (11^\circ,\ 6^\circ), \qquad \epsilon^{jet} \leq 3-5\% \tag{26}$$

The exact values of the cut parameters P_{tCUT}^{isol}, ϵ_{CUT}^{γ}, ϵ^{jet}, P_{tCUT}^{clust}, P_{tCUT}^{out} will be specified below, since they may be different, for instance, for various P_t^{γ} intervals (being looser for higher P_t^{γ}).

11. As we have already mentioned in Section 3.1, one can expect reasonable results of the jet energy calibration procedure modeling and subsequent practical realization only if one uses a set of selected events with small P_t^{miss}. So, we also use the following cut:

$$P_t^{miss} \ \leq P_{tCUT}^{miss}. \tag{27}$$

For this reason we shall study in the next Section 4 the influence of P_t^{miss} parameter on the selection of events with a reduced value of the total sum of neutrino contribution into P_t^{Jet}, i.e. $P_{t(\nu)}^{Jet}$. The aim of the event selection with small $P_{t(\nu)}^{Jet}$ is quite obvious: we need a set of events with a reduced P_t^{Jet} uncertainty due to a possible presence of a non-detectable particle contribution to a jet [9].

To conclude this section, let us write the basic P_t-balance equation (16) of the previous section with the notations introduced here in the form more suitable to present the final results. For this purpose we shall write equation (16) in the following scalar form (see also [13], [25] and [26]):

$$\frac{P_t^{\gamma} - P_t^{Jet}}{P_t^{\gamma}} = (1 - cos\Delta\phi) + P_t(O{+}\eta > 4.2)/P_t^{\gamma}, \tag{28}$$

where $P_t(O{+}\eta > 4.2) \equiv (\vec{P}_t^{\,O} + \vec{P}_t^{\,|\eta|>4.2}) \cdot \vec{n}^{Jet}$ with $\vec{n}^{Jet} = \vec{P}_t^{\,Jet}/P_t^{Jet}$.

As will be shown in Section 7, the first term on the right-hand side of equation (28), i.e. $(1 - cos\Delta\phi)$ is negligibly small as compared with the second term (in a case of Selection 1) and tends to decrease fast with growing P_t^{Jet}. So, in this case the main contribution to the P_t disbalance in the "$\gamma + Jet$" system is caused by the term $P_t(O{+}\eta > 4.2)/P_t^{\gamma}$.

4. ESTIMATION OF A NON-DETECTABLE PART OF P_t^{Jet}.

It is shown that by imposing an upper cut on the missing transverse momentum $P_t^{miss} < 10\ GeV/c$ one can reduce the correction to the measurable part of P_t^{jet} due to neutrino contribution down to the value of $\Delta_\nu = \langle P_{t(\nu)}^{Jet} \rangle_{all\ events} = 0.1\ GeV/c$ in all intervals of P_t^{γ}.

[9] In Section 8 we also underline the importance of this cut for reduction of $e^{\pm}$ events contribution to the background to the signal $\gamma^{dir} + jet$ events.

In Section 3.1 we have divided the transverse momentum of a jet, i.e. ${P_t}^{Jet}$, into two parts, a detectable ${P_t}^{jet}$ and non-detectable (${P_t}^{Jet} - {P_t}^{jet}$), consisting of $P^{Jet}_{t(\nu)}$ and $P^{Jet}_{t(\mu,|\eta|>2.5)}$ (see (11)). In the same way, according to equation (15), we divided the transverse momentum ${P_t}^{O}$ of "other particles" that are out of $\gamma^{dir} + jet$ system into a detectable part ${P_t}^{out}$ and a non-detectable part consisting of the sum of $P^{O}_{t(\nu)}$ and $P^{O}_{t(\mu,|\eta|>2.5)}$ (see (15)) [10].

We shall estimate here what part of ${P_t}^{Jet}$ may be carried out by non-detectable particles (mainly neutrinos originating from weak decays) [11].

We shall consider the case of switched-on decays of $\pi^\pm$ and $K^\pm$ mesons [12]. Here $\pi^\pm$ and $K^\pm$ meson decays are allowed inside the solenoid volume with the barrel radius $R_B = 80\ cm$ and the distance from the interaction vertex to Endcap along the z-axis $L = 130\ cm$ (D0 geometry).

For this aim we shall use the bank of the signal "$\gamma{+}Jet$" events, i.e. caused by subprocesses (1a) and (1b), generated for three ${P_t}^{\gamma}$ intervals: $40 < {P_t}^{\gamma} < 50$, $70 < {P_t}^{\gamma} < 90$ and $90 < {P_t}^{\gamma} < 140\ GeV/c$ and selected with conditions (17) – (24) (Selection 1) and the following cut values:

$$P^{isol}_{tCUT} = 4\ GeV/c,\ \ \epsilon^{\gamma}_{CUT} = 7\%,\ \ \Delta\phi{<}17^\circ,\ \ P^{clust}_{tCUT} = 30\ GeV/c. \qquad (29)$$

Here the cut $P^{clust}_{tCUT} = 30\ GeV/c$ has the meaning of a very weak restriction on mini-jets or clusters activity. No restriction was imposed on the ${P_t}^{out}$ value. The results of analysis of these events, based on the application of LUCELL jetfinder, are presented in Fig. 5, while more detailed tables of Appendix 1 contain the results found with UA1 and UA2 jetfinding algorithms as well.

The first row of Fig. 5 contains ${P_t}^{miss}$ spectra in the "$\gamma + Jet$" events for different ${P_t}^{\gamma}$ intervals and demonstrates (to a good accuracy) their practical independence on ${P_t}^{\gamma}$.

In the second row of Fig. 5 we present the spectra of ${P_t}^{miss}$ for those events (denoted as $P^{Jet}_{t(\nu)} > 0$) which contain jets having neutrinos, i.e. having a non-zero $P^{Jet}_{t(\nu)}$ component of ${P_t}^{Jet}$. These figures also show the practical independence of the ${P_t}^{miss}$ spectrum on the direct photon ${P_t}^{\gamma}$ (approximately equal to ${P_t}^{Jet}$): the peak position remains in the region of ${P_t}^{miss}{<}2.5\ GeV/c$. Comparison of the number of entries in the second row plots of Fig. 5 with those in the first row allows to conclude that the part of events with the jet having the non-zero neutrinos contribution ($P^{Jet}_{t(\nu)} > 0$) has practically the same size of about 15% in all ${P_t}^{\gamma}$ intervals.

The same spectra of ${P_t}^{miss}$ for events with $P^{Jet}_{t(\nu)}{>}0$ show how many of these events would remain after imposing a cut on ${P_t}^{miss}$ in every ${P_t}^{\gamma}$ interval. The important thing is that reduction of the number of events with $P^{Jet}_{t(\nu)} > 0$ in every ${P_t}^{\gamma}$ interval leads to reduction of the mean value of the $P^{Jet}_{t(\nu)}$, i.e. the value averaged over all collected events $\langle P^{Jet}_{t(\nu)}\rangle_{all\ events}$. This value, found from PYTHIA generation, serves as a model correction Δ_ν and it has to be estimated for proper determination of the total ${P_t}^{Jet}$ from the measurable part ${P_t}^{jet}$. Thus, the complete jet P_t can be defined as: ${P_t}^{Jet} = {P_t}^{jet} + \Delta_\nu + \Delta_\mu(|\eta^\mu| > 2.5)$ [13], where $\Delta_\nu = \langle P^{Jet}_{t(\nu)}\rangle_{all\ events}$ and $\Delta_\mu = \langle P^{Jet}_{t(\mu,|\eta>2.5|)}\rangle_{all\ events}$. (As we plan to use in this paper only events with jets belonging to CC part of calorimeter, Δ_μ is not important for our analysis.)

The effect of imposing general P^{miss}_{tCUT} in each event of our sample is shown in the third row of Fig. 5. The upper cut$P^{miss}_{tCUT} = 1000\ GeV/c$, as is seen from the comparison with the second

[10] But in a real experiment non-detectable part of ${P_t}^{Jet}$ may be also conditioned by energy leakage due to constructive/material features of a detector.

[11] In [17] and [26] it was shown that main source of high P_t neutrinos in background processes are $W^\pm$ decays, which also contain $e^\pm$ that in its turn may fake direct photons.

[12] According to the PYTHIA default agreement, $\pi^\pm$ and $K^\pm$ mesons are stable.

[13] With account of real processes in the detector, as we mentioned above, ${P_t}^{jet}$ should be also corrected by energy leakage from the detectable volume of the detector.

row pictures, means the absence of any upper limit for $P_{t(\nu)}^{Jet}$. The most important illustrative fact that in the absence of any restriction on P_t^{miss} the total neutrino P_t inside the jet averaged over all events can be as large as $P_{t(\nu)}^{Jet} \approx 0.32\ GeV/c$ at $90 < P_t^{\gamma} < 140\ GeV/c\ GeV/c$ comes from the right-hand plot of the third row in Fig. 5. In the $40 < P_t^{Jet} < 50\ GeV/c$ interval, which is less dangerous from the point of view of the neutrino P_t content in a jet, we have already a very small mean value of $P_{t(\nu)}^{Jet}$ equal to $0.12\ GeV/c$ even without imposing any P_{tCUT}^{miss}. From the same plots of the third row of Fig. 5 we see that with general $P_{tCUT}^{miss} = 10\ GeV/c$ the average correction due to neutrino contribution is $\Delta_\nu = 0.1\ GeV/c$ in all three intervals of P_t^{γ}.

At the same time, as it was demonstrated in [17] and [26], this cut essentially reduces the admixture of the $e^{\pm}$-events, in which $e^{\pm}$, mainly originating from the $W^{\pm} \to e^{\pm}\nu$ weak decays, may fake the direct photon signal. These events are characterized by big values of P_t^{miss} (it is higher, on the average, by about one order of magnitude than in the signal "$\gamma^{dir} + jet$" events) that may worsen the jet calibration accuracy.

The analogous (to neutrino) situation holds for the $P_{t(\mu)}^{Jet}$ contribution.

The detailed information about the values of non-detectable $P_{t(\nu)}^{Jet}$ averaged over all events (no cut on P_t^{miss} was used) as well as about mean P_t values of muons belonging to jets $\langle P_{t(\mu)}^{Jet} \rangle$ is presented in Tables 1–12 of Appendix 1 for the sample of events with jets which are entirely contained in the central region of the calorimeter ($|\eta^{jet}| < 0.7$) and found by UA1, UA2 and LUCELL jetfinders. In these tables the ratio of the number of events with non-zero $P_{t(\nu)}^{Jet}$ to the total number of events is denoted by $R_{event}^{\nu \in Jet}$ and the ratio of the number of events with non-zero $P_{t(\mu)}^{Jet}$ to the total number of events is denoted by $R_{event}^{\mu \in Jet}$.

The quantity P_t^{miss} in events with $P_{t(\nu)}^{Jet} > 0$ is denoted in these tables as $P_{t \nu \in Jet}^{miss}$ and is given there for four P_t^{γ} intervals ($40 < P_t^{\gamma} < 50$, $50 < P_t^{\gamma} < 70$, $70 < P_t^{\gamma} < 90$ and $90 < P_t^{\gamma} < 140$) and other P_{tCUT}^{clust} values ($P_{tCUT}^{clust} = 20, 15, 10, 5\ GeV/c$) complementary to $P_{tCUT}^{clust} = 30\ GeV/c$ used for the second row plots [14] of Fig. 5. From Tables 1–3 we see that the averaged value of P_t^{miss} calculated by using only the events with $P_{t(\nu)}^{Jet} > 0$, i.e. $\langle P_{t \nu \in Jet}^{miss} \rangle$, is about 2.3–2.4 GeV/c for the $40 < P_t^{\gamma} < 50\ GeV/c$ interval. It increases to about 3.4–3.5 GeV/c for the $90 < P_t^{\gamma} < 140\ GeV/c$ interval (see Tables 10–12). It should be noted that the averaged values of the modulus of $P_{t(\nu)}^{Jet}$ (see formula (8)) presented in the third lines of Tables 1–12 from Appendix 1 coincide with the averaged values of the difference $\langle P_t^{Jet} - P_t^{jet} \rangle \equiv \Delta_\nu$ (see Section 3.2 and second lines of Tables 1–12) to three digits, i.e. $<P_{t(\nu)}^{Jet}> = \Delta_\nu$. This is because the $\vec{P}_t^{Jet}$ and $\vec{P}_t^{jet}$ vectors are practically collinear and because we consider here the "CC-events" in which all jet muons may also be detected by the central muon system.

Let us mention that the 11-th lines of Tables 1–12 show the ratio ("$29 sub/all$") of the number of events due to the gluonic subprocess (1a) only (see also Section 10) to the number of events due to the sum of subprocesses (1a) and (1b). It is seen that this ratio drops with P_t^{γ} growth (see also Table 21). Two upper lines 9, 10 contain an additional information on the numbers of "$\gamma + Jet$" events, i.e. $Nevent_{(c)}$ and $Nevent_{(b)}$, produced in a case of the gluonic subprocess (1a) and having in the final state jets that originate from c and b quarks. These numbers correspond to the integrated luminosity $L_{int} = 300\ pb^{-1}$ and vary for different $P_t^{Jet}(\approx P_t^{\gamma})$ intervals. The averaged jet radii $<R_{jet}>$ and the number of entries are shown in last two lines.

[14]Please, note that the values of P_t^{miss} and $P_{t \nu \in Jet}^{miss}$ in the plots of Fig. 5 are slightly different from those of Appendix 1 as the numbers in from Fig. 5 were found for events in the whole $|\eta| < 4.2$ region.

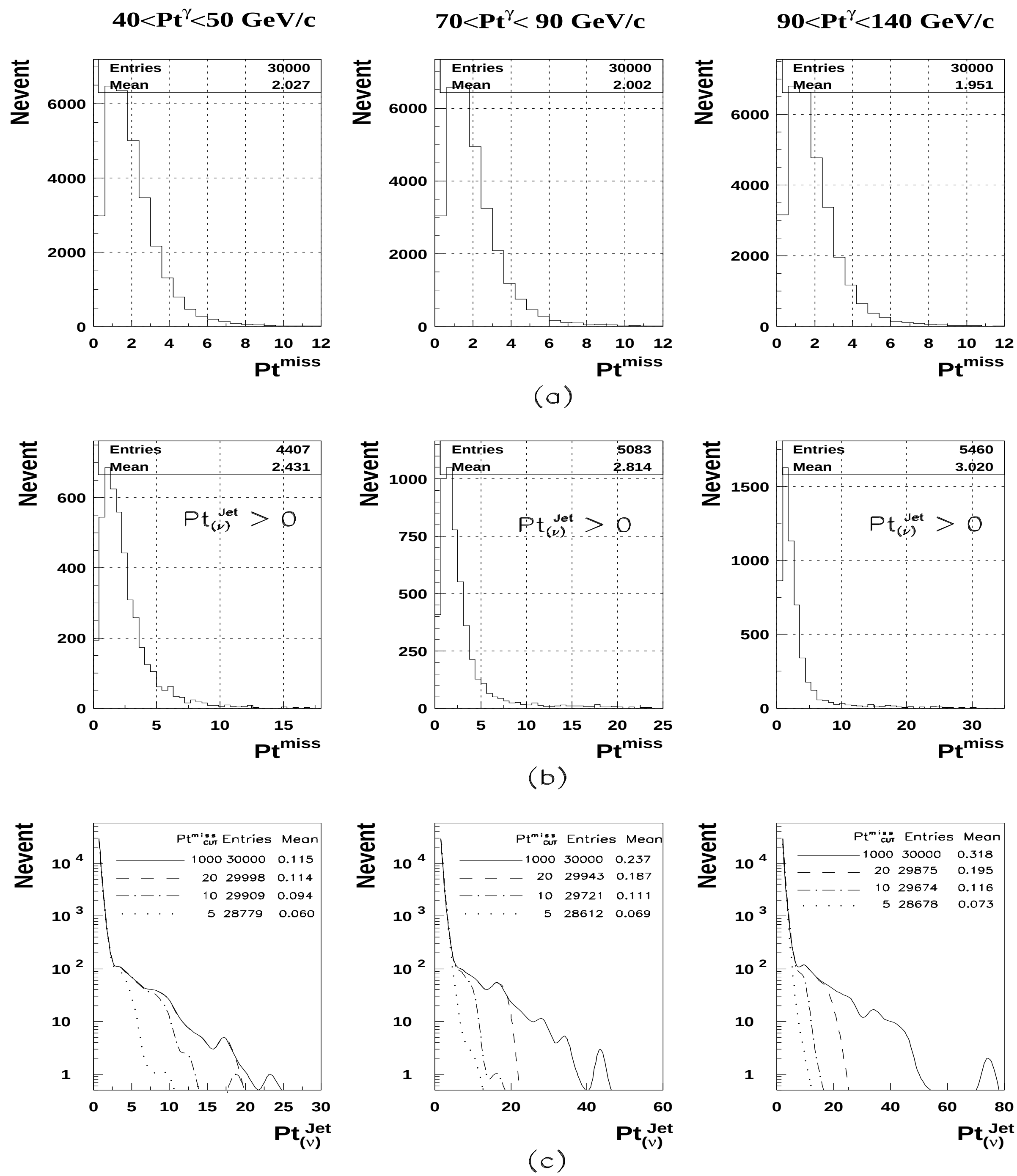

Fig. 5: a) P_t^{miss} spectra in all events; b) P_t^{miss} spectra in events having jets with non-zero P_t neutrinos, i.e. $P_{t(\nu)}^{Jet} > 0$; c) $P_{t(\nu)}^{Jet}$ spectra and their mean values dependence on the values of P_{tCUT}^{miss} in various $P_t{}^{\gamma}(\approx P_t{}^{Jet})$ intervals. $\pi^{\pm}$ and $K^{\pm}$ meson decays are allowed inside the solenoid of $R = 80\ cm$ and $L = 130\ cm$ ($P_{tCUT}^{clust} = 30\ GeV/c$).

5. EVENT RATES FOR DIFFERENT P_t^{γ} AND η^{Jet} INTERVALS.

The number of "$\gamma + Jet$" events distribution over P_t^{γ} and η^{γ} is studied here. It is found that in each interval of the $\Delta P_t^{\gamma} = 10\ GeV/c$ width the rates decrease by a factor more than 2. The number of events with jets which transverse momentum are completely (or with 5% accuracy) contained in CC, IC, EC and FC regions are presented in Tables 9–12 for integrated luminosity $L_{int} = 300\,pb^{-1}$.

5.1 Dependence of distribution of the number of events on the "back-to-back" angle $\phi_{(\gamma,\ jet)}$ and on P_t^{ISR}.

The definitions of the physical variables introduced in Sections 2 and 3 allow to study a possible way to select the events with a good P_t^{γ} and P_t^{Jet} balance. Here we shall be interested to get (by help of PYTHIA generator and the theoretical models therein) an idea about the form of the spectrum of the variable P_t56 (which is approximately proportional to P_t^{ISR} up to the value of intrinsic parton transverse momentum k_t inside a proton) at different values of P_t^{γ}. For this aim four samples of "$\gamma + Jet$" events were generated by using PYTHIA with 2 QCD subprocesses (1a) and (1b) being included simultaneously. In what follows we shall call these events as "signal events". The generations were done with the values of the PYTHIA parameter CKIN(3)($\equiv \hat{p}_{\perp}^{\,min}$) equal to 20, 25, 35 and 45 GeV/c in order to cover four P_t^{γ} intervals: 40–50, 50–70, 70–90 and 90–140 GeV/c, respectively. Each sample in these P_t^{γ} intervals had a size of $5 \cdot 10^6$ events. The cross sections for the two subprocesses were found to be as given in Table 1.

Table 1: The cross sections (in $microbarn$) of the $qg \to q + \gamma$ and $q\overline{q} \to g + \gamma$ subprocesses for four P_t^{γ} intervals.

Subprocess type	P_t^{γ} interval (GeV/c)			
	40 – 50	50 – 70	70 – 90	90 – 140
$qg \to q + \gamma$	$0.97{\cdot}10^{-2}$	$4.78{\cdot}10^{-3}$	$1.36{\cdot}10^{-3}$	$4.95{\cdot}10^{-4}$
$q\overline{q} \to g + \gamma$	$0.20{\cdot}10^{-2}$	$0.96{\cdot}10^{-3}$	$0.35{\cdot}10^{-3}$	$1.56{\cdot}10^{-4}$
Total	$1.17{\cdot}10^{-2}$	$5.75{\cdot}10^{-3}$	$1.71{\cdot}10^{-3}$	$6.51{\cdot}10^{-4}$

For our analysis we used "Selection 1" (formulae (17)–(24)) defined in Sections 3.2 and the values of cut parameters (29).

In Tables 2, 3 and 5, 6 we present P_t56 spectra for two most illustrative cases of P_t^{γ} intervals $40 < P_t^{\gamma} < 50\ GeV/c$ (Tables 2 and 5) and $70 < P_t^{\gamma} < 90\ GeV/c$ (Tables 3 and 6). The distributions of the number of events for the integrated luminosity $L_{int} = 300\,pb^{-1}$ in different P_t56 intervals ($\langle k_t \rangle$ was taken to be fixed at the PYTHIA default value, i.e. $\langle k_t \rangle = 0.44\,GeV/c$) and for different "back-to-back" angle intervals $\phi_{(\gamma,\ jet)} = 180^{\circ} \pm \Delta\phi$ ($\Delta\phi \leq 17^{\circ}$, 11° and 6° as well as without any restriction on $\Delta\phi$, i.e. for the whole ϕ interval $\Delta\phi \leq 180^{\circ}$) [15] are given there. The LUCELL jetfinder was used for determination of jets and clusters [16]. Tables 2 and 3 correspond to $P_t^{clust} < 30\,GeV/c$ and serve as an illustration since it is rather a weak cut condition, while Tables 5 and 6 correspond to a more restrictive selection cut $P_{tCUT}^{clust} = 5\,GeV/c$ (which leads to about twofold reduction of the number of events for $\Delta\phi \leq 17^{\circ}$; see summarizing Tables 4 and 7).

First, from the last summary lines of Tables 2, 3 and 5, 6 we can make a general conclusion about the $\Delta\phi$-dependence of the event spectrum. Thus, in the case of weak restriction $P_t^{clust} <$

[15] The value $\Delta\phi = 6^{\circ}$ approximately coincides with one D0 HCAL tower size in the ϕ-plane.

[16] More details connected with UA1 and UA2 jetfinders application can be found in Section 7 and Appendices 2–5 for a jet contained in CC region.

$30\ GeV/c$ we can see from Table 2 that for the $40 \leq P_t{}^{\gamma} \leq 50\ GeV/c$ interval about 76% of events are concentrated in the $\Delta\phi < 17°$ range, while 41% of events are in the $\Delta\phi < 6°$ range. At the same time the analogous summary line of Table 3 shows us that for higher $P_t{}^{\gamma}$ interval $70 \leq P_t{}^{\gamma} \leq 90\, GeV/c$ the $P_t 56$ spectrum for the same restriction $P_t{}^{clust} < 30\ GeV/c$ moves (as compared with low $P_t{}^{\gamma}$ intervals) to the small $\Delta\phi$ region: more than 80% of events have $\Delta\phi < 17°$ and 50% of them have $\Delta\phi < 6°$.

A tendency of distributions of the number of signal "$\gamma + Jet$" events to be very rapidly concentrated in a rather narrow back-to-back angle interval $\Delta\phi < 17°$ as $P_t{}^{\gamma}$ grows becomes more distinct with a more restrictive cut (see Tables 5, 6 and 7). From the last summary line of Table 5 we see that in the first interval $40 \leq P_t{}^{\gamma} \leq 50\, GeV/c$ more than 99% of the events, selected with $P_{tCUT}^{clust} = 5\, GeV/c$, have $\Delta\phi < 17°$, while 72% of them are in the $\Delta\phi < 6°$ range. It should be mentioned that after application of this cut only about 40% of events remain. For $70 \leq P_t{}^{\gamma} \leq 90\, GeV/c$ (see Table 6) more than 90% of the events, subject to the cut $P_{tCUT}^{clust} = 5\ GeV/c$, have $\Delta\phi < 6°$. It means that while suppressing cluster or mini-jet activity by imposing $P_{tCUT}^{clust} = 5\ GeV/c$ we can select the sample of events with a clean "back-to-back" (within 17° in ϕ) topology of γ and jet orientation. (Unfortunately, as it will be discussed below basing on the information from Tables 5 and 6, it does not mean that P_{tCUT}^{clust} allows to suppress completely the ISR as is seen from Tables 5 and 6.) [17].

So, one can conclude that PYTHIA simulation predicts that at Tevatron energies most of the "$\gamma + Jet$" events (more than 75%) may have the vectors $\vec{P}_t{}^{\gamma}$ and $\vec{P}_t{}^{jet}$ being back-to-back within $\Delta\phi < 17°$ after imposing $P_{tCUT}^{clust} = 30\ GeV/c$. The cut $P_{tCUT}^{clust} = 5\ GeV/c$ significantly improves [18] this tendency.

It is worth mentioning that this picture reflects the predictions of one of the generators based on the approximate LO values for the cross section. It may change if the next-to-leading order or soft physics [19] effects are included.

The other lines of Tables 2, 3 and 5, 6 contain the information about the $P_t 56$ spectrum or, up to intrinsic transverse parton momentum $\langle k_t \rangle = 0.44\ GeV/c$, about $P_t{}^{ISR}$ spectrum).

From Tables 2 and 3 one can see that in the case when there are no restrictions on $P_t{}^{clust}$ the $P_t 56$ spectrum becomes a bit wider for larger values of $P_t{}^{\gamma}$.

At the same time, one can conclude from the comparison of Table 2 with Table 5 that for lower $P_t{}^{\gamma}$ intervals the width of the most populated part of the $P_t 56$ (or $P_t{}^{ISR}$) spectrum reduces by about 40% with restricting P_{tCUT}^{clust}. So, for $\Delta\phi_{max} = 17°$ we see that it drops from $0 < P_t 56 < 20\ GeV/c$ for $P_{tCUT}^{clust} = 30\ GeV/c$ to a narrower interval of $0 < P_t 56 < 10\, GeV/c$ for the $P_{tCUT}^{clust} = 5\, GeV/c$. At higher $P_t{}^{\gamma}$ intervals (Tables 3 and 6) for the same value $\Delta\phi_{max} = 17°$ the reduction factor of the $P_t 56$ spectrum width (from the $0 < P_t 56 < 30\ GeV/c$ interval for $P_{tCUT}^{clust} = 30\, GeV/c$ to the $0 < P_t 56 < 10 - 15\ GeV/c$ interval for $P_{tCUT}^{clust} = 5\ GeV/c$) is more than two.

Thus, we can summarize that the PYTHIA generator predicts an increase in the $P_t{}^{ISR}$ spectrum with growing $P_t{}^{\gamma}$ (compare Tables 2 and 3), but this increase can be reduced by imposing a restrictive cut on $P_t{}^{clust}$ (for more details see Sections 6 and 7).

So, the $P_t 56$ spectra presented in Tables 2, 3 and 4, 5 show PYTHIA prediction that the

[17] See also the event spectra over $P_t{}^{clust}$ in Fig. 7 of the following Section 6.

[18] An increase in $P_t{}^{\gamma}$ produces the same effect, as is seen from comparison of Tables 2 and 3 and will be demonstrated in more detail in Section 6 and Appendices 2–5.

[19] We thank E. Pilon and J. Ph. Jouliet for the information about new Tevatron data on this subject and for clarifying the importance of NLO corrections and soft physics effects.

Table 2: Number of events dependence on P_t56 and $\Delta\phi_{max}$ for $40 \le Pt^{\gamma} \le 50\,GeV/c$ and $P_{tCUT}^{clust} = 30\,GeV/c$ for $L_{int} = 300\ pb^{-1}$.

P_t56 (GeV/c)	$\Delta\phi_{max}$			
	180°	17°	11°	6°
0 – 5	25859	24732	23583	20035
5 – 10	28712	27371	24597	14409
10 – 15	18899	15989	10903	5422
15 – 20	11830	6729	4399	2157
20 – 25	7542	2784	1825	900
25 – 30	5496	1642	1159	629
30 – 40	8506	2636	1800	952
40 – 50	3297	856	523	254
50 – 100	550	175	133	72
100 – 300	0	0	0	0
300 – 500	0	0	0	0
0 – 500	110691	82913	68921	44830

Table 3: Number of events dependence on P_t56 and $\Delta\phi_{max}$ for $70 \le Pt^{\gamma} \le 90\,GeV/c$ and $P_{tCUT}^{clust} = 30\,GeV/c$ for $L_{int} = 300\ pb^{-1}$.

P_t56 (GeV/c)	$\Delta\phi_{max}$			
	180°	17°	11°	6°
0 – 5	2734	2627	2506	2224
5 – 10	3318	3203	3059	2444
10 – 15	2356	2258	2081	1138
15 – 20	1680	1570	1187	579
20 – 25	1288	1072	735	354
25 – 30	1013	678	437	210
30 – 40	1150	626	421	216
40 – 50	545	265	192	109
50 – 100	768	427	300	144
100 – 300	1	0	0	0
300 – 500	0	0	0	0
0 – 500	14853	12727	10919	7418

Table 4: Number of events dependence on $\Delta\phi_{max}$ and on $P_t{}^{\gamma}$ for $L_{int} = 300\ pb^{-1}$, $P_{tCUT}^{clust} = 30\ GeV/c$ (summary).

P_t56 (GeV/c)	$\Delta\phi_{max}$			
	180°	17°	11°	6°
40 – 50	110691	82913	68921	44830
50 – 70	71075	55132	45716	29692
70 – 90	14853	12727	10919	7418
90 – 140	5887	5534	4974	3655

Table 5: Number of events dependence on P_t56 and $\Delta\phi_{max}$ for $40 \leq Pt^{\gamma} \leq 50\,GeV/c$ and $P_{tCUT}^{clust} = 5\,GeV/c$ for $L_{int} = 300\,pb^{-1}$.

P_t56 (GeV/c)	$\Delta\phi_{max}$			
	180°	17°	11°	6°
0 – 5	18462	18457	18361	16529
5 – 10	14774	14722	13881	8622
10 – 15	3195	3008	2298	1230
15 – 20	562	481	409	266
20 – 25	217	217	207	150
25 – 30	121	113	106	81
30 – 40	165	160	145	108
40 – 50	69	67	54	30
50 – 100	10	10	10	7
100 – 300	0	0	0	0
300 – 500	0	0	0	0
0 – 500	37576	37235	35473	27025

Table 6: Number of events dependence on P_t56 and $\Delta\phi_{max}$ for $70 \leq Pt^{\gamma} \leq 90\,GeV/c$ and $P_{tCUT}^{clust} = 5\,GeV/c$ for $L_{int} = 300\,pb^{-1}$.

P_t56 (GeV/c)	$\Delta\phi_{max}$			
	180°	17°	11°	6°
0 – 5	1671	1671	1670	1640
5 – 10	1553	1553	1552	1379
10 – 15	407	407	399	264
15 – 20	70	70	63	40
20 – 25	24	23	21	19
25 – 30	12	12	12	10
30 – 40	18	18	18	18
40 – 50	9	9	8	8
50 – 100	11	11	11	8
100 – 300	0	0	0	0
300 – 500	0	0	0	0
0 – 500	3773	3773	3755	3387

Table 7: Number of events dependence on $\Delta\phi_{max}$ and on $P_t{}^{\gamma}$ for $L_{int} = 300\ pb^{-1}$, $P_{tCUT}^{clust} = 5\ GeV/c$ (summary).

P_t56 (GeV/c)	$\Delta\phi_{max}$			
	180°	17°	11°	6°
40 – 50	37576	37235	35473	27025
50 – 70	19056	19017	18651	15149
70 – 90	3773	3773	3755	3387
90 – 140	1525	1525	1524	1468

ISR effect is a large one at Tevatron energies. Its P_t spectrum continues at least up to $P_t 56 = 10\ GeV/c$ in the case of P_t^{γ} (or P_t^{jet}) $\approx 90\ GeV/c$ (and up to higher values as P_t^{γ} grows) even for $P_{tCUT}^{clust} = 5\ GeV/c$. It cannot be completely suppressed by $\Delta\phi$ and P_t^{clust} cuts alone. (In Section 8 the effect of the additional P_{tCUT}^{out} will be discussed) Therefore we prefer to use the P_t balance equation for the event as a whole (see equations (16) and (28) of Sections 3.1 and 3.2), i.e. an equation that takes into account the ISR and FSR effects, rather than balance equation (2) for fundamental processes (1a) and (1b) as discussed in Section 2.1. (In Section 6 we shall study a behavior of each term that enter equation (28) in order to find the criteria that would allow to select events with a good balance of P_t^{γ} and P_t^{Jet}).

Since the last lines in Tables 2, 3 and 5, 6 contain an illustrative information on $\Delta\phi$ dependence of the total number of events, we supply these tables with the summarizing Tables 4 and 7. They include more P_t^{γ} intervals and contain analogous numbers of events that can be collected in different $\Delta\phi$ intervals for two different P_t^{clust} cuts at $L_{int} = 300\,pb^{-1}$.

5.2 P_t^{γ} and η^{γ} dependence of event rates.

Here we shall present the number of events for different P_t^{γ} and η^{γ} intervals as predicted by PYTHIA simulation with weak cuts defined mostly by (29) with only change of P_{tCUT}^{clust} value from 30 to 10 GeV/c. The lines of Table 8 correspond to P_t^{γ} intervals and the columns to η^{γ} intervals. The last column of this table contains the total number of events (at $L_{int} = 300\,pb^{-1}$) in the whole ECAL η^{γ}-region $|\eta^{\gamma}| < 2.5$ for a given P_t^{γ} interval. We see that the number of events decreases fast with growing P_t^{γ} (by more than 50% for each subsequent interval). For the fixed P_t^{γ} interval the dependence on η^{γ} is given in lines of Table 8 and illustrated by Fig. 6.

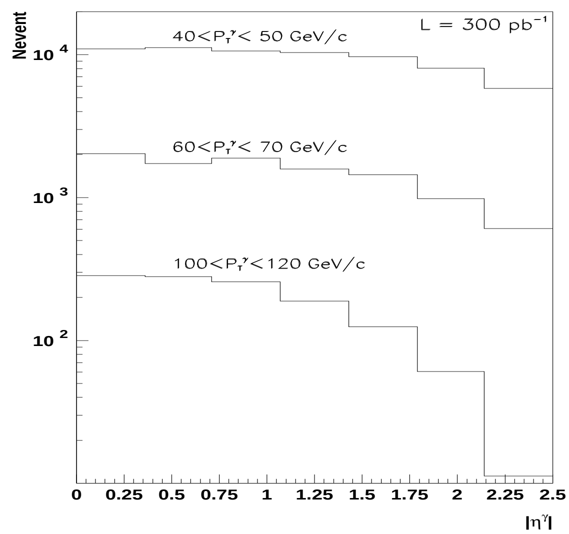

Fig. 6: η-dependence of rates for different P_t^{γ} intervals.

Table 8: Rates for $L_{int} = 300\,pb^{-1}$ for different P_t^{γ} intervals and η^{γ} ($P_{tCUT}^{clust} = 10\,GeV/c$ and $\Delta\phi \leq 17°$).

P_t^{γ}	η^{γ} intervals							all η^{γ}
(GeV/c)	0.0-0.4	0.4-0.7	0.7-1.1	1.1-1.4	1.4-1.8	1.8-2.1	2.1-2.5	0.0-2.5
40 – 50	10978	11232	10604	10337	9662	8051	5806	66679
50 – 60	4483	4210	4489	3938	3624	2814	1562	25121
60 – 70	2028	1732	1890	1587	1442	984	607	10270
70 – 80	949	931	937	753	637	392	170	4770
80 – 90	508	513	469	363	309	180	62	2405
90 –100	302	287	252	201	149	80	25	1295
100 –120	285	280	257	189	125	61	11	1207
120 –140	134	121	98	63	38	9	1	465
40 –140	19662	19302	18992	17427	15986	12571	8245	112216

5.3 Estimation of "$\gamma + Jet$" event rates for different calorimeter regions.

Since a jet is a wide-spread object, the η^{jet} dependence of rates for different P_t^{γ} intervals will be presented in a different way than in Section 5.2. Namely, Tables 9–12 include the rates of events ($L_{int} = 300\,pb^{-1}$) for different η^{jet} intervals, covered by the central, intercryostat, end and forward (CC, IC, EC and FC) parts of the calorimeter and for different $P_t^{\gamma}(\approx P_t^{Jet})$ intervals.

Table 9: Selection 1. $\Delta P_t^{jet}/P_t^{jet} = 0.00$ $\quad(P_{tCUT}^{clust} = 10\,GeV/c,\ \ \Delta\phi \leq 17^{\circ}$ and $L_{int} = 300\,pb^{-1}$).

P_t^{γ}	CC	$CC \to IC$	IC	$IC \to CC, EC$	EC	$EC \to IC, FC$	FC	$FC \to EC$
40 – 50	9965	13719	8152	22225	617	8854	554	1912
50 – 60	4009	5597	3104	8791	207	2766	109	413
60 – 70	1754	2515	1339	3615	71	979	14	93
70 – 80	930	1195	651	1593	21	348	1	23
80 – 90	503	596	328	811	9	136	0	6
90 – 100	283	352	165	421	3	59	0	1
100 – 120	263	351	137	389	2	37	0	0
120 – 140	118	143	50	142	1	7	0	0
40 – 140	17822	24462	13927	37988	930	13184	678	2448

Table 10: Selection 1. $\Delta P_t^{jet}/P_t^{jet} \leq 0.05$ $\quad(P_{tCUT}^{clust} = 10\,GeV/c,\ \ \Delta\phi \leq 17^{\circ}$ and $L_{int} = 300\,pb^{-1}$).

P_t^{γ}	CC	$CC \to IC$	IC	$IC \to CC, EC$	EC	$EC \to IC, FC$	FC	$FC \to EC$
40 – 50	17951	5733	20631	9746	4174	5296	1280	1186
50 – 60	7466	2141	8313	3583	1403	1570	253	269
60 – 70	3405	863	3553	1401	492	558	39	68
70 – 80	1699	426	1667	577	179	190	6	17
80 – 90	902	197	838	301	75	71	3	4
90 –100	528	107	440	146	31	31	0	0
100 –120	537	98	384	142	19	20	0	0
120 –140	223	37	143	48	5	3	0	0
40 –140	32701	9603	35971	15943	6377	7738	1582	1545

No restrictions on other parameters are used. The first columns of these tables CC give the number of events with the jets (found by the LUCELL jetfinding algorithm of PYTHIA), all particles of which are comprised (at the particle level of simulation) entirely (100%) in the CC part and there is a 0% sharing of P_t^{jet} ($\Delta P_t^{jet} = 0$) between the CC and the neighboring IC part of the calorimeter. The second columns of the tables $CC \to IC$ contain the number of events in which P_t of the jet is shared between the CC and IC regions. The same sequence of restriction conditions takes place in the next columns. Thus, the IC, EC and FC columns include the number of events with jets entirely contained in these regions, while the $EC \to IC, FC$ column gives the number of events where the jet covers both the EC and IC or EC and FC regions. From these tables we can see what number of events can, in principle, most suitable for the precise jet energy absolute scale setting, carried out separately for the CC, EC and FC parts of the calorimeter in different P_t^{γ} intervals.

The selection cuts are as those of Section 3.2 specified by the following values of the cut parameters:

$$P_{tCUT}^{isol} = 4\ GeV/c; \quad \epsilon_{CUT}^{\gamma} = 7\%; \quad \Delta\phi < 17^{\circ}; \quad P_{tCUT}^{clust} = 10\ GeV/c. \tag{30}$$

Table 11: Selection 2. $\Delta P_t^{jet}/P_t^{jet} = 0.00$ ($\epsilon^{jet} < 3\%, P_{tCUT}^{clust} = 10\ GeV/c, \Delta\phi \leq 17^{\circ}$ and $L_{int} = 300\,pb^{-1}$).

P_t^{γ}	CC	$CC\to IC$	IC	$IC\to CC, EC$	EC	$EC\to IC, FC$	FC	$FC\to EC$
40- 50	4274	5119	3916	8287	321	3543	261	776
50- 60	2031	2472	1766	3879	121	1215	66	194
60- 70	989	1330	852	1834	52	503	9	41
70- 80	586	663	444	923	17	192	0	14
80- 90	338	367	241	505	8	81	0	3
90-100	207	233	126	287	3	43	0	0
100-120	223	251	112	282	2	28	0	0
120-140	97	110	42	115	0	7	0	0
40-140	8743	10544	7499	16108	523	5611	337	1028

Table 12: Selection 2. $\Delta P_t^{jet}/P_t^{jet} \leq 0.05$ ($\epsilon^{jet} < 3\%, P_{tCUT}^{clust} = 10\ GeV/c, \Delta\phi \leq 17^{\circ}$ and $L_{int} = 300\,pb^{-1}$).

P_t^{γ}	CC	$CC\to IC$	IC	$IC\to CC, EC$	EC	$EC\to IC, FC$	FC	$FC\to EC$
40- 50	7384	2009	8858	3344	1912	1952	557	480
50- 60	3689	813	4157	1488	729	606	150	110
60- 70	1907	412	1991	695	305	251	23	27
70- 80	1027	223	1040	326	116	93	3	11
80- 90	598	108	572	173	47	41	2	1
90-100	375	64	320	93	23	22	0	0
100-120	408	66	295	89	14	15	0	0
120-140	179	28	118	39	5	2	0	0
40-140	15563	3724	17349	6247	3151	2983	736	630

Less restrictive conditions, when up to 5% of the jet P_t are allowed to be shared between the CC, EC and FC parts of the calorimeter, are given in Tables 10 and 12. Tables 9 and 10 correspond to the case of Selection 1. Tables 11 and 12 contain the number of events collected with Selection 2 criteria (defined in Section 3.2), i.e. they include only the events with "isolated jets" satisfying the isolation criterion $\epsilon^{jet} < 3\%$. The reduction factor of 2 for the number of events can be found by comparing those tables with Tables 9, 10. This is a cost of passing to Selection 2.

Table 9 corresponds to the most restrictive selection $\Delta P_t^{jet} = 0$ and gives the number of events most suitable for jet energy calibration. From its last summarizing line we see that for the entire interval $40 < P_t^{\gamma} < 140\ GeV/c$ PYTHIA predicts around 18000 events for CC and 1000 events for EC at integrated luminosity $L_{int} = 300\ pb^{-1}$.

An additional information on the number of "CC-events" (i.e. events, corresponding to CC column of Table 11) with jets produced by c and b quarks in gluonic subprocess (1a), i.e. $Nevent_{(c)}$ and $Nevent_{(b)}$ (given for the integrated luminosity $L_{int} = 300\ fb^{-1}$) for different $P_t^{Jet}(\approx P_t^{\gamma})$ intervals $40-50, 50-70, 70-90$ and $90-140\ GeV/c$ are contained in Tables 1–12 of Appendix 1. The ratio ("$29 sub/all$") of the number of events caused by gluonic subprocess (1a)

$(= 29sub)$, summed over quark flavours, to the number of events due to the sum of subprocesses (1a) and (1b) $(= all)$, also averaged over all quark flavours, is also shown there.

6. FEATURES OF "$\gamma + Jet$" EVENTS IN THE CENTRAL CALORIMETER REGION.

The influence of P_{tCUT}^{clust} parameter (defining the upper limit on P_t of clusters or mini-jets in the event) on the variables characterizing the ${P_t}^{\gamma} - {P_t}^{Jet}$ balance as well as on the P_t distribution in jets and out of them is studied.

In this section we shall study the specific sample of events considered in the previous section that may be most suitable for the jet energy calibration in the CC region, with jets entirely (100%) contained in this region, i.e. having 0% sharing of ${P_t}^{jet}$ (at the PYTHIA particle level of simulation) with IC. *Below we shall call them "CC-events".* The ${P_t}^{\gamma}$ spectrum for this particular set of events for ${P_t}^{clust} = 10\ GeV/c$ was presented in the first column (CC) of Table 9. Here we shall use three different jetfinders, namely, LUCELL from PYTHIA and UA1 and UA2 from CMSJET [24]. The ${P_t}^{clust}$ distributions for generated events found by the all three jetfinders in two ${P_t}^{\gamma}$ intervals, $40 < {P_t}^{\gamma} < 50\ GeV/c$ and $70 < {P_t}^{\gamma} < 90\ GeV/c$, are shown in Fig. 7 for $P_{tCUT}^{clust} = 30\ GeV/c$. It is interesting to note an evident similarity of the ${P_t}^{clust}$ spectra with P_t56 spectra (for $\Delta\phi \leq 17°$) shown in Tables 2 and 3 (see also Figs. 8, 9), what support our intuitive picture of ISR and cluster connection described in Section 2.2.

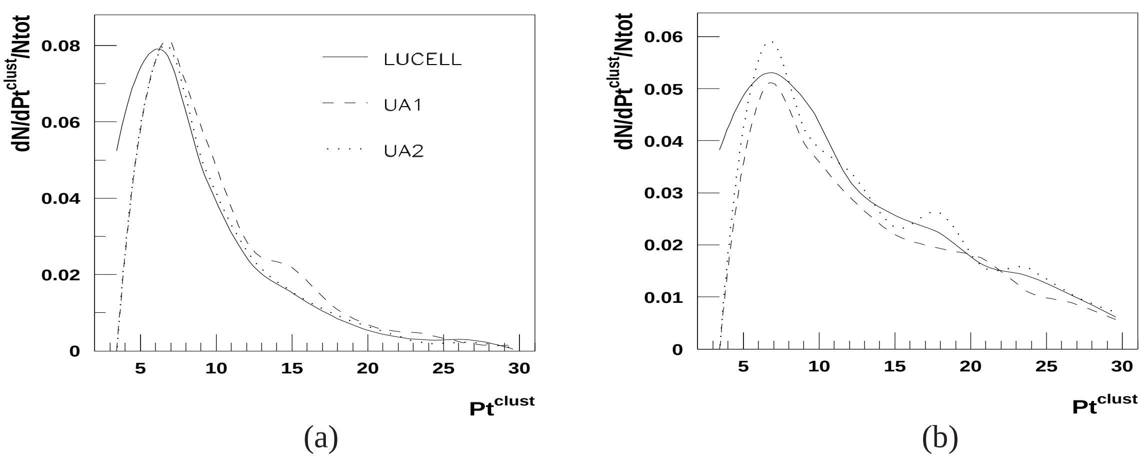

Fig. 7: ${P_t}^{clust}$ distribution in "$\gamma + Jet$" events from two ${P_t}^{\gamma}$ intervals: (a) $40 < {P_t}^{\gamma} < 50\, GeV/c$ and (b) $70 < {P_t}^{\gamma} < 90\, GeV/c$ with the same cut $P_{tCUT}^{clust} = 30\ GeV/c$ ($\Delta\phi \leq 17°$).

6.1 Influence of the P_{tCUT}^{clust} parameter on the photon and jet P_t balance and on the initial state radiation suppression.

Here we shall study in more detail correlation of ${P_t}^{clust}$ with ${P_t}^{ISR}$ mentioned above. The averaged value of intrinsic parton transverse momentum will be fixed at $\langle k_t \rangle = 0.44\ GeV/c$ [20].

The banks of 1-jet "$\gamma + Jet$" events gained from the results of PYTHIA generation of $5 \cdot 10^6$ signal "$\gamma + Jet$" events in each of four ${P_t}^{\gamma}$ intervals (40 – 50, 50 – 70, 70 – 90, 90 – 140 GeV/c) [21] will be used here. The observables defined in Sections 3.1 and 3.2 will be restricted here by Selection 1 cuts (17) – (24) of Section 3.2 and the cut parameters defined by (29).

We have chosen two of these intervals to illustrate the influence of the P_{tCUT}^{clust} parameter on the distributions of physical variables, that enter the balance equation (28). These distributions

[20] The influence of possible $\langle k_t \rangle$ variation on the ${P_t}^{\gamma} - {P_t}^{Jet}$ balance is discussed in Section 9. See also [13]–[17].
[21] they were discussed in Section 5

are shown in Fig. 8 ($40 < P_t{}^{\gamma} < 50\ GeV/c$) and Fig. 9 ($70 < P_t{}^{\gamma} < 90\ GeV/c$). In these figures, in addition to three variables P_t56, $P_t{}^{|\eta|>4.2}$, $P_t{}^{out}$, already explained in Sections 2.2, 3.1 and 3.2, we present distributions of two other variables, $P_t(O+\eta > 4.2)$ and $(1 - cos\Delta\phi)$, which define the right-hand side of equation (28). The distribution of the γ-jet back-to-back angle $\Delta\phi$ (see (22)) is also presented in Figs. 8, 9.

The ISR describing variable P_t56 (defined by formula (3)) and both components of the experimentally observable disbalance measure $(P_t{}^{\gamma}–P_t{}^{Jet})/P_t{}^{\gamma}$ (see (28)) as a sum of $(1-cos\Delta\phi)$ and $P_t(O+\eta > 4.2)/P_t{}^{\gamma}$, as well as two others, $P_t{}^{out}$ and $\Delta\phi$, show a tendency, to become smaller (the mean values and the widths) with the restriction of the upper limit on the $P_t{}^{clust}$ value (see Figs. 8, 9). It means that the jet energy calibration precision may increase with decreasing P_{tCUT}^{clust}, which justifies the intuitive choice of this new variable in Section 3. The origin of this improvement becomes clear from the P_t56 density plot, which demonstrates the decrease of P_t56 (or $P_t{}^{ISR}$) values with decrease of P_{tCUT}^{clust}. In Section 2.3 we gave arguments why it may also influence FSR.

Comparison of Fig. 8 (for $40 < P_t{}^{\gamma} < 50\ GeV/c$) and Fig. 9 (for $70 < P_t{}^{\gamma} < 90\ GeV/c$) also shows that the values of $\Delta\phi$ as a degree of back-to-backness of the photon and jet P_t vectors in the ϕ-plane decreases with increasing $P_t{}^{\gamma}$. At the same time $P_t{}^{out}$ and $P_t{}^{ISR}$ distributions become slightly wider. It is also seen that the $P_t{}^{|\eta|>4.2}$ distribution practically does not depend on $P_t{}^{\gamma}$ and $P_t{}^{clust}$ [22].

It should be mentioned that the results presented in Figs. 8 and 9 were obtained with the LUCELL jetfinder of PYTHIA [23].

6.2 P_t distribution inside and outside of a jet.

Now let us see what spatial distribution may have the P_t activity in the volume outside the jet (i.e. in the calorimeter cells outside the jet cone) in these CC "$\gamma + Jet$" events collected with the Selection 1 cuts. For this purpose we calculate a vector sum $\vec{P}_t{}^{sum}$ of individual transverse momenta of $\Delta\eta \times \Delta\phi$ cells included by a jetfinder into a jet and of cells in a larger volume that surrounds a jet. In the latter case this procedure can be viewed as straightforward enlarging of the jet radius in the $\eta - \phi$ space.

The figures that show the ratio $P_t{}^{sum}/P_t{}^{\gamma}$ as a function of the distance $R(\eta, \phi)$ counted from the jet gravity center towards its boundary and further into the space outside the jet are shown in the left-hand columns of Figs. 10 and 11 for two different $P_t{}^{\gamma}$ intervals ($40 < P_t{}^{\gamma} < 50\ GeV/c$ in Fig. 10 and the $70 < P_t{}^{\gamma} < 90\ GeV/c$ in Fig. 11).

From these figures we see that the space surrounding the jet in general, i.e. for Selection 1, is far from being an empty in the case of "$\gamma + Jet$" events considered here. We also see that an average value of the total $P_t{}^{sum}$ increases with increasing volume around the jet and it exceeds $P_t{}^{\gamma}$ at $R = 0.8 - 1.0$ (see Figs. 10 and 11).

From the right-hand columns of Figs. 10 and 11 we also see that the disbalance measure (the analog of (4))

$$P_t{}^{\gamma+sum} = \left|\vec{P}_t{}^{\gamma} + \vec{P}_t{}^{sum}\right| \tag{31}$$

achieves its minimum at $R \approx 0.9 - 1.1$ for all three jetfinding algorithms.

The value of $P_t{}^{\gamma+sum}$ continues to grow with increasing R after the point $R = 1.0$ for $40 < P_t{}^{\gamma} < 50\ GeV/c$ (see Figs. 10), while for higher $P_t{}^{\gamma}$ (see Figs. 11 for the $70 < P_t{}^{\gamma} < 90\ GeV/c$

[22] see also Appendices 2–5

[23] The results obtained with all jetfinders and $P_t{}^{\gamma} - P_t{}^{Jet}$ balance will be discussed in Section 7 in more detail.

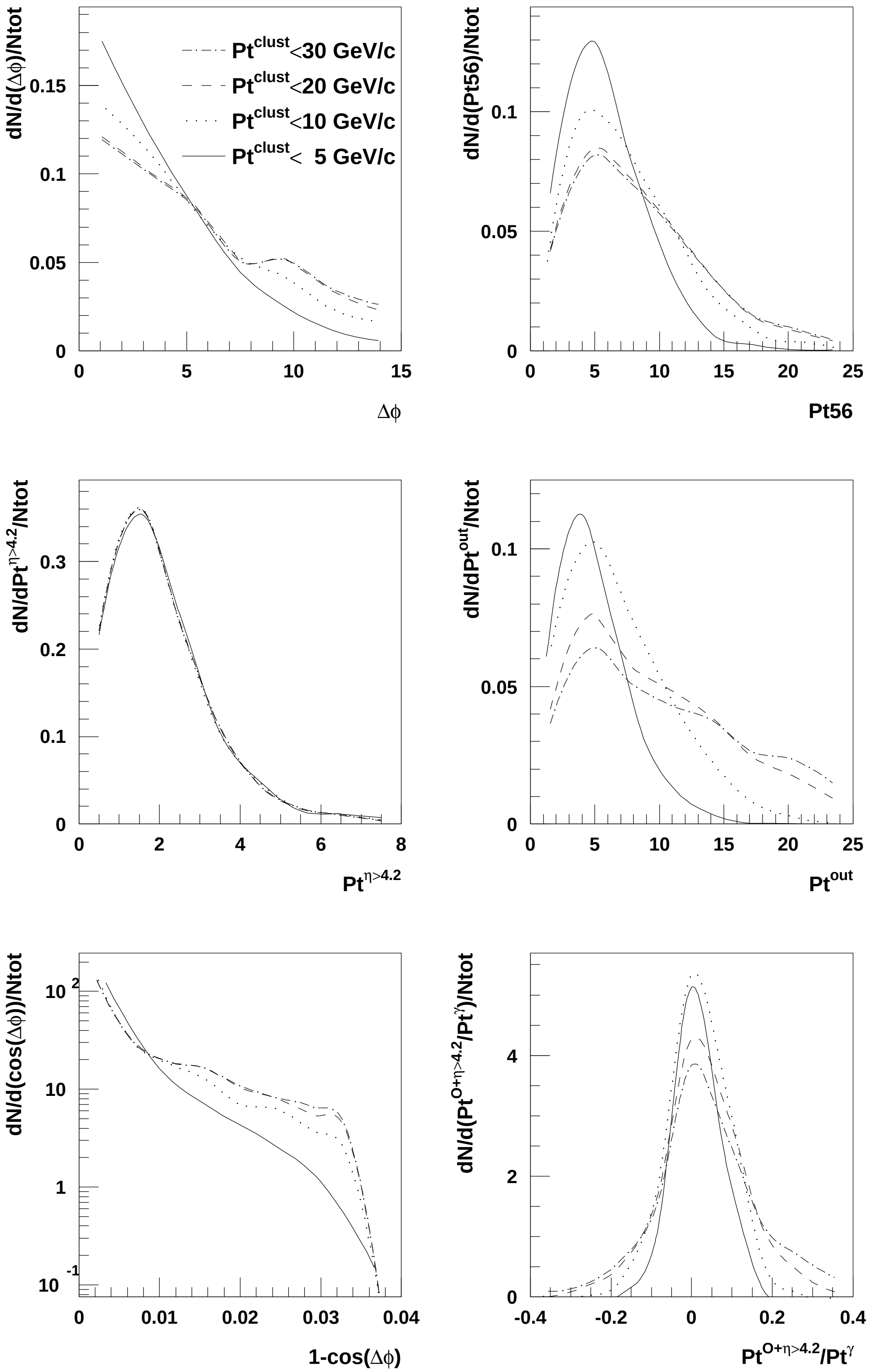

Fig. 8: LUCELL algorithm, $\Delta\phi < 17°$; $40 < {P_t}^{\gamma} < 50\,GeV/c$. Selection 1.

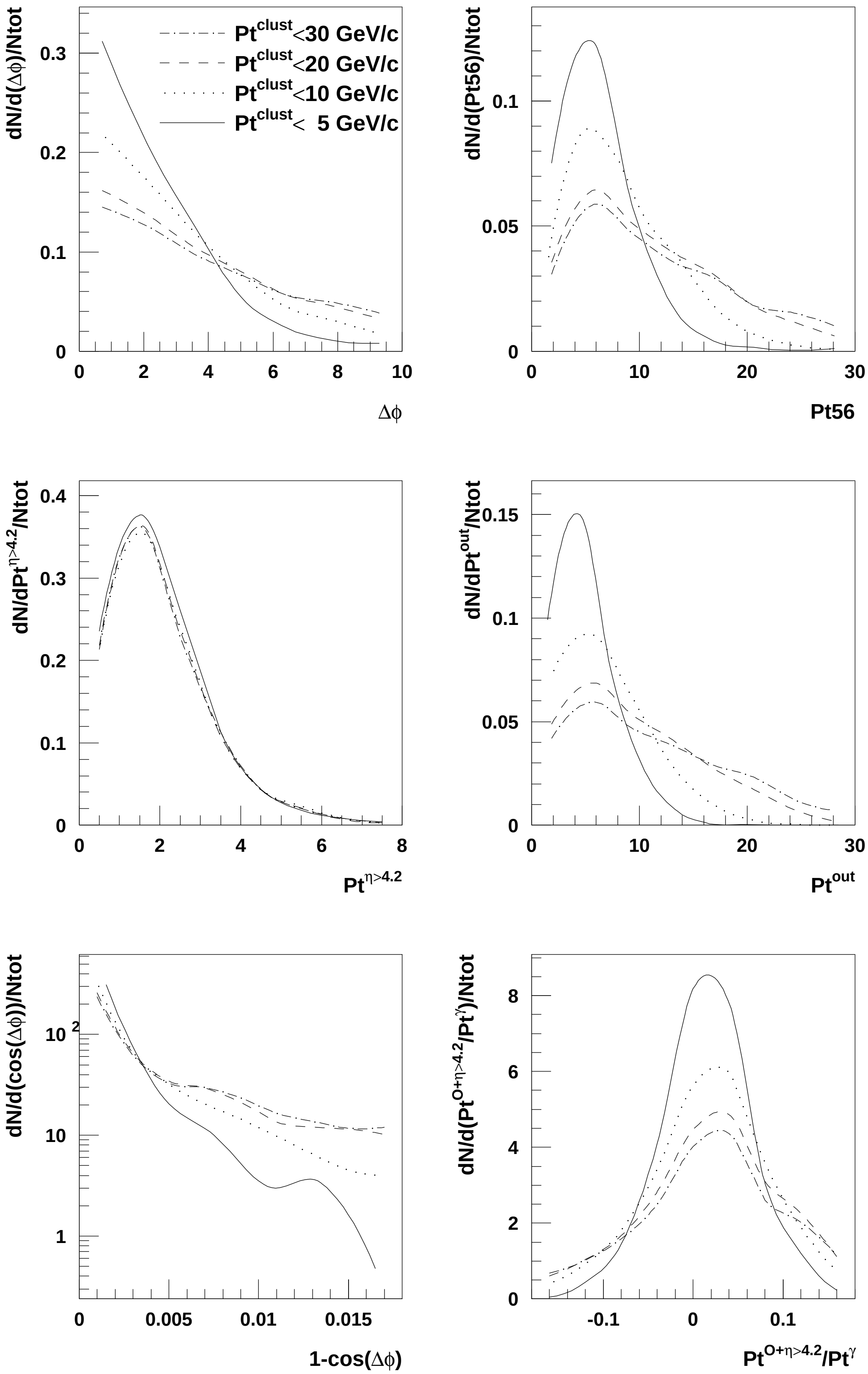

Fig. 9: LUCELL algorithm, $\Delta\phi < 17°$; $70 < {P_t}^{\gamma} < 90\,GeV/c$. Selection 1.

interval) the ratio P_t^{sum}/P_t^{γ} and the disbalance measure $P_t^{\gamma+sum}$ increase more slowly with increasing R after the point $R = 1.0$.

This means that at higher P_t^{γ} (or P_t^{Jet}) the topology of "$\gamma + Jet$" events becomes more pronounced and we get a clearer picture of an "isolated" jet. This feature clarifies the motivation of introducing following [13]–[17] the "Selection 2" criteria in Section 3.2 (see point 9) for selection of events with "isolated jets".

7. DEPENDENCE OF THE P_t-DISBALANCE IN THE "$\gamma + Jet$" SYSTEM ON P_{tCUT}^{clust} and P_{tCUT}^{out} PARAMETERS.

It is shown that with Selection 2 (that leads to about twice reduction of the number of events $Nevent$ for $P_t^{\gamma} < 70\ GeV/c$ and to about $30-40\%$ loss of them at $P_t^{\gamma} > 70\ GeV/c$) one can select (at the particle level) the events with the value of a fractional $(P_t^{\gamma} - P_t^{Jet})/P_t^{\gamma}$ disbalance better than 1%. Selection 3 leads to further about 25% reduction of $Nevent$. The number of events (at $L_{int} = 300\ pb^{-1}$) and other characteristics of "$\gamma + Jet$" events are presented in tables of Appendices 2–5 for interval $40 < P_t^{\gamma} < 140\ GeV/c$.

In the previous sections we have introduced physical variables for studying "$\gamma+Jet$" events (Section 3) and discussed what cuts for them may lead to a decrease in the disbalance of P_t^{γ} and P_t^{Jet} (Sections 6, 7). One can make these cuts to be tighter if more events would be collected during data taking.

Here we shall study in detail the dependence of the P_t disbalance in the "$\gamma + Jet$" system on P_{tCUT}^{clust} and P_{tCUT}^{out} values. For this aim we shall use the same samples of events as in Section 5 that were generated by using PYTHIA with 2 QCD subprocesses (1a) and (1b) and collected to cover four P_t^{γ} intervals: 40–50, 50–70, 70–90, 90–140 GeV/c. These events were selected with

$$P_t^{\gamma} \geq 40\ GeV/c, \quad P_t^{jet} \geq 30\ GeV/c \tag{32}$$

and with the use of the set of cut parameters defined by (29).

The dependence of the number of events (selected with above-mentioned set of cut parameters) on the value of P_{tCUT}^{clust} is shown for the case of $\Delta\phi \leq 17^{\circ}$ and for four P_t^{γ} intervals in Fig. 13 for Selection 1, in Fig. 15 for Selection 2 and in Fig. 17 for Selection 3. Each of these plots is accompanied at the same page by four additional plots that show the dependence of the fractional disbalance $(P_t^{\gamma} - P_t^{Jet})/P_t^{\gamma}$ on P_{tCUT}^{clust} in different P_t^{γ} intervals. The dependence of this ratio is presented for three different jetfinders LUCEL, UA1 and UA2 used to determine a jet in the same event. It is worth mentioning that in contrast to UA1 and LUCELL algorithms that use a fixed value of jet radius $R^{jet}(= 0.7)$, the value of R^{jet} is not restricted directly for UA2 [24] and, thus, it may take different values (see [14] and R values in Appendices 1). More details about the differences in the results of these three jetfinders application can be found in Section 6.2, Appendices 1–5 and in [25].

The normalized event distributions over $(P_t^{\gamma} - P_t^{Jet})/P_t^{\gamma}$ for two most illustrative P_t^{γ} intervals $40 < P_t^{\gamma} < 50$ and $70 < P_t^{\gamma} < 90\ GeV/c$ are shown for a case of $\Delta\phi \leq 17^{\circ}$ in Fig. 12 in different plots for three jetfinders. These plots demonstrate the dependence of the mean square deviations on P_{tCUT}^{clust} value, not shown in Fig. 14. From the comparison of Figs. 14, 16 and 18 one can easily see that passing from Selection 1 to Selection 2 and 3 allows to select events with a better balance of P_t^{γ} and P_t^{Jet} (about 1% and better) on the PYTHIA particle level. It is also

[24] The only radii defining in UA2 algorithm are cone radius for preclusters search ($= 0.4$) and cone radius for subsequent precluster dressing ($= 0.3$) (see [24]).

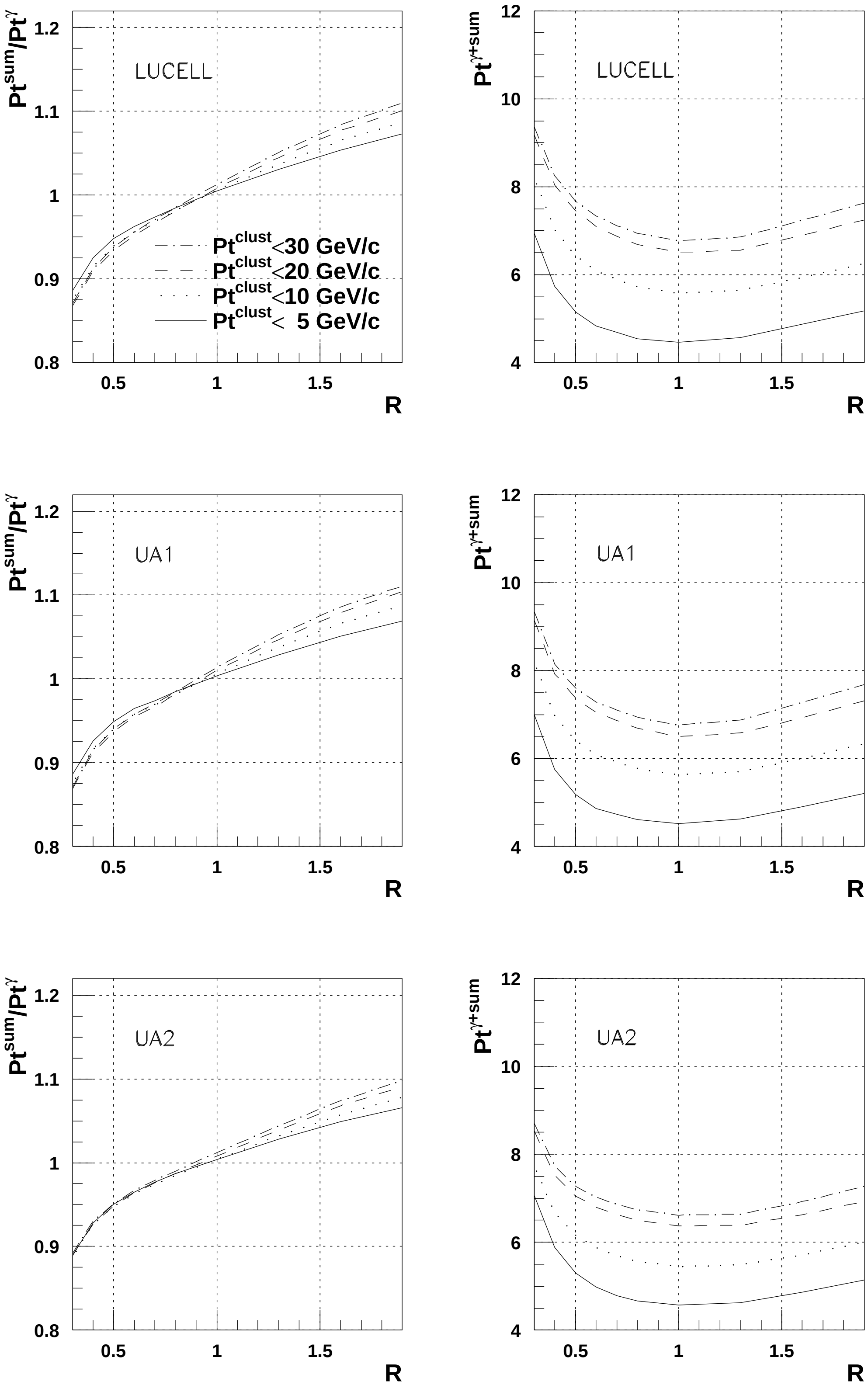

Fig. 10: LUCELL, UA1 and UA2 algorithms, $\Delta\phi < 17°$; $40 < P_t{}^{\gamma} < 50\,GeV/c$. Selection 1.

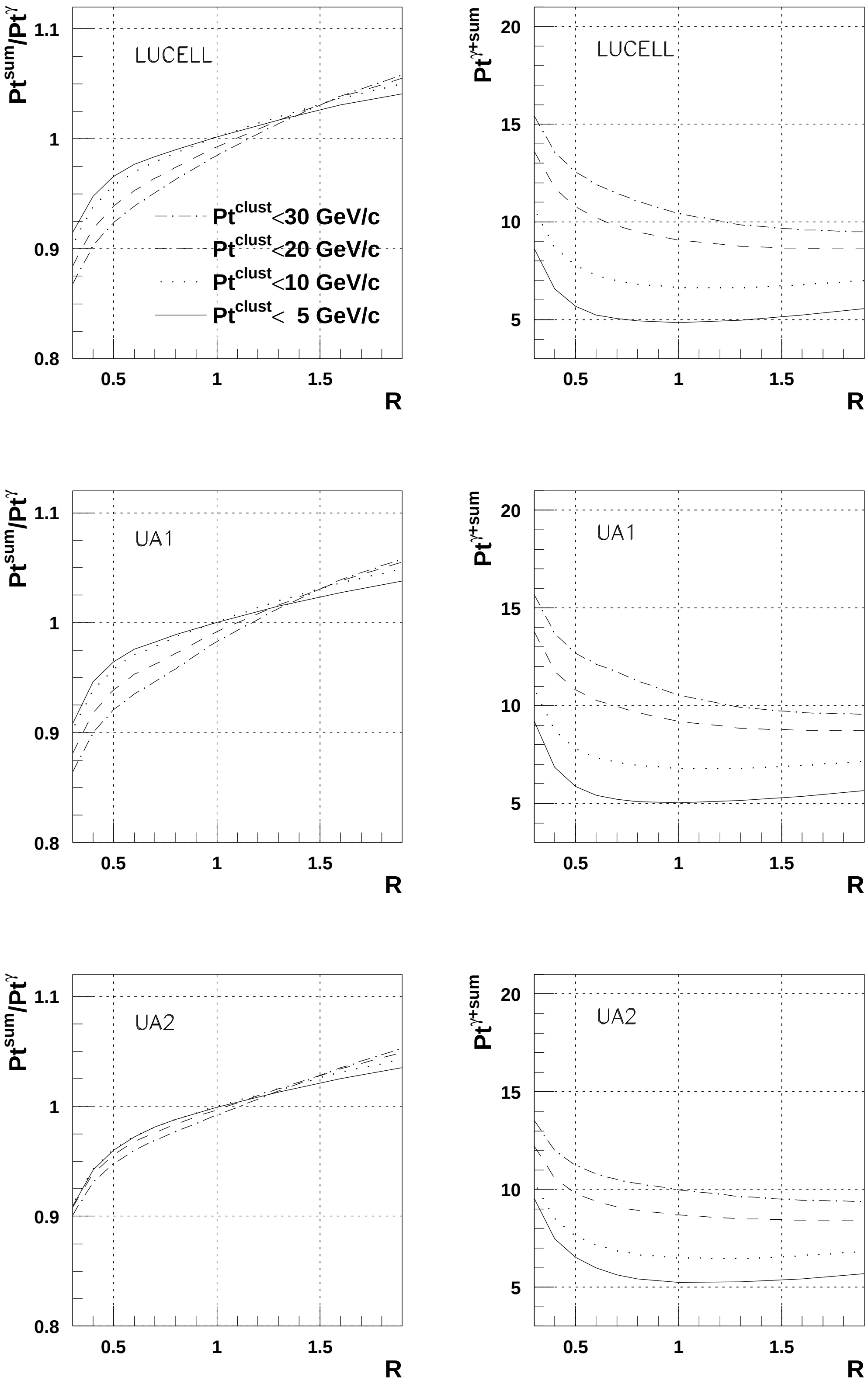

Fig. 11: LUCELL, UA1 and UA2 algorithms, $\Delta\phi < 17°$; $70 < P_t{}^{\gamma} < 90\,GeV/c$. Selection 1.

seen that in events with "isolated jets" there is no such a strong dependence on P_{tCUT}^{clust} value in the events with ${P_t}^{\gamma} > 50\ GeV/c$.

More details on P_{tCUT}^{clust} dependence of different important features of "$\gamma + Jet$" events (as predicted by PYTHIA. i.e. without account of detector effects) are presented in tables of Appendices 2 – 5. They include the information about a topology of events and mean values of most important variables that characterize ${P_t}^{\gamma} - {P_t}^{Jet}$ disbalance [25]. This information can be useful as a model guideline while performing jet energy calibration procedure and also serve for fine tuning of PYTHIA paramters while comparing its predictions with the collected data.

Appendix 2 contains the tables for events with ${P_t}^{\gamma}$ varying from 40 to $50\ GeV/c$. In these tables we present the values of interest found with the UA1, UA2 and LUCELL jetfinders [26] for three different Selections mentioned in Section 3.2. Each page corresponds to a definite value of $\Delta\phi$ (see (22)) as a measure of deviation from the absolute back-to-back orientation of two $\vec{P_t}^{\gamma}$ and $\vec{P_t}^{Jet}$ vectors.

So, Tables 1 – 3 on the first page of each of Appendices 2–5 correspond to $\Delta\phi < 180°$, i.e. to the case when no restriction on the back-to-back $\Delta\phi$ angle is applied. Tables 4–6 on the second page correspond to $\Delta\phi < 17°$. The third and fourth pages correspond to $\Delta\phi < 11°$ and $\Delta\phi < 6°$ respectively.

The first four pages of each Appendix contain information about variables that characterize the ${P_t}^{\gamma}$ – ${P_t}^{Jet}$ balance for Selection 1, i.e. when only cuts (17)–(24) of Section 3.2 are used.

On the fifth page of each of Appendices 2–5 we present Tables 13 – 15 for the cut $\Delta\phi < 17°$ that correspond to Selection 2 described in Section 3.2. Selection 2 differs from Selection 1 presented in Tables 1 – 12 by addition of cut (25). It allows one to select events with the "isolated jet", i.e. events with the total P_t activity in the $\Delta R = 0.3$ ring around the jet not exceeding 3% of jet P_t [27]. The results obtained with Selection 3 [28] are given on the sixth page of Appendices 2–5.

The columns in all Tables 1 – 18 correspond to five different values of cut parameter $P_{tCUT}^{clust} = 30,\ 20,\ 15,\ 10$ and $5\ GeV/c$. The upper lines of Tables 1 – 15 in Appendices 2–5 contain the expected numbers N_{event} of "CC events" (i.e. the number of signal "$\gamma + Jet$" events in which the jet is entirely fitted into the CC region of the calorimeter; see Section 5) for the integrated luminosity $L_{int} = 300\ pb^{-1}$.

In the next four lines of the tables we put the values of $P_t 56$, $\Delta\phi$, ${P_t}^{out}$ and ${P_t}^{|\eta|>4.2}$ defined by formulae (3), (22), (24) and (5) respectively and averaged over the events selected with a chosen P_{tCUT}^{clust} value.

From the tables we see that the values of $P_t 56$, $\Delta\phi$, ${P_t}^{out}$ decrease fast with decreasing P_{tCUT}^{clust}, while the averaged values of ${P_t}^{|\eta|>4.2}$ show very weak dependence on it (practically constant) [29].

The following three lines (from 6-th to 8-th) present the average values of the variables $({P_t}^{\gamma} - {P_t}^{part})/{P_t}^{\gamma}$, $({P_t}^{J} - {P_t}^{part})/{P_t}^{J}$, $({P_t}^{\gamma} - {P_t}^{J})/{P_t}^{\gamma}$ (here J≡Jet) that serve as the measures

[25] Please note that the information about averaged values of jet radius as well as ${P_t}^{miss}$ and non-detectable content of a jet is included in the tables of Appendix 1 for the same ${P_t}^{\gamma}$ intervals.

[26] the first two are taken from CMSJET fast Monte Carlo program [24]

[27] In contrast to the case of LHC energies, where we required in Selection 2 $\epsilon^{jet} \leq 6 - 8\%$ for $40 < {P_t}^{\gamma} < 50$ (see [25]), at FNAL energies, due to less P_t activity in the space beyond the jet, one can impose the tighter cut $\epsilon^{jet} \leq 3\%$.

[28] Selection 3 (see Section 3.2, point 10) leaves only those events in which jets are found simultaneously by UA1, UA2 and LUCELL jetfinders i.e. events with jets having up to a good accuracy equal coordinates of the center of gravity, ${P_t}^{jet}$ and $\phi_{(\gamma,\ jet)}$.

[29] Compare also with Figs. 8 and 9.

of the P_t disbalance in the "$\gamma + parton$" and "$\gamma + Jet$" systems as well as the measure of the parton-to-hadrons (Jet) fragmentation effect.

The 9-th and 10-th lines include the averaged values of $P_t(O\!+\!\eta > 4.2)/P_t^{\gamma}$ and $(1 - cos(\Delta\phi))$ quantities that appear on the right-hand side of equation (28) that has the meaning of the scalar variant of vector equation (16) for the total transverse momentum conservation in a physical event.

After application of the cut $\Delta\phi < 17^{\circ}$ the value of $\langle 1 - cos(\Delta\phi)\rangle$ becomes smaller than the value of $\langle P_t(O\!+\!\eta > 4.2)/P_t^{\gamma}\rangle$ in the case of Selection 1 and tends to decrease faster with growing energy[22,29]. So, we can conclude that the main contribution into the P_t disbalance in the "$\gamma + Jet$" system, as defined by equation (28), comes from the term $P_t(O\!+\!\eta > 4.2)/P_t^{\gamma}$, while in Selections 2 and 3 the contribution of $\langle P_t(O\!+\!\eta > 4.2)/P_t^{\gamma}\rangle$ reduces with growing P_t^{clust} to the level of that of $\langle 1 - cos(\Delta\phi)\rangle$ and even to smaller values.

We have estimated separately the contributuions two terms $\vec{P}_t^{\,O} \cdot \vec{n}^{Jet}$ and $\vec{P}_t^{\,|\eta|>4.2} \cdot \vec{n}^{Jet}$ (with $\vec{n}^{Jet} = \vec{P}_t^{\,Jet}/P_t^{Jet}$, see (28)) that enter $P_t(O\!+\!\eta > 4.2)$. Firstly from tables it is easily seen that $P_t^{|\eta|>4.2}$ has practically the same value in all P_t^{γ} intervals and it does not depend neither on $\Delta\phi$ nor on P_t^{clust} values being equal to $2\ GeV/c$ up to a good precision. Let us emphasize that it is a prediction of PYTHIA. $\vec{P}_t^{\,|\eta|>4.2} \cdot \vec{n}^{Jet}$ contribution is also practically constant ($\approx 0.6\ GeV/c$) and also does not depend on P_t^{γ} or P_t^{clust}. The value of the fraction $\vec{P}_t^{\,|\eta|>4.2} \cdot \vec{n}^{Jet}/P_t^{\gamma}$ is 0.015 at $40 < P_t^{\gamma} < 50\ GeV/c$ and decreases to 0.008 at $70 < P_t^{\gamma} < 90\ GeV/c$ (and to 0.006 at $90 < P_t^{\gamma} < 140\ GeV/c$). Among these two terms the first one, $\vec{P}_t^{\,O} \cdot \vec{n}^{Jet}$, is a measurable one (its value can be found from the numbers in lines with $P_t(O\!+\!\eta > 4.2)$). Below in this section the cuts on the value of P_t^{out} is applied to select events with better P_t^{γ} and P_t^{Jet} balance.

The following two lines contain the averaged values of the standard deviations $\sigma(Db[\gamma, J])$ and $\sigma(Db[\gamma, part])$ of $(P_t^{\gamma} - P_t^{J})/P_t^{\gamma} (\equiv\ Db[\gamma, J])$ and $(P_t^{\gamma} - P_t^{part})/P_t^{\gamma} (\equiv\ Db[\gamma, part])$ respectively. These two variables drop approximately by about 50% (and even more for $P_t^{\gamma} > 70\ GeV/c$) as one goes from $P_{tCUT}^{clust} = 30\ GeV/c$ to $5\ GeV/c$ for all P_t^{γ} intervals and for all jetfinding algorithms.

The last lines of the tables present the number of generated events (i.e. entries) left after cuts.

Three features are clearly seen from these tables:

(1) after passing from tables with $\Delta\phi \leq 180^{\circ}$ to those with $\Delta\phi \leq 17^{\circ}$, the $\Delta\phi$ cut, supposed to be most effective in low P_t^{γ} intervals, does not affect the $(P_t^{\gamma} - P_t^{Jet})/P_t^{\gamma}$ disbalance strongly as compared with "jet isolation" criterion or cut on P_t^{clust};

(2) in events with $\Delta\phi < 17^{\circ}$ the fractional disbalance on the *parton-photon* level $(P_t^{\gamma} - P_t^{part})/P_t^{\gamma}$ reduces to about 1% (or even less) after imposing $P_t^{clust} < 10\ GeV/c$. It means that $P_{tCUT}^{clust} = 10\ GeV/c$ is really effective for ISR suppression as it was supposed in Section 3.1.

(3) *parton-to-jet* hadronization/fragmentation effect, that includes also FSR, can be estimated by the value of the following ratio $(P_t^{J} - P_t^{part})/P_t^{J}$. It always has a negative value. It means that a jet loses some part of the parent parton transverse momentum P_t^{part}. It is seen that in the case of Selection 1 this effect gives a big contribution into P_t^{γ} and P_t^{Jet} disbalance even after application of $P_{tCUT}^{clust} = 10\ GeV/c$. The value of the fractional $(P_t^{J} - P_t^{part})/P_t^{J}$ disbalance does not vary strongly with P_{tCUT}^{clust} in the cases of Selections 2 and 3.

We also see from the tables that more restrictive cuts on the observable P_t^{clust} lead to a decrease in the values of $P_t 56$ variable (non-observable one) that serves, according to (3), as a measure of the initial state radiation transverse momentum P_t^{ISR}, i.e. of the main source of the

P_t disbalance in the fundamental $2 \to 2$ subprocesses (1a) and (1b). Thus, variation of P_{tCUT}^{clust} from $30\ GeV/c$ to $5\ GeV/c$ (for $\Delta\phi < 17^\circ$) leads to suppression of the P_t56 value (or P_t^{ISR}) approximately by 40% for $40 < P_t^{\gamma} < 50\ GeV/c$ and by $\approx 60\%$ for $P_t^{\gamma} \geq 90\ GeV/c$.

In the first three intervals with $P_t^{\gamma} < 90\ GeV/c$ the decrease in P_{tCUT}^{clust} leads to some decrease in the $(P_t^{\gamma} - P_t^{J})/P_t^{\gamma}$ ratio. In the case of $90 < P_t^{\gamma} < 140\ GeV/c$ (for $\Delta\phi < 17^\circ$) the mean value of $(P_t^{\gamma} - P_t^{J})/P_t^{\gamma}$ drops from $3.9-4.2\%$ to $1.1-1.3\%$ (see Tables 4, 6 of Appendix 5). But the value of the fractional disbalance is higher than 1%. After we pass to Selections 2 and 3 this disbalance becomes of the 1% level and smaller but at the cost of statistics loss (by about $40-60\%$). Tables 13–18 clearly show the prediction of PYTHIA about the best level of jet calibration precision that can be achieved after application of Selections 2 and 3 and with the use of the above-mentioned jet finding algorithms. The difference in the fractional disbalance $(P_t^{\gamma} - P_t^{Jet})/P_t^{\gamma}$ caused by their applications defines one of parts of systematical error of the calibration procedure.

Thus, to summarize the results presented in tables of Appendices 2–5, we want to underline that only after imposing the jet isolation requirement (see Tables 13 – 15 of Appendices 2–5) the mean values of P_t^{γ} and P_t^{Jet} disbalance, i.e. $(P_t^{\gamma} - P_t^{J})/P_t^{\gamma}$, for all P_t^{γ} intervals are contained inside the 1% window for any $P_t^{clust} \leq 20\ GeV/c$. The reduction of P_t^{clust} leads to lower values of mean square deviations of the photon-parton $Db[\gamma, part]$ and of photon-jet $Db[\gamma, J]$ balances. The Selection 2 (with $P_{tCUT}^{clust} = 10\ GeV/c$, for instance) leaves after its application the following number of events with jets *entirely contained* (see Section 5) *in the CC region* (at $L_{int} = 300\ pb^{-1}$):
(1) about 4000 for $40 < P_t^{\gamma} < 50\ GeV/c$, (2) about 3000 for $50 < P_t^{\gamma} < 70\ GeV/c$,
(3) about 850 for $70 < P_t^{\gamma} < 90\ GeV/c$ and (4) about 500 for the $90 < P_t^{\gamma} < 140\ GeV/c$.

The analogous results for Selection 3 are presented in Tables 16–18 of Appendices 2–5. This selection leads to approximately $25-30\%$ further reduction of the number of selected events as compared with Selection 2 and practically does not change values of the $P_t^{\gamma} - P_t^{Jet}$ balance and other variables, presented in Tables 13–15. The advantage of Selection 3 is that it includes only events containing jets simultaneously found by all three used jetfinders.

So, we can say that Selections 2 and 3, besides improving the $P_t^{\gamma} - P_t^{Jet}$ balance value, are also important for selecting events with a clean jet topology and for rising the confidence level of a jet determination.

Up to now we have been studying the influence of the P_{tCUT}^{clust} parameter on the balance. Let us see, in analogy with Fig. 12, what effect is produced by P_{tCUT}^{out} variation [30].

If we constrain this variable to 5 GeV/c, keeping P_t^{clust} slightly restricted by $P_{tCUT}^{clust} = 30\ GeV/c$ (practically unbound), then, as can be seen from Fig. 19, the mean and RMS values of the $(P_t^{\gamma} - P_t^{J})/P_t^{\gamma}$ in the case of the LUCELL algorithm in the case of $40 < P_t^{\gamma} < 50\ GeV/c$ decrease from 3.6% to 1.3% and from 14.5% to 7.1%, respectively. For $70 < P_t^{\gamma} < 90\ GeV/c$ the mean and RMS values drop from 4.5% to 0.7% and from 11.5% to 3.7% respectively. From these plots we also may conclude that variation of P_{tCUT}^{out} improves the disbalance, in fact, in the same way as the variation of P_{tCUT}^{clust}. It is not surprising as the cluster P_t activity is a part of the P_t^{out} activity.

The influence of the P_{tCUT}^{out} variation (with the fixed value $P_{tCUT}^{clust} = 10\ GeV/c$) on the distribution of $(P_t^{\gamma} - P_t^{J})/P_t^{\gamma}$ is shown in Fig. 20 for Selection 1. In this case the mean value of $(P_t^{\gamma} - P_t^{J})/P_t^{\gamma}$ drops from 3.2% to 1.3% for LUCELL and from 2.7% to 1.3% for UA2

[30] This variable enters into the expression $P_t(O+\eta > 4.2)/P_t^{\gamma}$, which makes a dominant contribution to the right-hand side of P_t balance equation (28), as we mentioned above.

algorithms for the $40 < {P_t}^{\gamma} < 50\ GeV/c$ interval. At the same time the RMS value changes from 12% to 7% for all algorithms. For interval $70 < {P_t}^{\gamma} < 90\ GeV/c$ the mean value of fractional disbalance $({P_t}^{\gamma} - {P_t}^{J})/{P_t}^{\gamma}$ decrease to less then 1% at $P_{tCUT}^{out} = 5\ GeV/c$ (and to $1.1 - 1.4\%$ at $P_{tCUT}^{out} = 10\ GeV/c$). Simultaneously, RMS decreases to about 3.7% for all three jetfinders. More detailed study of P_{tCUT}^{out} influence on the $({P_t}^{\gamma} - {P_t}^{Jet})/{P_t}^{\gamma}$ disbalance will be continued in the following Section 8 (see also Appendix 6).

So, we conclude basing on the analysis of PYTHIA simulation (as a model) that the new cuts P_{tCUT}^{clust} and P_{tCUT}^{out} introduced in Section 3 as well as introduction of a new object, the "isolated jet", are found as those that may be very efficient tools to improve the jet calibration accuracy [31]. Their combined usage for this aim and for the background suppression will be a subject of a further more detailed study in Section 8.

The results of our preliminary estimation of the number of "$\gamma + Jet$" events taken in D0 Run II experiment during January 2002 and satisfying the discussed above cuts on ${P_t}^{clust}$ and ${P_t}^{out}$ can be found in our talk at QCD group [27].

Some comments have to be added about the impact of $\Delta\phi$ cut onto the P_t disbalance. Let us consider the case of Selection 1. In this case, as one can easily see from Appendices 2–5, the restriction of $\Delta\phi$ leads to improving of the positive $({P_t}^{\gamma} - {P_t}^{part})/{P_t}^{\gamma}$ disbalance for all jetfinders. For the low ${P_t}^{\gamma}$ interval (${P_t}^{\gamma} < 50\ GeV/c$), as one can see from Appendix 2, the application of $\Delta\phi$ cut alone, i.e. for the fixed value of $P_{tCUT}^{clust} = 30\ GeV/c$, allows to reduce the fractional disbalance ${P_t}^{\gamma} - {P_t}^{part}$ to the level less than 1% for LUCELL and UA1 jetfinders. In a case of UA2 this disbalance became less than 1% already after the first cut $\Delta\phi < 17^{\circ}$. As for higher ${P_t}^{\gamma}$ intervals, the P_{tCUT}^{clust} becomes more effective than the $\Delta\phi$ cut for the ${P_t}^{\gamma} - {P_t}^{part}$ disbalance improvement mainly due to the presence of more energetic clusters in an event at higher ${P_t}^{\gamma}$.

Now let us turn to a case of Selections 2 and 3. If we look at the corresponding Tables 13–18 of Appendices 2–5, we can find out that in events with isolated jet the sign of $({P_t}^{\gamma} - {P_t}^{part})/{P_t}^{\gamma}$ disbalance has a negative value. It was mentioned previously that for all ${P_t}^{\gamma}$ intervals the hadronization effect $({P_t}^{J} - {P_t}^{part})/{P_t}^{J}$ has also negative value. Thus, the "negative sign" parton-to-jet hadronization effect compensates partially the $({P_t}^{\gamma} - {P_t}^{part})/{P_t}^{\gamma}$ disbalance when passing to the photon–jet final state P_t disbalance $({P_t}^{\gamma} - {P_t}^{Jet})/{P_t}^{\gamma}$ as ${P_t}^{Jet} < {P_t}^{part}$ (compare three corresponding lines with disbalance values in Tables 13–18).

So, diminishing $({P_t}^{\gamma} - {P_t}^{part})/{P_t}^{\gamma}$ disbalance by restricting P_{tCUT}^{clust} and keeping in mind that the hadronization effect practically rather weakly depends on P_{tCUT}^{clust} we can get in the line $({P_t}^{\gamma} - {P_t}^{Jet})/{P_t}^{\gamma}$ of Tables 13–18 the achieved values of final state photon–jet disbalance.

The extreamly strong cut $P_{tCUT}^{clust} = 5\ GeV/c$, as it is seen from Tables 13–18, leads to a very small value of $({P_t}^{\gamma} - {P_t}^{part})/{P_t}^{\gamma}$ disbalance. It means that we have chosen the events with a good balance at the parton level, i.e. those really corresponding to LO diagrams, shown in Fig. 1 of Section 2. In this case the parton-to-jet hadronization effect, that practically is not affected by P_{tCUT}^{clust}, naturally leads to worsening $({P_t}^{\gamma} - {P_t}^{Jet})/{P_t}^{\gamma}$ disbalance at $P_{tCUT}^{clust} < 10\ GeV/c$ as is seen from Figs. 16 and 18.

[31] We plan to continue this study on the level of the full event reconstruction after D0GSTAR simulation.

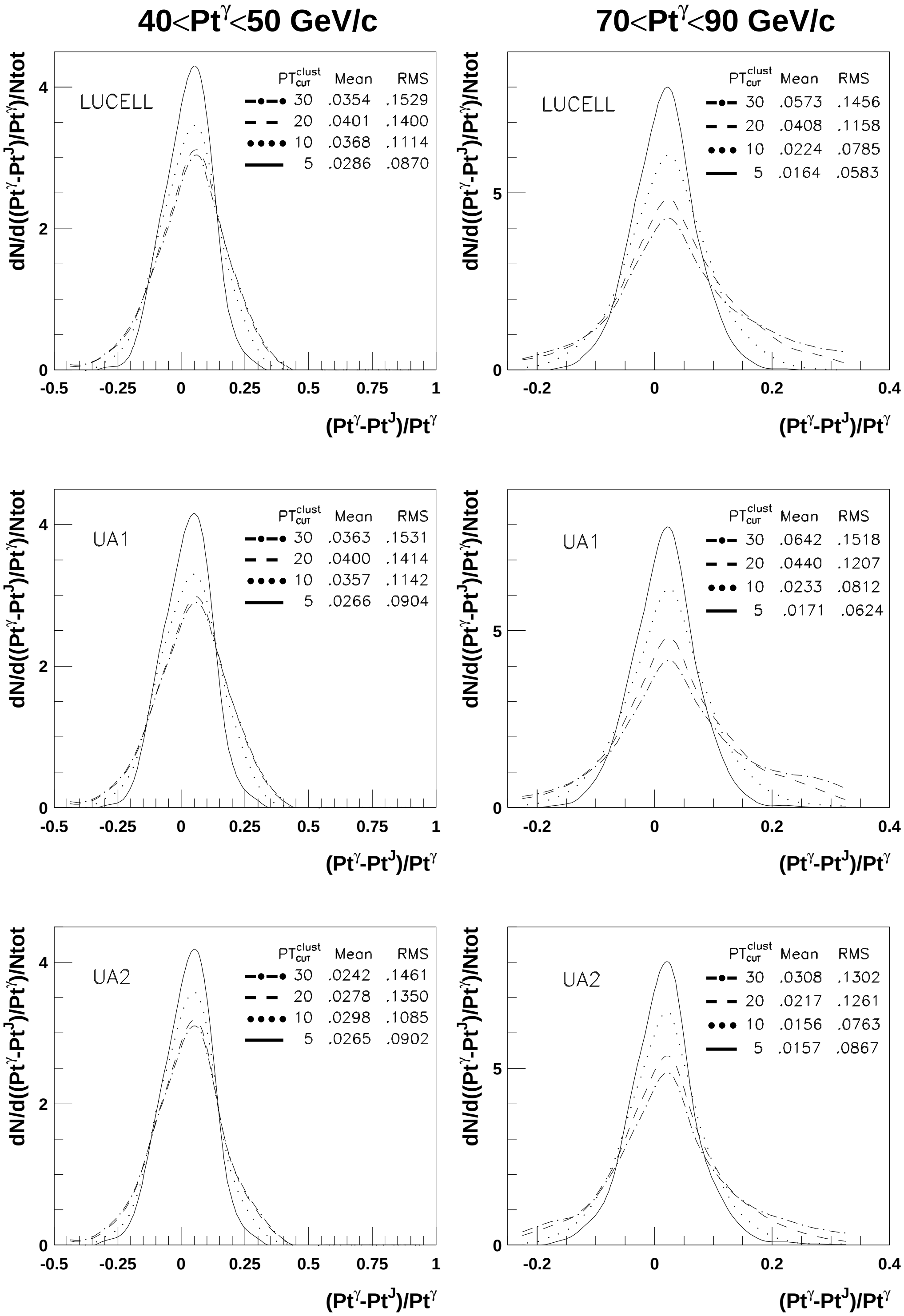

Fig. 12: A dependence of $(P_t{}^{\gamma} - P_t{}^{J})/P_t{}^{\gamma}$ on P_{tCUT}^{clust} for LUCELL, UA1 and UA2 jetfinding algorithms and two intervals of $P_t{}^{\gamma}$. The mean and RMS of the distributions are displayed on the plots. $\Delta\phi < 17^{\circ}$. $P_t{}^{out}$ is not limited. Selection 1.

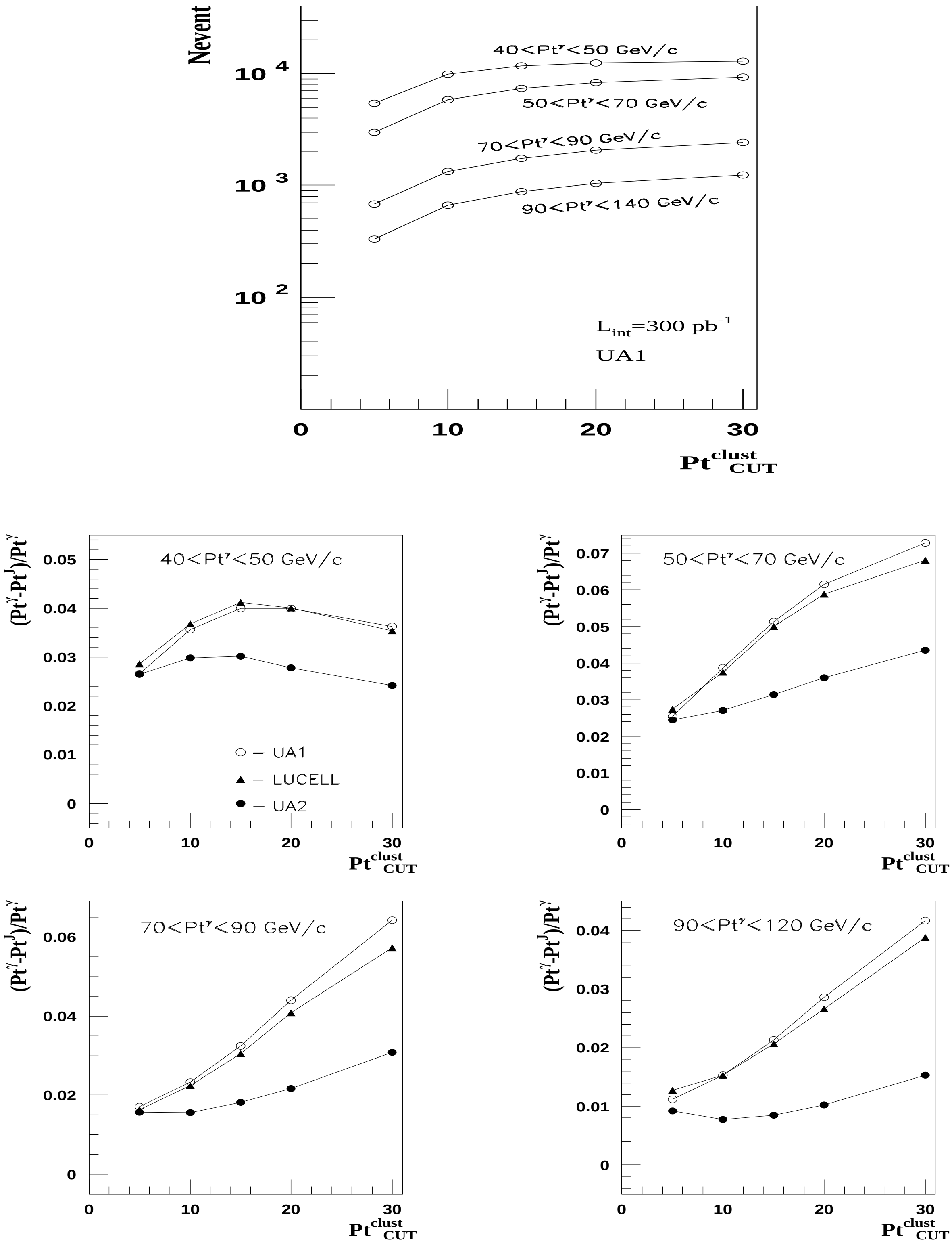

Selection 1. Dependence of the number of events for $L_{int} = 300\,pb^{-1}$ (Fig. 13, top) and $(P_t{}^{\gamma} - P_t{}^{J})/P_t{}^{\gamma}$ (Fig. 14, four bottom plots) on P_{tCUT}^{clust} in cases of LUCELL, UA1 and UA2 jetfinding algorithms. $\Delta\phi \leq 17^{\circ}$. $P_t{}^{out}$ is not limited.

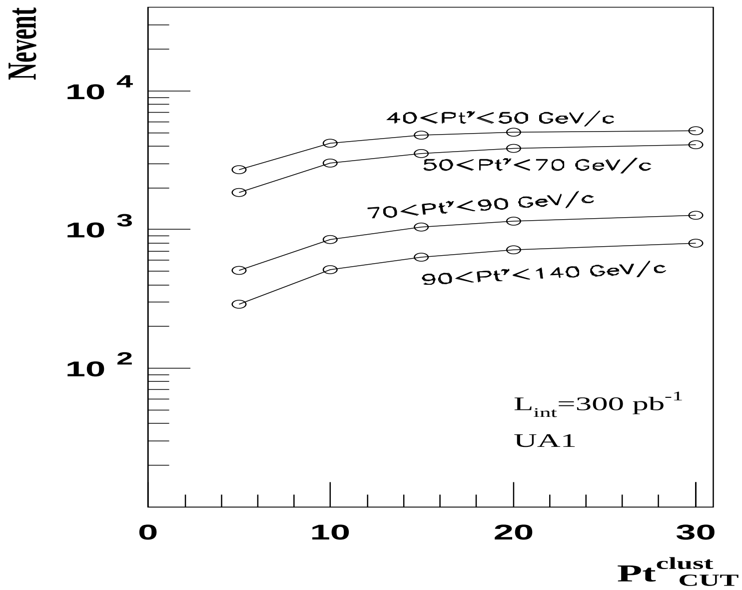

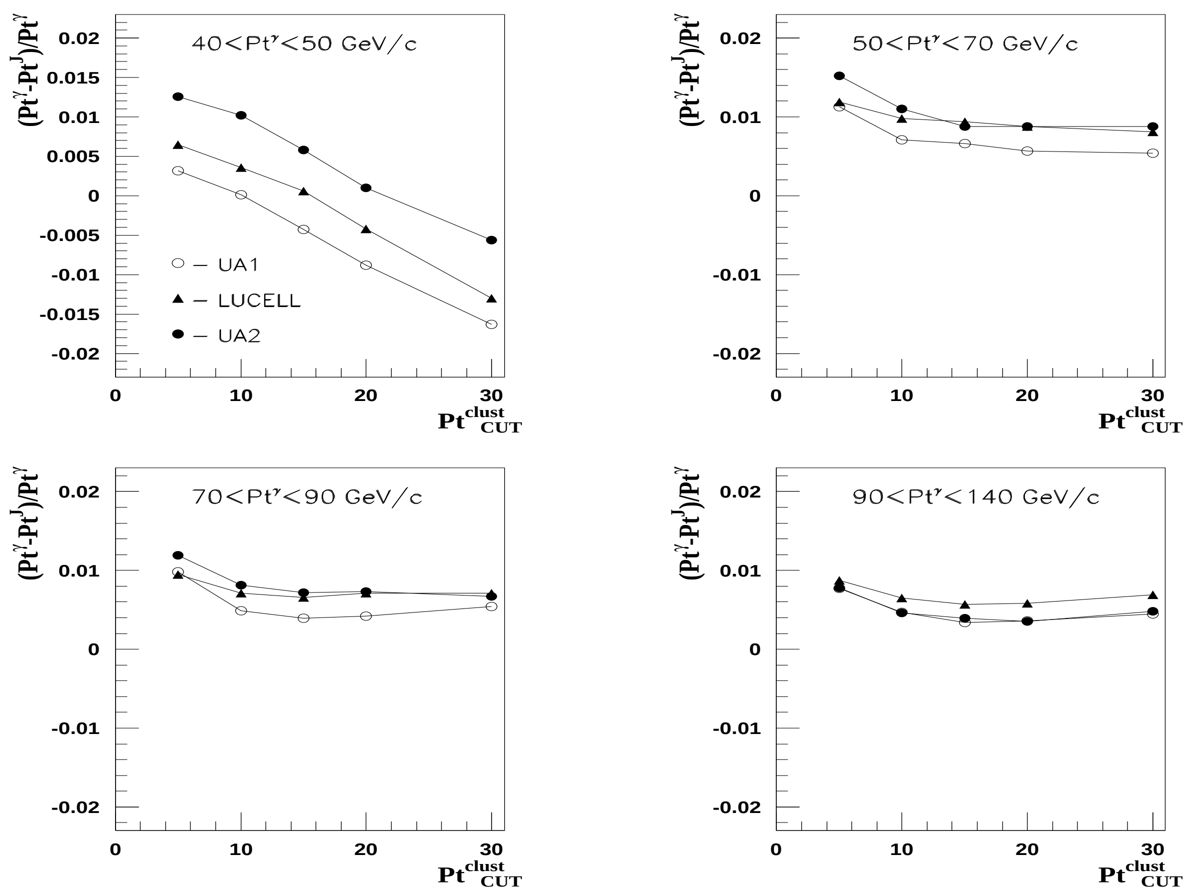

Selection 2. Dependence of the number of events for $L_{int} = 300\ pb^{-1}$ (Fig. 15, top) and $(P_t{}^{\gamma} - P_t{}^{J})/P_t{}^{\gamma}$ (Fig. 16, four bottom plots) on P_{tCUT}^{clust} in cases of LUCELL, UA1 and UA2 jetfinding algorithms. $\Delta\phi \leq 17°$. $P_t{}^{out}$ is not limited. $\epsilon^{jet} < 3\%$.

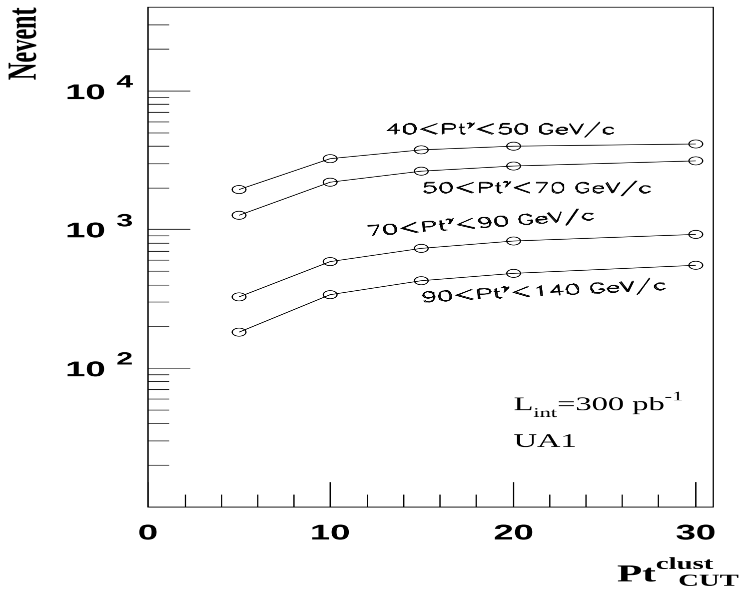

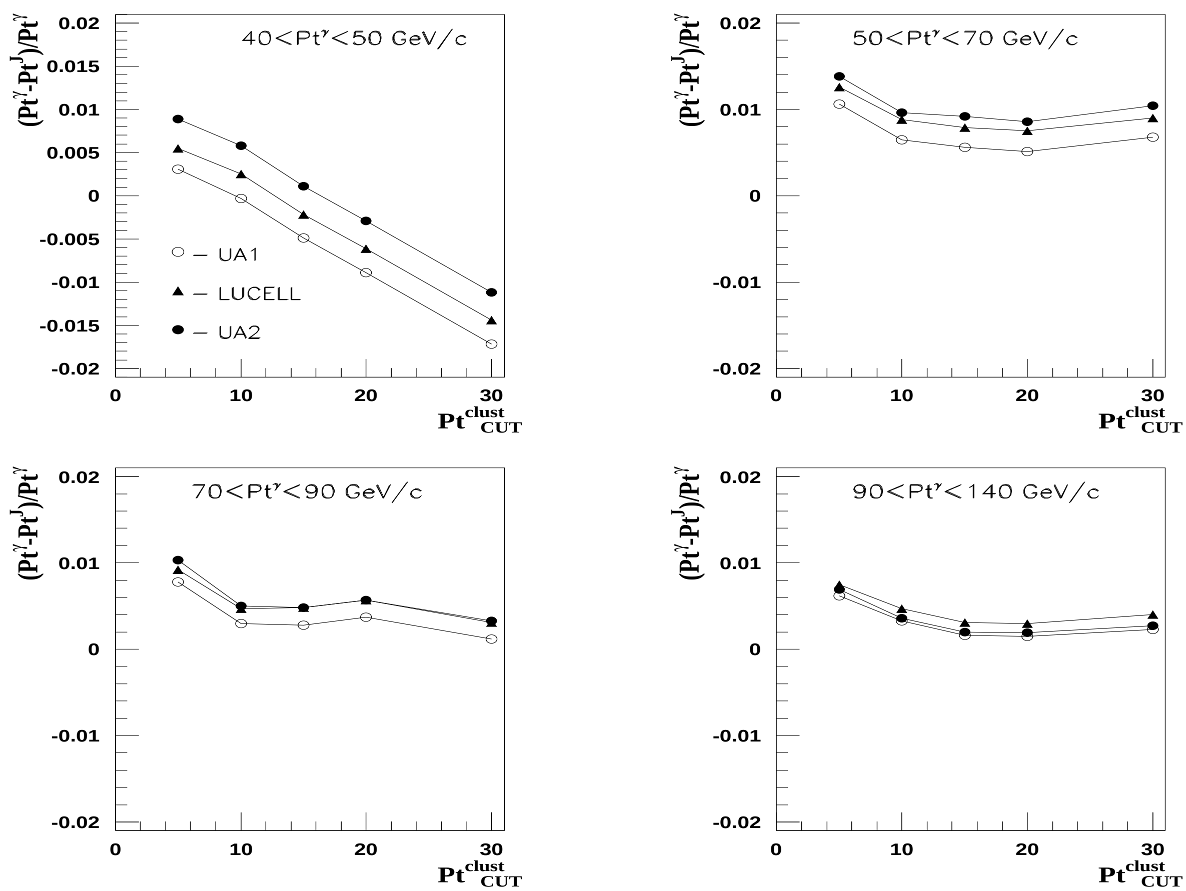

Selection 3. Dependence of the number of events for $L_{int} = 300pb^{-1}$ (Fig. 17, top) and $(P_t{}^{\gamma} - P_t{}^{J})/P_t{}^{\gamma}$ (Fig. 18, four bottom plots) on P_{tCUT}^{clust} in cases of LUCELL, UA1 and UA2 jetfinding algorithms. $\Delta\phi \leq 17^{\circ}$. $P_t{}^{out}$ is not limited. $\epsilon^{jet} < 3\%$.

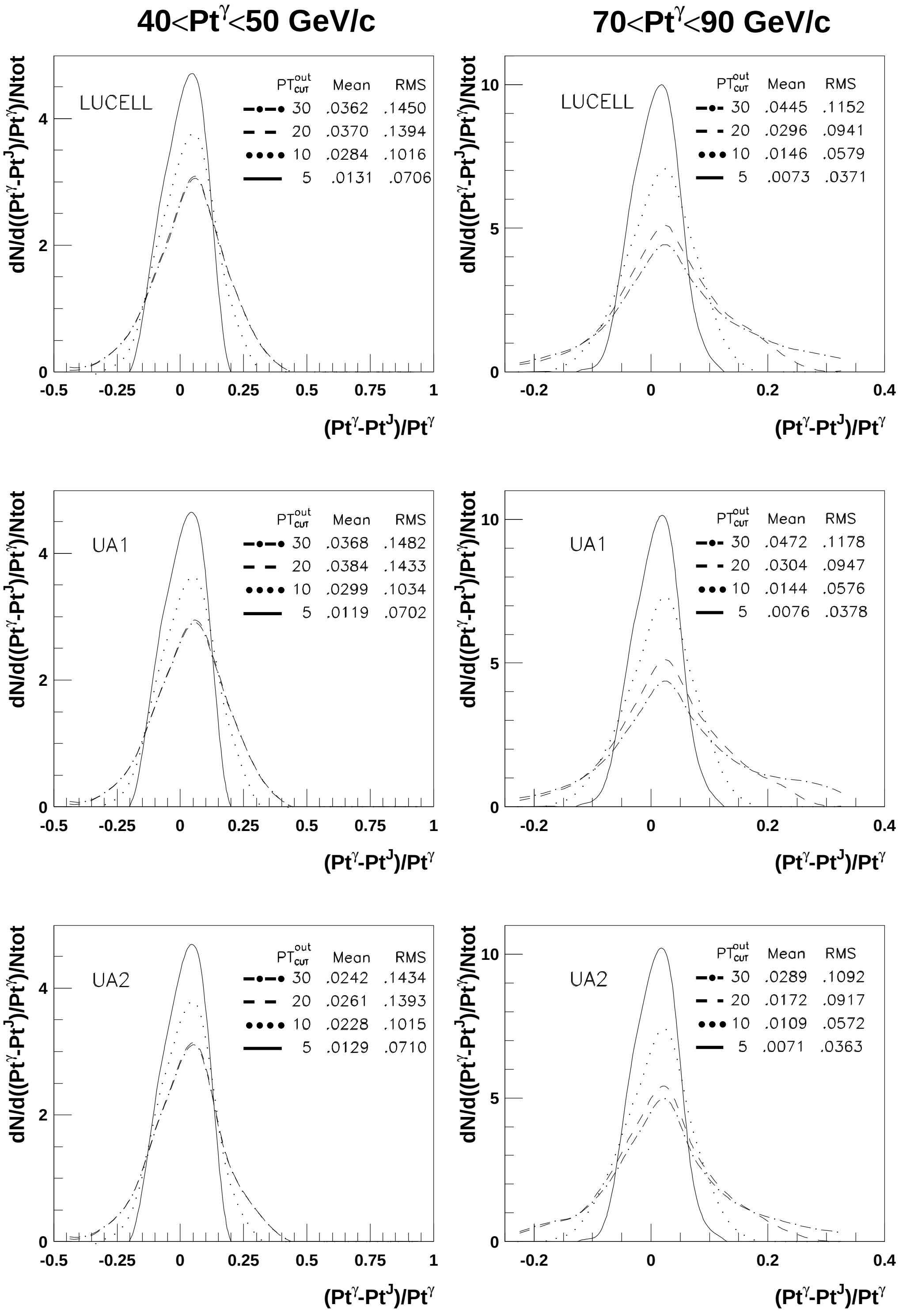

Fig. 19: A dependence of $({P_t}^{\gamma} - {P_t}^{J})/{P_t}^{\gamma}$ on P_{tCUT}^{out} for LUCELL, UA1 and UA2 jetfinding algorithms and two intervals of ${P_t}^{\gamma}$. The mean and RMS of the distributions are displayed on the plots. $\Delta\phi \leq 17^{\circ}$, $P_{tCUT}^{clust} = 30\; GeV/c$. Selection 1.

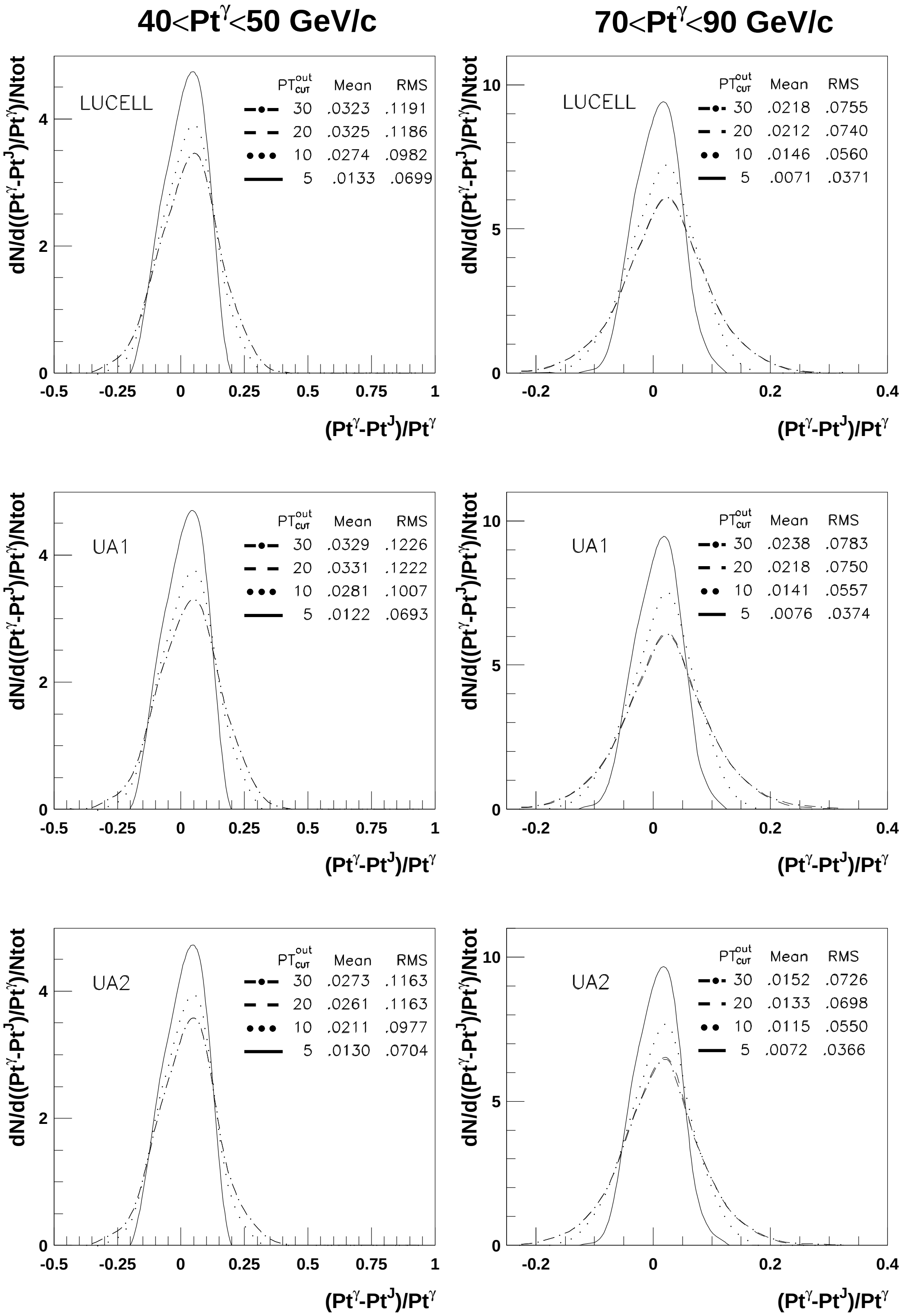

Fig. 20: A dependence of $({P_t}^{\gamma} - {P_t}^{J})/{P_t}^{\gamma}$ on P_{tCUT}^{out} for LUCELL, UA1 and UA2 jetfinding algorithms and two intervals of ${P_t}^{\gamma}$. The mean and RMS of the distributions are displayed on the plots. $\Delta\phi \leq 17°$, $P_{tCUT}^{clust} = 10\ GeV/c$. Selection 1.

8. ESTIMATION OF BACKGROUND SUPPRESSION CUTS EFFICIENCY.

The relative efficiency of "hadronic" cuts that are added to "photonic" ones, used to suppress the background in the case of inclusive photon measurement, is estimated at the particle level. It is shown that an imposing of new cuts on P_t of "clusters" (P_{tCUT}^{clust}) and on P_t activity in the region out of "$\gamma + Jet$" system (P_{tCUT}^{out}) and also an application of "jet isolation" criterion would allow to achieve further (after "photonic" cuts) fourteen-fold background suppression at the cost of four-fold loss of the signal "$\gamma^{dir} + jet$" events.

It is also shown that the imposing of P_{tCUT}^{out}, P_{tCUT}^{clust} together with a usage of jet isolation criterion would lead to a substantial improvement of $P_t^{\gamma} - P_t^{Jet}$ balance.

The potentially dangerous role of a new source of background to the signal "$\gamma^{dir} + jet$" events caused by hard bremsstrahlung photons ("$\gamma - brem$") is demonstrated. It is shown that at Tevatron energy this new "$\gamma - brem$" irreducible background may be compatible at low P_t^{γ} intervals with the π^0 contribution and it may grow faster with P_t^{γ} increasing than the latter one.

To estimate the efficiency of the cuts proposed in Section 3.2 we carried out the simulation [32] with a mixture of all QCD and SM subprocesses with large cross sections existing in PYTHIA (namely, in notations of PYTHIA, with ISUB=1, 2, 11–20, 28–31, 53, 68). The events caused by this set of the subprocesses may give a large background to the "$\gamma^{dir} + jet$" signal events defined by the subprocesses (1a) and (1b) [33] (ISUB=29 and 14) that were also included in this simulation.

Three generations with the above-mentioned set of subprocesses were performed. Each of them was done with a different value of $CKIN(3) \equiv \hat{p}_{\perp}^{min}$ PYTHIA parameter that defines the minimal value of P_t appearing in the final state of a hard $2 \to 2$ parton level fundamental subprocess in the case of ISR absence. These values were $\hat{p}_{\perp}^{min} = 40, 70$ and $100\ GeV/c$. By 40 million events were generated for each of $\hat{p}_{\perp}^{min}$ value. The cross sections of the above-mentioned subprocesses define the rates of corresponding physical events and, thus, appear in simulation as weight factors.

We selected "γ^{dir}-candidate +1 Jet" events containing one γ^{dir}-candidate (denoted in what follows as $\tilde{\gamma}$) and one jet (found by LUCELL) with $P_t^{Jet} > 30\ GeV/c$. Here and below, as we work at the PYTHIA particle level of simulation, speaking about the γ^{dir}-candidate we actually mean, apart from γ^{dir}, a set of particles like electrons, bremsstrahlung photons and also photons from neutral meson decays that may be registered in one D0 calorimeter tower of the $\Delta\eta \times \Delta\phi = 0.1 \times 0.1$ size.

Here we consider a set of 17 cuts that are separated into 2 subsets: a set of "photonic" cuts and a set of "hadronic" ones. The first set consists of 6 cuts used to select an isolated photon candidate in some $P_t^{\tilde{\gamma}}$ interval. The second one includes 11 cuts applied after the first six cuts. They are connected mostly with jets and clusters and are used to select events having one "isolated jet" and limited P_t activity out of "$\tilde{\gamma} + jet$" system.

The used cuts are listed in Table 13. To give an idea about their physical meaning and importance we have done an estimation of their possible influence on the signal-to-background ratios S/B. The letter were calculated after application of each cut. Their values are presented in Table 14 for a case of the most illustrative intermediate interval of event generation with $\hat{p}_{\perp}^{min} = 70\ GeV/c$. In Table 14 the number in each line corresponds to the number of the cut in Table 13 (three important lines of Table 14 are darkened because they will be often referenced to while

[32] PYTHIA 5.7 version with default CTEQ2L parameterization of structure functions is used here.

[33] A contribution of another possible NLO channel $gg \to g\gamma$ (ISUB=115 in PYTHIA) was found to be still negligible even at Tevatron energies.

discussing the following Tables 15–17).

Table 13: List of the applied cuts (will be used also in Tables 14 – 17).

1. $a)\ P_t^{\tilde{\gamma}} \geq 40\ GeV/c,\ \ b)\ \vert\eta^{\tilde{\gamma}}\vert \leq 2.5,\ \ c)\ P_t^{jet} \geq 30\ GeV/c,\ \ d) P_t^{hadr} < 7\ GeV/c^*$;	
2. $P_t^{isol} \leq 5\ GeV/c,\ \epsilon^{\tilde{\gamma}} < 15\%$;	**10**. $\Delta\phi < 17^\circ$;
3. $P_t^{\tilde{\gamma}} \geq \hat{p}_{\perp}^{\,min}$;	**11**. $P_t^{clust} < 20\ GeV/c$;
4. $P_{t\,ring}^{isol} \leq 1\ GeV/c^{**}$;	**12**. $P_t^{clust} < 15\ GeV/c$;
5. $P_{t\,max}^{ch}(R=0.4) < 2\ GeV/c$;	**13**. $P_t^{clust} < 10\ GeV/c$;
6. $P_t^{isol} \leq 2\ GeV/c,\ \epsilon^{\tilde{\gamma}} < 5\%$;	**14**. $P_t^{out} < 20\ GeV/c$;
7. $Njet \leq 3$;	**15**. $P_t^{out} < 15\ GeV/c$;
8. $Njet \leq 2$;	**16**. $P_t^{out} < 10\ GeV/c$;
9. $Njet = 1$;	**17**. $\epsilon^{jet} \leq 3\%$.

$*$ P_t of a hadron in the tower containing a γ^{dir}-candidate;

$**$ A scalar sum of P_t in the ring: $P_t^{sum}(R=0.4) - P_t^{sum}(R=0.2)$.

Line number 1 of Table 13 makes primary preselection. It includes and specifies our first general cut (17) of Section 3.2 as well as the cut connected with ECAL geometry and the cut (21) that excludes γ^{dir}-candidates accompanied by hadrons.

Line number 2 of Table 13 fixes the values of P_{tCUT}^{isol} and ϵ_{CUT}^{γ} that, according to (18) and (19), define the isolation parameters of $\tilde{\gamma}$.

The third cut selects the events with γ^{dir}-candidates having P_t higher than $CKIN(3) \equiv \hat{p}_{\perp}^{\,min}$ threshold. We impose the third cut to select the samples of events with $P_t^{\tilde{\gamma}} \geq 40, 70$ and $100\ GeV/c$ as ISR may smear the sharp kinematical cutoff defined by $CKIN(3)$ [9]. This cut reflects an experimental viewpoint when one is interested in how many events with γ^{dir}-candidates are contained in some definite interval of $P_t^{\tilde{\gamma}}$.

The forth cut restricts a value of $P_{t\,ring}^{isol} = P_{t\,R=0.4}^{isol} - P_{t\,R=0.2}^{isol}$, where $P_{t\,R}^{isol}$ is a sum of P_t of all ECAL cells contained in the cone of radius R around the tower fired by γ^{dir}-candidate [35], [36]. Here it is taken to be even stricter than that one used in [35], [36]. As it is seen from line 4 of Table 14 the fourth cut leads to about 25% reduction of background contribution. It makes not so big effect as compared with the transition from line 1 to line 2 because in line 2 we have already imposed a strict enough isolation cut that covers a wide region of $R = 0.7$ around γ^{dir}-candidate. So, the restriction for $P_{t\,ring}^{isol}$, realized in the fourth line, acts already on the events having a rather clean surrounding space near γ^{dir}-candidate. The reduction of the number of events happens mainly due to a passing from general isolation $P_t^{isol} \leq 5\ GeV/c$ to a small value of $P_{t\,ring}^{isol} \leq 1\ GeV/c$.

The fifth cut corresponds to that one described in point 4 of Section 3.2 and it excludes events having the tracks of charged particles with $P_t^{ch} > 2\ GeV/c$ that are contained in the cone of $R = 0.4$ around $\tilde{\gamma}$. It gives about 10% reduction of background that is achieved practically without any loss of signal events [34].

Here we take the efficiency of each cut to be equal to 100% as we study the results of simulation at the particle level. The estimations of detector effects are given in [35], [36], where track finding efficiency was found to be 83%.

Having in mind this value (83%) we have not included the $e^{\pm}$ events contribution (i.e. with $\tilde{\gamma} = e^{\pm}$) to the background values B presented in Table 14. Nevertheless, let us mention that

[34] In our PYTHIA particle level simulation this cut stands for the effective account of three criteria used in Section 6.1.1 of [1] for reduction of events with a track presence (ECAL cluster–track matching, total charge in TRD and the ionization losses in the central tracking detectors).

their number was estimated and presented in [26] for a slightly different set of selection cuts. The expected contribution of events with $\tilde{\gamma} = e^{\pm}$ at the level of the last cut 17 of Table 14 to the value of total background was found to be about 10%. Now, accepting the value of track finding efficiency for electrons as mentioned above, we conclude that the contribution of $e^{\pm}$ events to the total background would not exceed 2% [35].

The sixth cut makes tighter the isolation criterion of γ^{dir}-candidate (within $R = 0.7$) than it was required by the second line of Table 13. It gives further 30% reduction of the background at the cost of 10% loss of signal events. It should be noted that this cut includes the restriction of "infrared" cut (20) of Section 3.2 which was not included to this reason into Table 13.

The data taken in D0 Run II experiment during January 2002 were analyzed to select events with γ^{dir}-candidates satisfying the photonic cuts 1–5 of Table 13. The very preliminary plot of the number of events dependence on $P_t^{\tilde{\gamma}}$ can be found in the slides from our talk at QCD group [27].

Table 14: Values of significance and efficiencies for $\hat{p}_{\perp}^{\,min} = 70\ GeV/c$.

Cut	S	B	$Eff_S(\%)$	$Eff_B(\%)$	S/B
1	38890	1279436	100.00± 0.00	100.000± 0.000	0.03
2	35603	46023	94.56± 0.70	54.733± 0.317	0.77
3	29235	16221	77.64± 0.61	19.291± 0.165	1.80
4	27301	12228	72.51± 0.58	14.542± 0.141	2.23
5	27293	10903	72.49± 0.58	12.966± 0.132	2.50
6	24657	7714	65.48± 0.54	9.174± 0.109	3.20
7	24610	7613	65.36± 0.54	9.054± 0.108	3.23
8	24129	6920	64.08± 0.53	8.230± 0.103	3.49
9	19905	4041	52.86± 0.46	4.806± 0.077	4.93
10	18781	3401	49.88± 0.45	4.045± 0.071	5.52
11	16225	2474	43.09± 0.40	2.942± 0.060	6.56
12	14199	1884	37.71± 0.37	2.241± 0.052	7.54
13	11023	1232	29.28± 0.32	1.465± 0.042	8.95
14	10915	1208	28.99± 0.32	1.437± 0.042	9.04
15	10481	1128	27.84± 0.31	1.341± 0.040	9.29
16	8774	896	23.30± 0.28	1.066± 0.036	9.79
17	6264	551	16.64± 0.23	0.655± 0.028	11.37

The cuts considered up to now, apart from general preselection cut $P_t^{jet} \geq 30\ GeV/c$ used in the first line of Table 13, were connected with photon selection ("photonic" cuts). Before we go further, some words of caution must be said here. Firstly, we want to emphasize that the starting numbers of the signal (S) and background (B) events (first line of Table 14) may be specific only for PYTHIA generator and for the way of preparing primary samples of the signal and background events described above. So, we want to underline here that the starting values of S and B in the first columns of Table 14 are model dependent [36].

[35] This number agrees with our estimation of the electron contribution to the total background to $\gamma^{dir} + jet$ events done in [17], [25] for LHC energies. It is also worth mentioning that a sizeable rejection of $e^{\pm}$ events, that are characterized, as discussed in Section 4, by noticeable P_t^{miss} values, can be achieved by applying $P_{t\,CUT}^{miss} = 10\ GeV/c$ (not included in present Table 13 but shown in analogous table in [26]). This cut reduces strongly the number of the events with $e^{\pm}$ produced in weak decays (see [17] and [26] for details).

[36] Let us notice that S/B ratio, obtained after application of photon isolation cuts $1-5$, is equal to 2.5. This

But nevertheless, for our aim of investigation of new cuts 11–17 (see [10]–[17]) efficiency the important thing here is that we can use these starting model numbers of S- and B-events for studying the further relative influence of these cuts on S/B ratio (also as for the conventional normalization to 100% of the cut efficiencies [37] for S- and B-events in line 1).

In spite of self-explaining nature of the cuts 7–10 let us mention, before passing to cuts 11–17, that the cuts 7–10 are connected with the selection of events having only one jet and the definition of jet-photon spatial orientation. Usage of these four cuts leads to the almost two-fold relative improvement of model S/B ratio (compare lines 6 and 10 of Table 14).

Moving further we see from Table 14 that the cuts 11–16 of Table 13 reduce the values of ${P_t}^{clust}$ and ${P_t}^{out}$ down to the values less than $10\ GeV/c$. The 17-th cut of Table 13 imposes the jet isolation requirement. It leaves only the events with jets having the sum of P_t in a ring surrounding a jet to be less than 3% of ${P_t}^{Jet}$. From comparison of the numbers in 10-th and 17-th lines we make the important conclusion that all these new cuts (11–17), despite of model dependent nature of starting S/B value in line 10, may, in principle, lead to the following about two-fold improvement of S/B ratio. This improvement is reached by reducing the P_t activity out of "$\tilde{\gamma} + 1\ jet$" system.

It is also rather interesting to mention that the total effect of "hadronic cuts" 7–17 consist of about fourteen-fold decrease of background contribution at the cost of four-fold loss of signal events. So, in this sense, we may conclude that from the viewpoint of S/B ratio the study of "$\gamma + Jet$" events may be more preferable as compared with a case of inclusive photon production.

Below we shall demonstrate in some plots how new selection criteria 11–17 work to choose the events with further almost two-fold improvement of S/B ratio.For this reason we have built the distributions that correspond to the three above-mentioned values of $\hat{p}_{\perp}^{\,min}$ and for the "$\tilde{\gamma} + 1\ jet$" events that have passed the set of cuts 1–9 defined in Table 13. Thus, no special cuts were imposed on $\Delta\phi$, ${P_t}^{out}$ and ${P_t}^{clust}$ (the values of ${P_t}^{clust}$ are automatically bounded from above since we select "$\tilde{\gamma} + 1\ jet$" events with ${P_t}^{jet} > 30\ GeV/c$).

These distributions are given here to show the dependence of the number of events on the physical observables $\Delta\phi$, ${P_t}^{out}$ and ${P_t}^{clust}$ introduced in Sections 3.1 and 3.2. We present them separately for the signal "γ-dir" and background events contained in each of three generated samples. The distributions are given for three different ${P_t}^{\tilde{\gamma}}$ intervals in Figs. 21, 23, 25 and are accompanied by scatter plots 22, 24, 26. So, each pair of a figure and a scatter plot does correspond to one ${P_t}^{\tilde{\gamma}}$ interval. Thus, Fig. 21 and scatter plot 22 correspond to ${P_t}^{\tilde{\gamma}} \geq 40\ GeV/c$ and so on.

The first columns in these figures, denoted by "γ - dir", show the distributions in the signal events, i.e. in the events corresponding to processes (1a) and (1b). The second columns, denoted as "γ - brem", correspond to the events in which the photons were emitted from quarks (i.e. bremsstrahlung photons). The distributions in the third columns were built on the basis of the events containing "γ-mes" photons, i.e. those photons which originate from multiphoton decays of mesons (π^0, η, ω and K_S^0).

First, we see that in the case of ${P_t}^{\tilde{\gamma}} \geq 100\ GeV/c$ (see Fig. 25) practically all "signal events" are within $\Delta\phi < 17°$. In the case of ${P_t}^{\tilde{\gamma}} \geq 70\ GeV/c$ (see Fig. 23) most of them are

number is close to that one stemming from the value of photon purity $P \approx 0.75 - 0.80$ found in inclusive photon measurement [36] for interval $P_t \geq 70\ GeV/c$ and for CC region, but it is still lower, what is quite expectable as we have not taken into account the detector effects.

[37] In Table 14 the efficiencies $Eff_{S(B)}$ (with their errors) are defined as a ratio of the number of signal (background) events that passed under a cut (1–17) to the number of the preselected events (1st cut of this table).

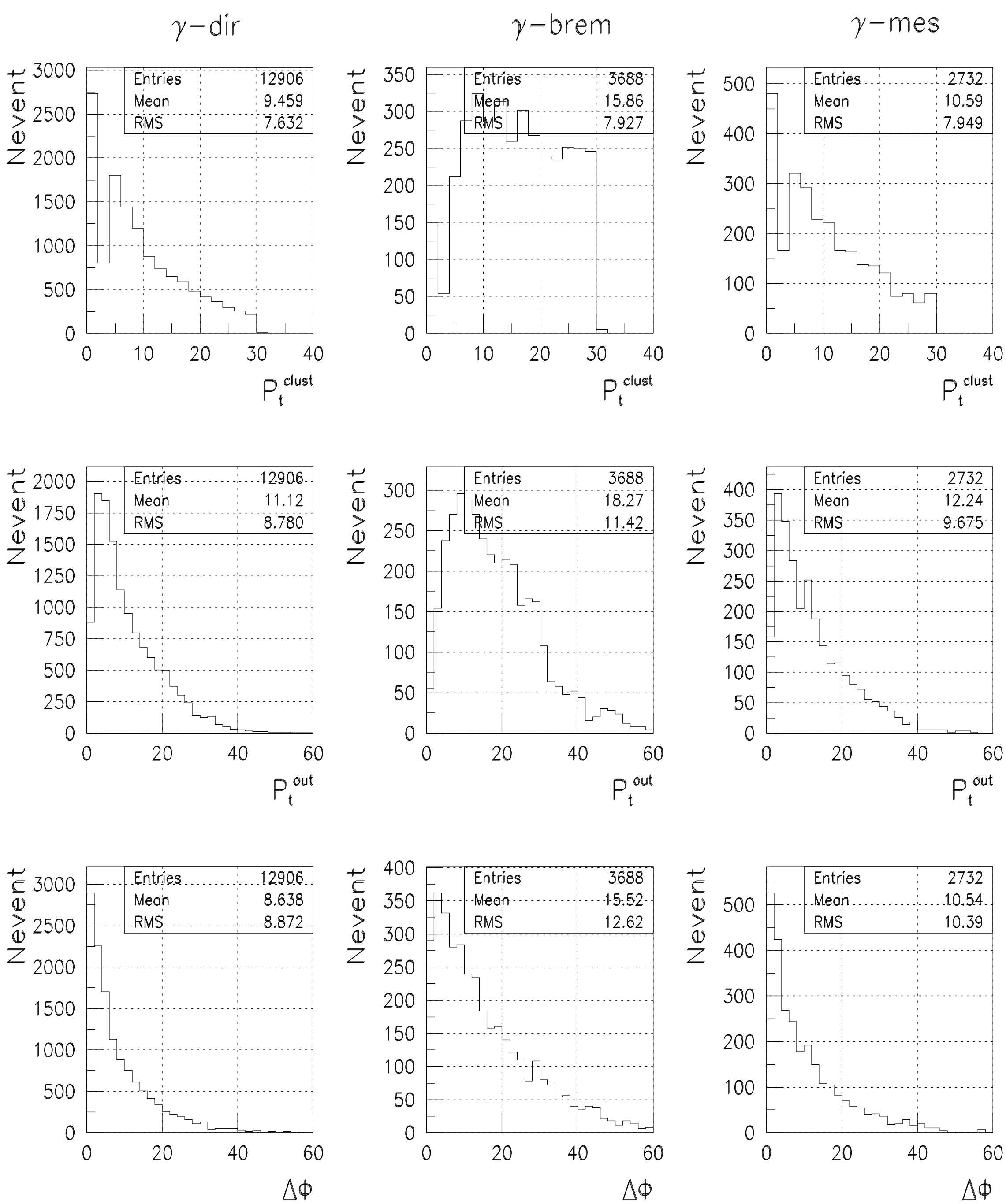

Fig. 21: Signal & Backgrounds: Number of events distribution over ${P_t}^{clust}$, ${P_t}^{out}$, $\Delta\phi$ (${P_t}^{\tilde{\gamma}} \geq 40\ GeV/c$).

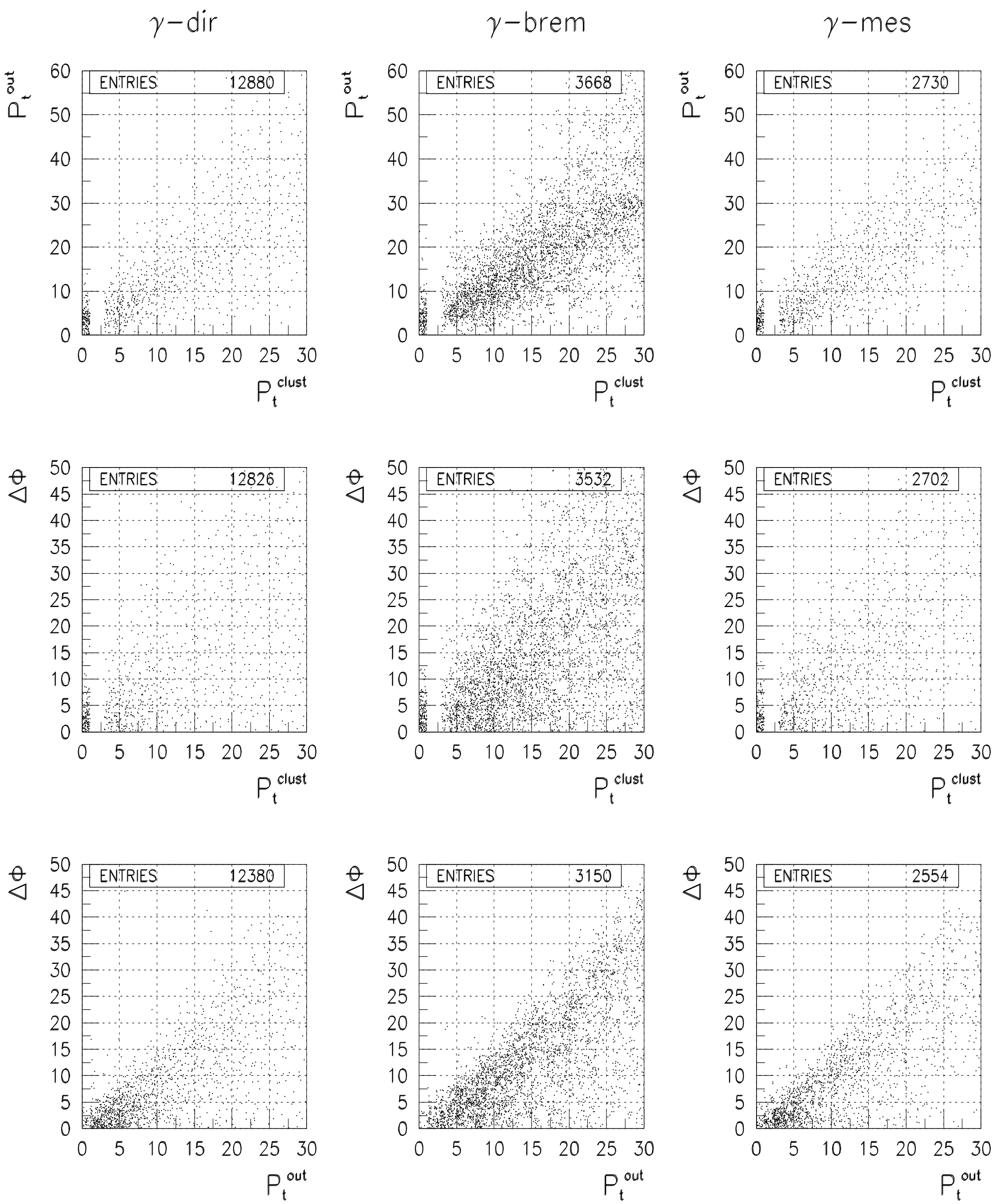

Fig. 22: Signal & Backgrounds: ${P_t}^{clust}$ vs. ${P_t}^{out}$, ${P_t}^{clust}$ vs. $\Delta\phi$, ${P_t}^{out}$ vs. $\Delta\phi$ (${P_t}^{\tilde{\gamma}} \geq 40\, GeV/c$).

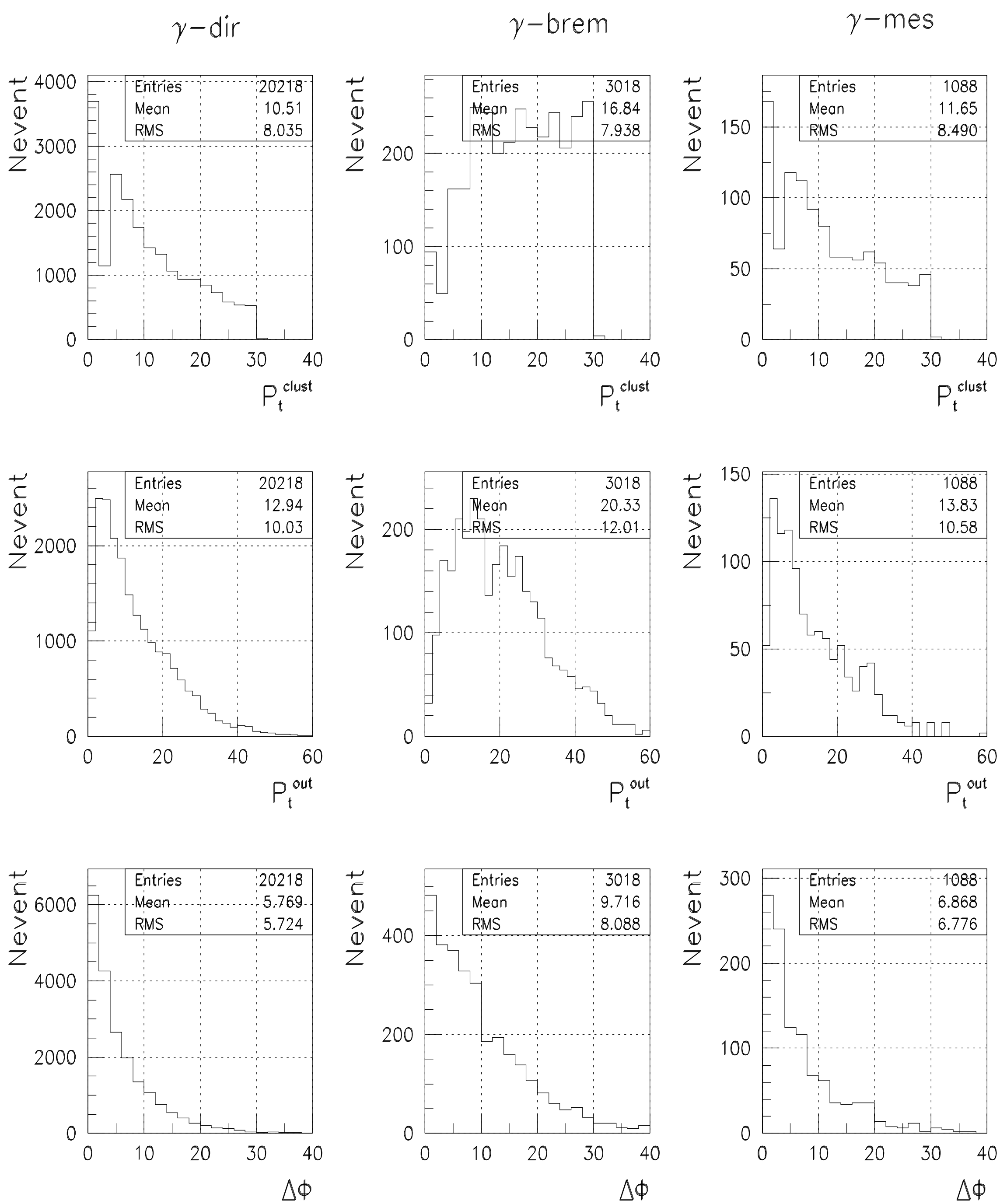

Fig. 23: Signal & Backgrounds: Number of events distribution over ${P_t}^{clust}$, ${P_t}^{out}$, $\Delta\phi$ (${P_t}^{\tilde{\gamma}} \geq 70\ GeV/c$).

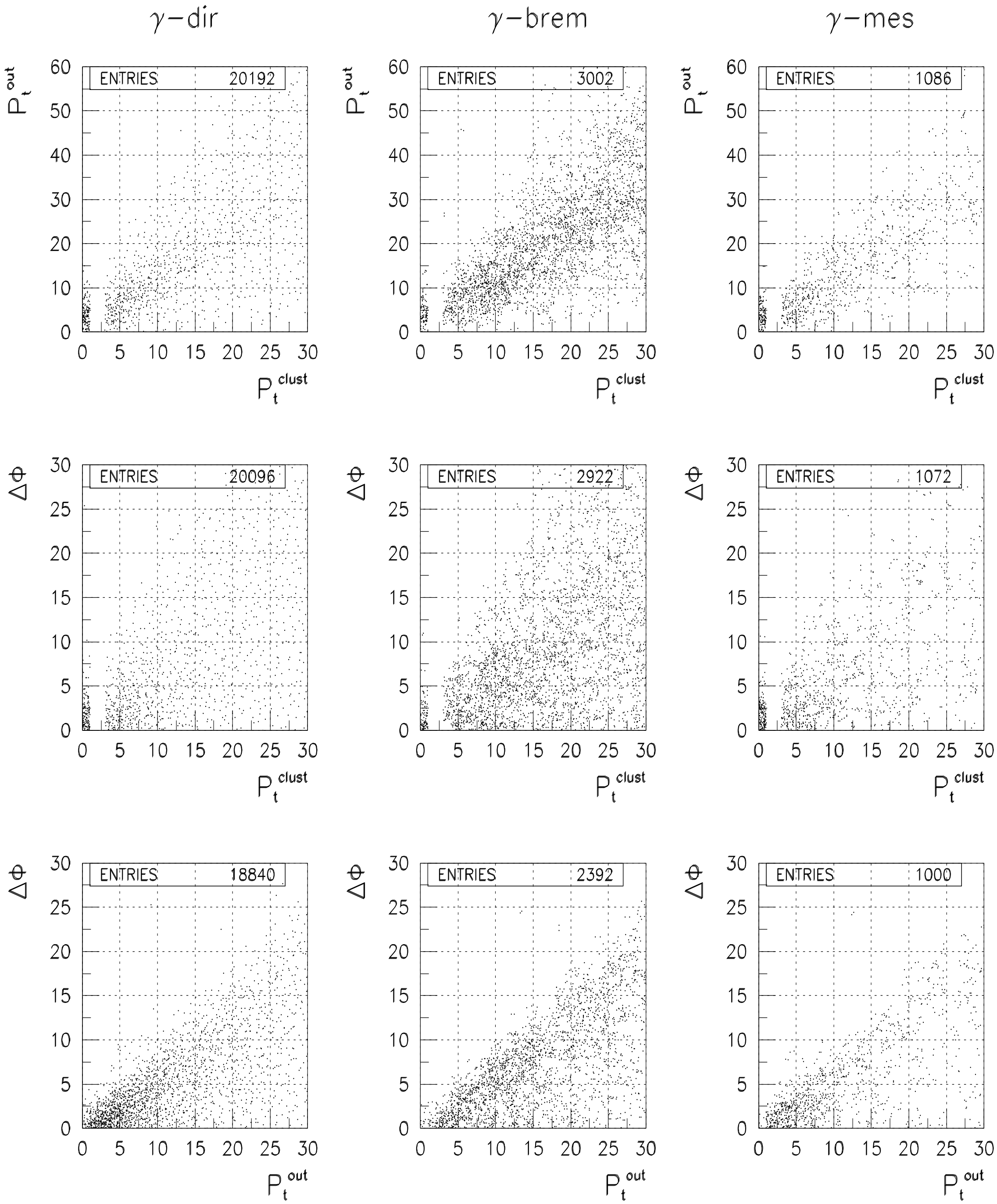

Fig. 24: Signal & Backgrounds: ${P_t}^{clust}$ vs. ${P_t}^{out}$, ${P_t}^{clust}$ vs. $\Delta\phi$, ${P_t}^{out}$ vs. $\Delta\phi$ (${P_t}^{\tilde{\gamma}} \geq 70\,GeV/c$).

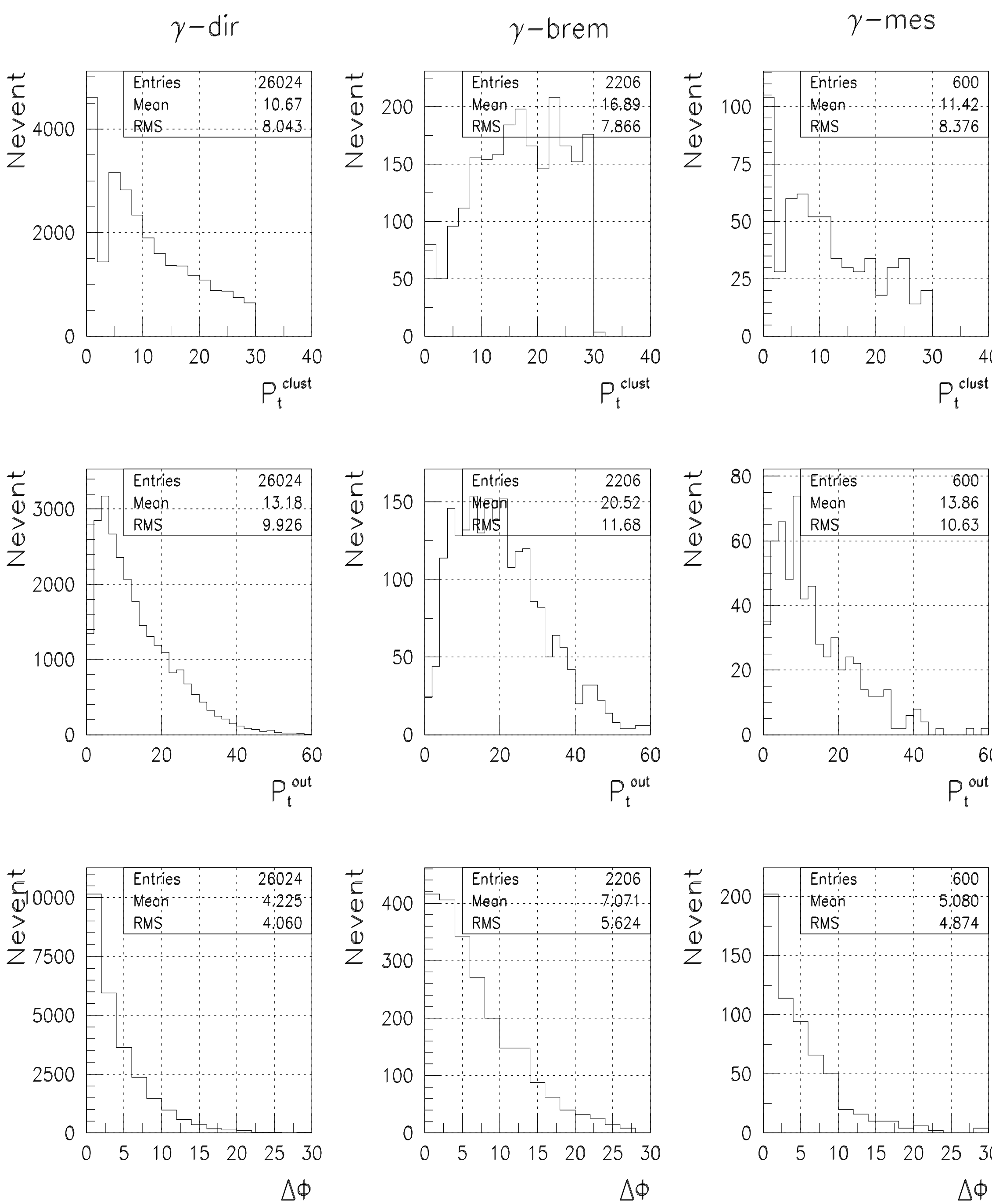

Fig. 25: Signal & Backgrounds: Number of events distribution over $P_t{}^{clust}$, $P_t{}^{out}$, $\Delta\phi$ ($P_t{}^{\tilde{\gamma}} \geq 100\ GeV/c$).

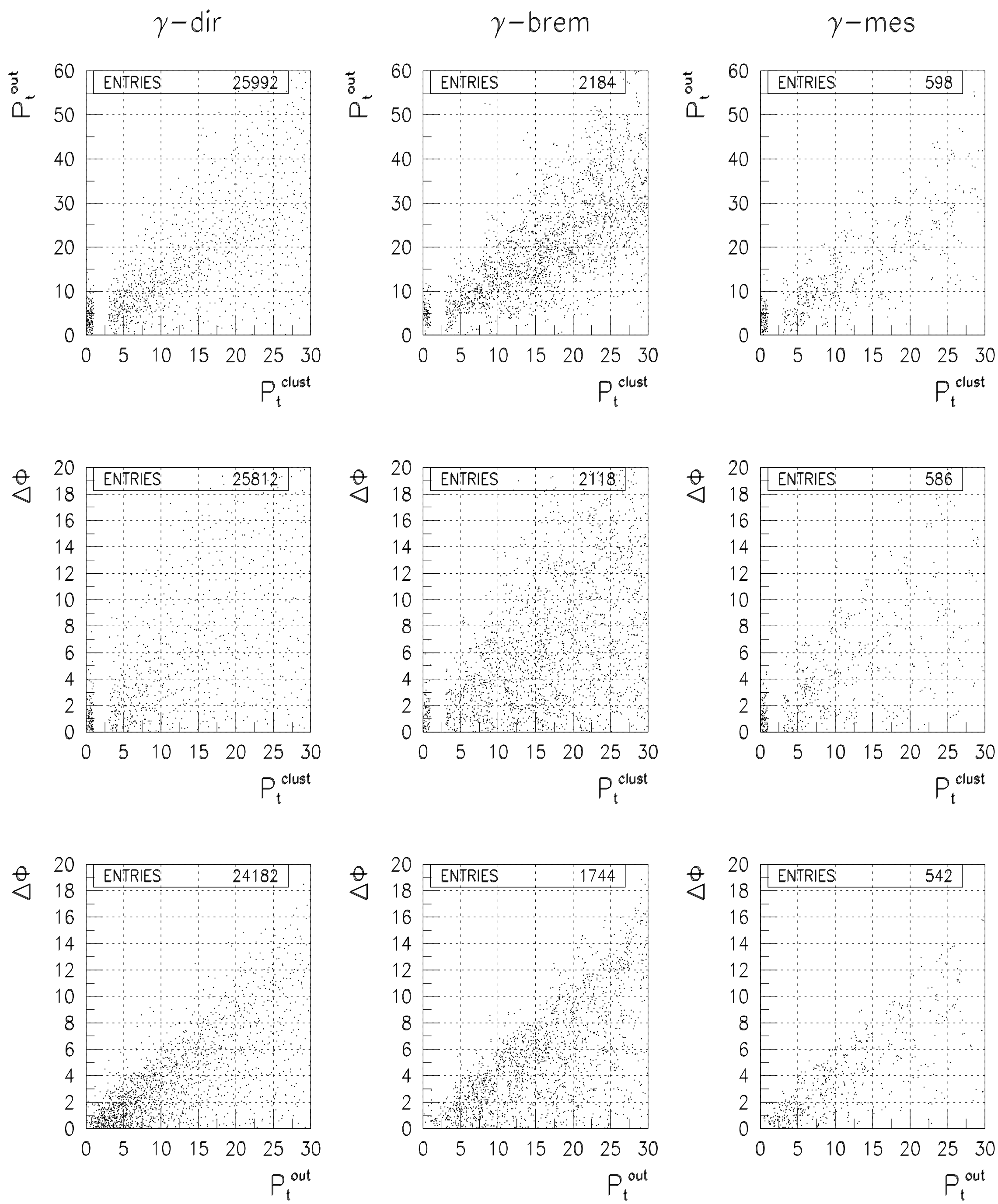

Fig. 26: Signal & Backgrounds: ${P_t}^{clust}$ vs. ${P_t}^{out}$, ${P_t}^{clust}$ vs. $\Delta\phi$, ${P_t}^{out}$ vs. $\Delta\phi$ (${P_t}^{\tilde{\gamma}} \geq 100\, GeV/c$).

also within $\Delta\phi < 17^{\circ}$. It is seen from Fig. 21 that for $P_t^{\tilde{\gamma}} \geq 40\ GeV/c$ there is still a large number of signal events (about 70%) belonging to the $\Delta\phi < 17^{\circ}$ interval. From here and from the comparison of plots in the "γ-dir" and "γ-brem" columns (showing the $\Delta\phi$ dependence) in the same figures 21–26 we conclude that the upper cut $\Delta\phi < 17^{\circ}$, used in previous sections, is reasonable, and moreover, it does discard a lot of "γ-brem" background events in the intervals with $P_t^{\tilde{\gamma}} < 100\ GeV/c$.

From the second "γ-brem" columns of Figs. 21, 23 and 25 one can also see that P_t^{clust} spectra of the events with bremsstrahlung photons look quite different from the analogous P_t^{clust} distributions of the signal "γ-dir" photons. The latter distributions have the most of the events in the region of small P_t^{clust} values (there is a deep in spectra between $P_t^{clust} = 0$, caused by events having no clusters, and the second peak appearing due to cluster definition as of the object with $3 < P_t^{clust} < 30\ GeV/c$).

Since the bremsstrahlung ("γ-brem") photons give the most sizeable background [38], (compare the numbers of entries in the second "γ-brem" and the third "γ-mes" columns of Figs. 21–26) the observed difference of the spectra prompts an idea of using an upper cut for the value of P_t^{clust} to reduce the "γ-brem" background which dominates at large P_t^{clust} values (that was not a primary guideline for introduction of P_t^{clust} in Sections 2 and 3 as a physical variable and a cut on it).

The analogous difference of P_t^{out} spectra of signal "γ-dir" events (which are concentrated at low P_t^{out} values) from those of the background "γ-brem" events having longer tails at high P_t^{out} enables us to impose an upper cut on the P_t^{out} value.

Now from the scatter plots in Figs. 22, 24 and 26 as well as from Figs. 21, 23 and 25 we can conclude that the use of cuts [39]: $\Delta\phi < 17^{\circ}$, $P_{tCUT}^{clust} = 10\ GeV/c$, $P_{tCUT}^{out} = 10\ GeV/c$ would allow to keep a big number of the signal "γ-dir" events and to reduce noticeably the contribution from the background "γ-brem" and "γ-mes" events in all intervals of $P_t^{\tilde{\gamma}}$. At the same time the Figs. 21–26 give the information about what parts of different spectra are lost with the imposed cuts.

So, Figs. 21–26 illustrate well that the new physical variables P_t^{clust} and P_t^{out} [10]–[17], described in Sections 3.1 and 3.2 may be useful for separation of the "$\gamma^{dir} + jet$" events from the background ones (the latter, in principle, are not supposed to have the well-balanced $P_t^{\tilde{\gamma}}$ and P_t^{Jet}).

Table 15 includes the numbers of signal and background events left in three generated event samples after application of cuts 1–16 and 1–17. They are given for all three intervals of $P_t^{\tilde{\gamma}}$. Tables 15 and 14 are complementary to each other. The summary of Table 14 is presented in the middle section ($\hat{p}_{\perp}^{min} = 70\ GeV/c$) of Table 15 where the line "Preselected" corresponds to the cut 1 of Table 13 and, respectively, to the line number 1 of Table 14 presented above. The line "After cuts" corresponds to the line 16 of Table 14 and line "+jet isolation" corresponds to the line 17 of Table 14.

Table 15 is done to show in more detail the origin of γ^{dir}-candidates. The numbers in the "$\gamma - direct$" column correspond to the respective numbers of signal events left in each of $P_t^{\tilde{\gamma}}$ intervals after application of the cuts defined in lines 1, 16 and 17 of Table 13 (and column "S"

[38] The numbers in Table 15 below supports this remark. But it is also necessary to keep in mind the results obtained in [37] that the PYTHIA/JETSET fragmentation may underestimate the π^0, η contribution to the isolated photon background.

[39] rather soft here, but the results of their further restriction were already shown in tables of Appendices 2–5 and Figs. 12–20 and will be discussed below

of Table 14). Analogously the numbers in the "$\gamma - brem$" column of Table 15 correspond to the numbers of events with the photons radiated from quarks participating in the hard interactions. Their P_t^{clust} and P_t^{out} distributions were presented in the central columns of Figs. 21 – 26. Columns 5 – 8 of Table 15 illustrate the numbers of the "$\gamma - mes$" events with photons originating from $\pi^0,\ \eta,\ \omega$ and K_S^0 meson decays. Their distributions were shown in the right-hand columns of Figs. 21 – 26. In a case of $P_t^{\tilde{\gamma}} > 70\ GeV/c$ the total numbers of background events, i.e. a sum over the numbers presented in columns 4 – 8 of Table 15, are shown in the lines 1, 16 and 17 of column "B" of Table 14. The other lines of Table 15 for $\hat{p}_\perp^{min} = 40$ and $100\ GeV/c$ have the meaning analogous to that described above for $\hat{p}_\perp^{min} = 70\ GeV/c$.

Table 15: Number of signal and background events remained after cuts.

$\hat{p}_\perp^{min}$ (GeV/c)	Cuts	γ direct	γ brem	photons from the mesons π^0	η	ω	K_S^0	$e^\pm$
40	Preselected	18550	14054	151254	55591	18699	15257	2890
	After cuts	6814	711	660	369	101	111	0
	+ jet isol.	3529	272	283	136	45	56	0
70	Preselected	38890	63709	773208	275524	93967	73028	18510
	After cuts	8774	445	230	144	45	32	0
	+ jet isol.	6264	289	132	75	33	22	0
100	Preselected	54007	105715	919932	328259	112553	86327	38874
	After cuts	11038	300	116	76	24	20	0
	+ jet isol.	9188	226	84	52	22	18	0

Table 16: Efficiency, S/B ratio and significance values in the selected events without jet isolation cut.

$\hat{p}_\perp^{min}$ (GeV/c)	S	B	$Eff_S(\%)$	$Eff_B(\%)$	S/B	$S/\sqrt{B}$
40	6814	1952	36.91 ± 0.52	4.767 ± 0.110	3.5	154.2
70	8774	896	23.30 ± 0.28	1.066 ± 0.036	9.8	293.1
100	11038	536	20.58 ± 0.22	0.571 ± 0.025	20.6	476.8

Table 17: Efficiency, S/B ratio and significance values in the selected events with jet isolation cut.

$\hat{p}_\perp^{min}$ (GeV/c)	S	B	$Eff_S(\%)$	$Eff_B(\%)$	S/B	$S/\sqrt{B}$
40	3529	792	19.12 ± 0.35	1.934 ± 0.069	4.5	125.4
70	6264	551	16.64 ± 0.23	0.655 ± 0.028	11.4	266.9
100	9188	402	17.13 ± 0.19	0.428 ± 0.021	22.9	459.3

The last column of Table 15 shows the number of preselected events with $e^\pm$ (see our notes above while discussing the fifth cut of Table 13).

The numbers in Tables 16 (without jet isolation cut) and 17 (with jet isolation cut) accumulate in a compact form the final information of Tables 13 – 15. Thus, for example, the columns S and B of the line that corresponds to $\hat{p}_\perp^{min} = 70\ GeV/c$ contain the total numbers of the selected signal and background events taken at the level of 16-th (for Table 16) and 17-th (for Table 17) cuts from Table 14.

It is seen from Table 16 that in the case of Selection 1 the ratio S/B grows from 3.5 to 20.6 while $P_t^{\tilde{\gamma}}$ increases from $P_t^{\tilde{\gamma}} \geq 40\ GeV/c$ to $P_t^{\tilde{\gamma}} \geq 100\ GeV/c$ interval.

The jet isolation requirement (cut 17 from Table 13) noticeably improves the situation at low $P_t^{\tilde{\gamma}}$ (see Table 17). After application of this criterion the value of S/B increases from 3.5 to 4.5 at $P_t^{\tilde{\gamma}} \geq 40\ GeV/c$ and from 20.6 to 22.9 at $P_t^{\tilde{\gamma}} \geq 100\ GeV/c$. Remember on this occasion the conclusion that the sample of events selected with our criteria has a tendency to contain more events with an isolated jet as $P_t^{\tilde{\gamma}}$ increases (see Sections 5–7 and Appendices 2–5). Thus, from Appendices 4 and 5 it can be seen that the main part of jets with $P_t^{jet} \geq 70\ GeV/c$ appears to be isolated (compare also the last two lines in each $\hat{p}_{\perp}^{min}$ section of Table 15) [40].

Let us underline here that, in contrast to other types of background, "$\gamma - brem$" background has an irreducible nature. So, the number of "$\gamma - brem$" events should be carefully estimated for each $P_t^{\tilde{\gamma}}$ interval using the particle level of simulation in the framework of event generator like PYTHIA. They are also have to be taken into account in experimental analysis of the prompt photon production data at high energies.

Table 18 shows the relative contributions of fundamental QCD subprocesses (having the largest cross sections) with ISUB=11, 12, 28, 53 and 68 (see [9]) that define the main production of "$\gamma - brem$" background in event samples selected with criteria 1–13 of Table 13 in three $P_t^{\tilde{\gamma}}$ intervals.

Accepting the results of simulation with PYTHIA, we found from the event listing analysis that in the main part of selected "$\gamma - brem$" events these photons are produced in the final state of the fundamental $2 \rightarrow 2$ subprocess [41]. Namely, they are mostly radiated from the outgoing quarks in the case of the first three sets of subprocesses (ISUB=28, 11, 12 and 53). They may also appear as a result of string breaking in a final state of $gg \rightarrow gg$ scattering (ISUB=68). But this subprocess, naturally, gives a small contribution into "$\tilde{\gamma} + jet$" events production.

Table 18: Relative contribution (in per cents) of different QCD subprocesses into the "$\gamma - brem$" events production.

P_t^{γ} (GeV/c)	fundamental QCD subprocess			
	ISUB=28	ISUB=11,12	ISUB=53	ISUB=68
40–70	62.1±6.6	31.8±4.0	3.3±1.0	2.8±0.9
70–100	52.3±7.7	42.4±6.4	3.8±1.4	1.5±0.9
> 100	41.8±6.0	56.9±7.2	1.3±0.7	—

It may be noted also from the first two columns of Table 18 that the most of "$\gamma - brem$" background events (92% at least) originate from the ISUB=28 ($fg \rightarrow fg$) and ISUB=11, 12 ($f_i f_j \rightarrow f_i f_j$, $f_i \bar{f}_i \rightarrow f_j \bar{f}_j$) subprocesses. Table 18 shows also a tendency of increasing the contribution from the sum of two subprocess "11+12" (given in the second column of Table 18) with growing $P_t^{\tilde{\gamma}}$.

From Tables 15 – 17 we have seen that the cuts listed in Table 13 (having rather moderate values of P_{tCUT}^{clust} and P_{tCUT}^{out}) allow to suppress the major part of the background events. The influence of these two cuts on:

(a) the number of selected events (for $L_{int} = 300\,pb^{-1}$);

(b) the signal-to-background ratio S/B;

(c) the mean value of $(P_t^{\tilde{\gamma}} - P_t^{Jet})/P_t^{\tilde{\gamma}} \equiv F$ and its standard deviation value $\sigma(F)$

is presented in Tables 1 – 12 of Appendix 6 for their variation in a wide range.

Let us emphasize that the tables of Appendix 6 include, in contrast to Appendices 2–5, the results obtained after analyzing three generated samples (described in the beginning of this section) of *signal and background* events. These events were selected with the cuts of Table 13.

[40] see also Fig. 11 for $P_t^{\gamma} \geq 70\ GeV/c$

[41] i.e. from lines 7, 8 in Fig. 3

Namely, the cuts (1) – (10) of Table 13 were applied for preselection of "$\tilde{\gamma} + 1\ jet$" events. The jets in these events as well as clusters were found by use of only one jetfinder LUCELL (for the whole η region $|\eta^{jet}| < 4.2$).

Tables 1 – 4 of Appendix 6 correspond to the simulation with $\hat{p}_{\perp}^{\,min} = 40\ GeV/c$. Analogously, the values of $\hat{p}_{\perp}^{\,min} = 70\ GeV/c$ and $\hat{p}_{\perp}^{\,min} = 100\ GeV/c$ were used for Tables 5 – 8 and Tables 9 – 12 respectively. The rows and columns of Tables 1 – 12 illustrate, respectively, the influence of P_{tCUT}^{clust} and P_{tCUT}^{out} on the quantities mentioned above (in the points (a), (b), (c)).

First of all, we see from Tables 2, 6 and 10 that a noticeable reduction of the background take place while moving along the table diagonal from the right-hand bottom corner to the left-hand upper one, i.e. with reinforcing P_{tCUT}^{clust} and P_{tCUT}^{out}. So, we see that for $\hat{p}_{\perp}^{\,min} = 40\ GeV/c$ the value of S/B ratio changes in the table cells along the diagonal from $S/B = 2.5$ (in the case of no limits on these two variables), to $S/B = 3.5$ for the cell with $P_{tCUT}^{clust} = 10\ GeV/c$ and $P_{tCUT}^{out} = 10\ GeV/c$. Analogously, for $\hat{p}_{\perp}^{\,min} = 100\ GeV/c$ the value of S/B changes in the same table cells from 9.8 to 20.6 (compare with the numbers in Table 10 of Appendix 6).

The second observation from Appendix 6. The restriction of P_{tCUT}^{clust} and P_{tCUT}^{out} improves the calibration accuracy. Table 3 shows that in the interval ${P_t}^{\tilde{\gamma}} > 40\ GeV/c$ the mean value of the fraction $F (\equiv ({P_t}^{\tilde{\gamma}} - {P_t}^{Jet})/{P_t}^{\tilde{\gamma}})$ decreases from 0.049 (the bottom right-hand corner) to 0.024 for the table cell with $P_{tCUT}^{clust} = 10\ GeV/c$ and $P_{tCUT}^{out} = 10\ GeV/c$. At the same time, the both cuts lead to a noticeable decrease of the gaussian width $\sigma(F)$ (see Table 4 and also Tables 8 and 12). For instance, for $\hat{p}_{\perp}^{\,min} = 40\ GeV/c$ $\sigma(F)$ drops by about a factor of two: from 0.159 to 0.080. It should be also noted that Tables 4, 8 and 12 demonstrate that for any fixed value of P_{tCUT}^{clust} further improvement in $\sigma(F)$ can be achieved by limiting ${P_t}^{out}$ (e.g. in line with $P_{tCUT}^{clust} = 10\ GeV/c$ $\sigma(F)$ drops by a factor of 2 with variation of ${P_t}^{out}$ from 1000 to $5\ GeV/c$).

The explanation is simple. The balance equation (28) contains 2 terms on the right-hand side ($1 - cos\Delta\phi$) and $P_t(O{+}\eta > 4.2)/{P_t}^{\tilde{\gamma}}$. The first one is negligibly small in a case of Selection 1 and tends to decrease with growing ${P_t}^{\tilde{\gamma}}$ (see tables in Appendices 2–5). So, we see that in this case the main source of the disbalance in equation (28) is the term $P_t(O{+}\eta > 4.2)/{P_t}^{\tilde{\gamma}}$. This term can be diminished by decreasing P_t activity beyond the jet, i.e. by decreasing ${P_t}^{out}$.

The behavior of the number of selected events (for $L_{int} = 300\,pb^{-1}$), the mean values of $F = ({P_t}^{\tilde{\gamma}} - {P_t}^{Jet})/{P_t}^{\tilde{\gamma}}$ and its standard deviation $\sigma(F)$ as a function of P_{tCUT}^{out} (with fixed $P_{tCUT}^{clust} = 10\,GeV/c$) are also displayed in Fig. 27 for events with non-isolated (left-hand column) and isolated jets (right-hand column, see also Tables 13–24 of Appendix 6).

Thus, we can conclude that application of two criteria introduced in Section 3.2, i.e. P_{tCUT}^{clust} and P_{tCUT}^{out}, results in two important consequences: significant background reduction and essential improvement of the calibration accuracy.

The numbers of events (for $L_{int} = 300\ pb^{-1}$) for different P_{tCUT}^{clust} and P_{tCUT}^{out} are given in the cells of Tables 1, 5 and 9 of Appendix 6. One can see that even with such strict P_{tCUT}^{clust} and P_{tCUT}^{out} values as, for example, $10\ GeV/c$ for both we would have a sufficient number of events (about 100 000, 7 000 and 1 300 for ${P_t}^{\tilde{\gamma}} \geq 40\ GeV/c$, ${P_t}^{\tilde{\gamma}} \geq 70\ GeV/c$ and ${P_t}^{\tilde{\gamma}} \geq 100\ GeV/c$, respectively) with low background contamination ($S/B = 3.5,\ 9.8$ and 20.6) and a good accuracy of the ${P_t}^{\tilde{\gamma}} - {P_t}^{Jet}$ balance: $F = 2.4\%, 1.5\%$ and 1.2%, respectively, for the case of Selection 1.

In addition, we also present Tables 13–24 of Appendix 6. They contain the information analogous to that in Tables 1 – 12 but for the case of isolated jets with $\epsilon^{jet} < 3\%$. From these tables we see that with the same cuts $P_{tCUT}^{clust} = P_{tCUT}^{out} = 10\ GeV/c$ one can expect about 47 000, 5 000 and 1000 events for ${P_t}^{\tilde{\gamma}} \geq 40\ GeV/c$, ${P_t}^{\tilde{\gamma}} \geq 70\ GeV/c$ and ${P_t}^{\tilde{\gamma}} \geq 100\ GeV/c$, respectively, with a much more better fractional ${P_t}^{\tilde{\gamma}} - {P_t}^{Jet}$ balance: $F = 0.5\%, 0.7\%$ and 0.1%.

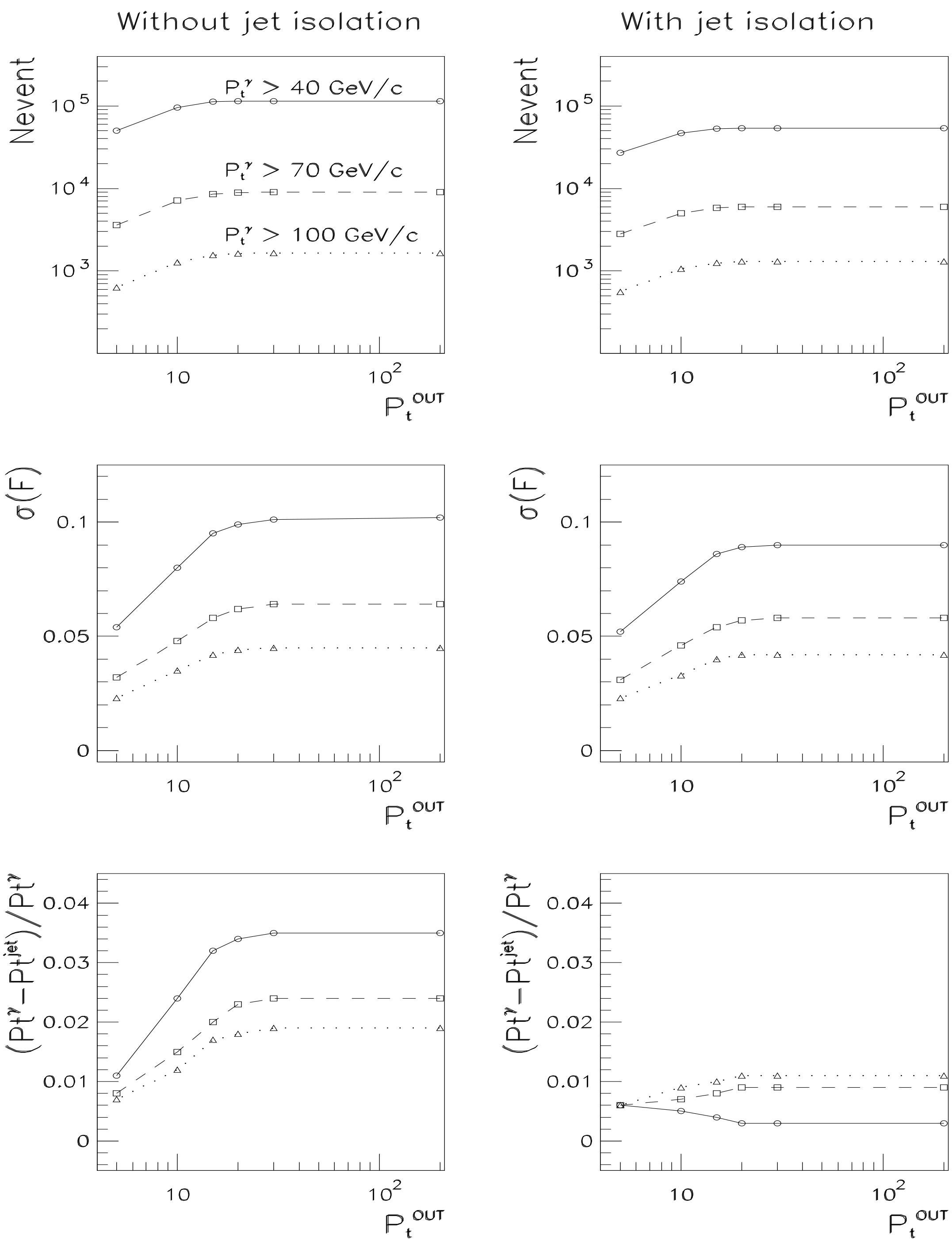

Fig. 27: Number of events (for $L_{int} = 300\,pb^{-1}$), mean value of $(P_t^{\tilde{\gamma}} - P_t^{Jet})/P_t^{\tilde{\gamma}}$ ($\equiv F$) and its standard deviation $\sigma(F)$ distributions over P_t^{out} for the cases of nonisolated (left-hand column) and isolated (right-hand column) jet and for three intervals: $P_t^{\tilde{\gamma}} > 40, 70$ and $100\ GeV/c$. $P_{tCUT}^{clust} = 10\ GeV/c$.

Let us mention that all these PYTHIA results give us an indication of a tendency and may serve as a guideline for further full GEANT simulation that would allow to come to a final conclusion.

To conclude this section we would like to stress, firstly, that, as is seen from Tables 15, the "$\gamma - brem$" background defines a dominant part of the total background. One can see from Table 15 that π^0 contribution being about the same as "$\gamma - brem$" at $\hat{p}_\perp^{min} > 40\ GeV/c$ becomes three times less than "$\gamma - brem$" contribution at $\hat{p}_\perp^{min} > 100\ GeV/c$. We would like to emphasize here that this is a strong prediction of the PYTHIA generator that has to be compared with predictions of another generator like HERWIG, for example.

Secondly, we would like to mention also that, as it is seen from Tables 14 and 15, the photon isolation and selection cuts 1–6, usually used in the study of inclusive photon production (see, for instance, [34], [35], [36]), increase the S/B ratio up to 3.20 only (for $P_t^{\tilde{\gamma}} \geq 70\ GeV/c$). The other "hadronic" cuts 7–17, that select events with a clear "$\gamma + Jet$" topology and limited P_t activity beyond "$\gamma + Jet$" system, lead to quite a significant improvement of S/B ratio by a factor of four (to $S/B = 11.37$) as they suppress the background events contamination by a factor of about fourteen at the cost of four-fold loss of signal events.

The numbers in the tables of Appendix 6 were obtained with inclusion of the contribution from the background events. The tables show that their account does not spoil the $P_t^{\gamma} - P_t^{Jet}$ balance in the event samples preselected with the cuts 1–10 of Table 13. The estimation of the number of these background events would be important for the gluon distribution determination (see Section 10).

9. STUDY OF DEPENDENCE OF THE P_t^{γ} and P_t^{Jet} BALANCE ON PARTON k_t.

It is shown that in the case of ISR presence the value of fractional disbalance $(P_t^{\gamma} - P_t^{Jet})/P_t^{\gamma}$ *depends weakly on the variation of the average value of intrinsic parton transverse momentum* $\langle k_t \rangle$.

This section is dedicated to the study (within PYTHIA simulation) of a possible influence of the intrinsic parton transverse momentum k_t on the P_t balance of the "$\gamma + Jet$" system. For this aim we consider two samples of signal events gained by simulation with subprocesses (1a) and (1b) in two different ranges of $\hat{p}_\perp^{min}$: $\hat{p}_\perp^{min} \geq 40\ GeV/c$ and $\hat{p}_\perp^{min} \geq 100\ GeV/c$. For these two $\hat{p}_\perp^{min}$ intervals Tables 19 and 20 demonstrate the average values of P_t56 (defined by (3)) for two different cases of generation: without initial state radiation ("ISR is OFF") and with it ("ISR is ON"). Four different generations were done for each $\hat{p}_\perp^{min}$ interval. They correspond to four

Table 19: Effect of k_t on the P_t^{γ} - P_t^{Jet} balance with $\hat{p}_\perp^{min}$=40 GeV/c $(F = (P_t^{\gamma} - P_t^{Jet})/P_t^{\gamma})$.

$\langle k_t \rangle$	ISR is OFF			ISR is ON		
(GeV/c)	$\langle P_t56 \rangle$	$\langle F \rangle$	$\sigma(F)$	$\langle P_t56 \rangle$	$\langle F \rangle$	$\sigma(F)$
0.0	0.0	0.021	0.050	6.4	0.022	0.080
1.0	1.8	0.023	0.053	6.7	0.024	0.082
2.0	3.5	0.024	0.062	7.2	0.024	0.084
5.0	8.4	0.027	0.096	9.0	0.026	0.100

values of parton $\langle k_t \rangle$: [42] $\langle k_t \rangle = 0.0, 1.0, 2.0$ and $5.0\ GeV/c$ (the values $\langle k_t \rangle > 1\ GeV/c$ are given here only for illustration of a tendency).

[42] $\equiv$ PARP(91) parameter in PYTHIA

Table 20: Effect of k_t on ${P_t}^{\gamma}$ -${P_t}^{Jet}$ balance with $\hat{p}_{\perp}^{\ min}$=100 GeV/c $\ (F=({P_t}^{\gamma}-{P_t}^{Jet})/{P_t}^{\gamma})$.

$\langle k_t \rangle$	ISR is OFF			ISR is ON		
(GeV/c)	$\langle P_t56 \rangle$	$\langle F \rangle$	$\sigma(F)$	$\langle P_t56 \rangle$	$\langle F \rangle$	$\sigma(F)$
0.0	0.0	0.011	0.033	7.2	0.012	0.045
1.0	1.8	0.012	0.035	7.5	0.013	0.045
2.0	3.6	0.014	0.039	8.1	0.013	0.046
5.0	8.5	0.014	0.050	10.3	0.014	0.054

$*$ All numbers in the tables above are given in GeV/c.

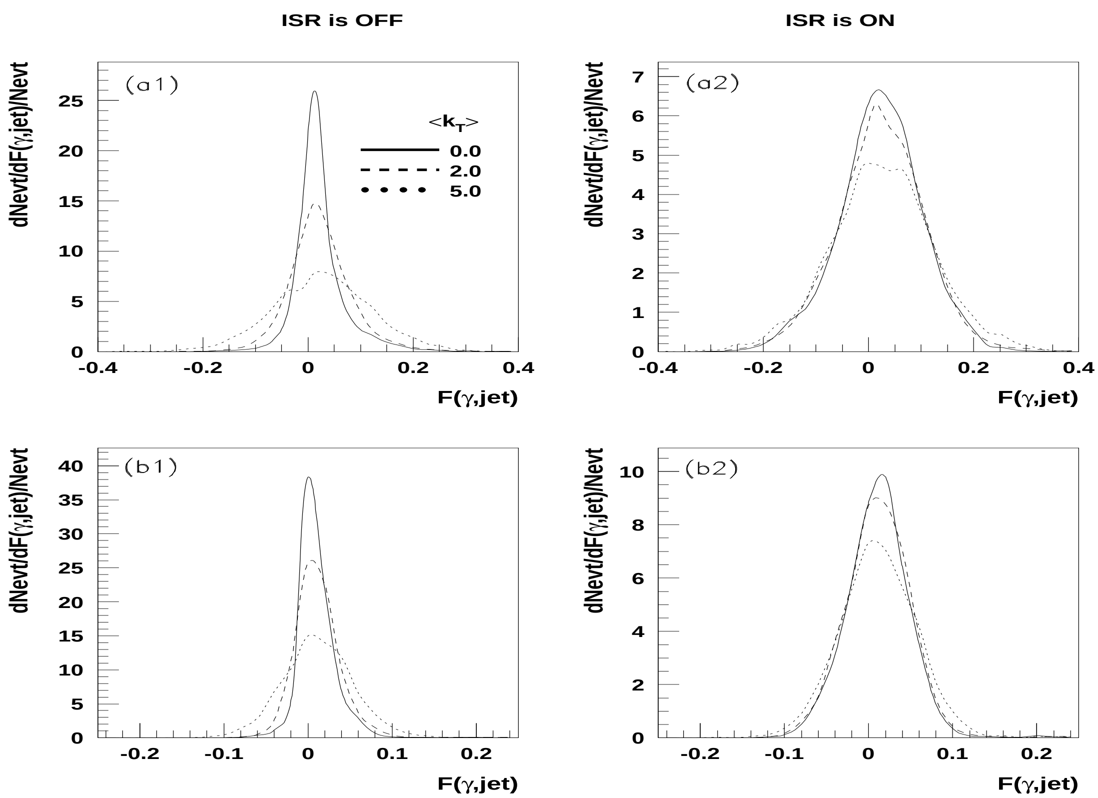

Fig. 28: $({P_t}^{\gamma}-{P_t}^{Jet})/{P_t}^{\gamma} \equiv F(\gamma,jet)$ as a function of primordial k_t value for the cases of switched on (a1, b1) and switched off (a2, b2) initial radiation and for $\hat{p}_{\perp}^{\ min}=40$ (a1, a2) and $\hat{p}_{\perp}^{\ min}=100\ \ GeV/c$ (b1, b2).

Let us consider firstly the case with ISR switched off during the simulation. The numbers in Tables 19 and 20 (obtained from the set of events selected by the cuts $\Delta\phi < 17^{\circ}$, $P_{tCUT}^{out} = 10\ GeV/c$ and $P_{tCUT}^{clust} = 10\ GeV/c$) show that in the case when "ISR is OFF" the value of $\langle P_t56 \rangle$ grows rapidly with increasing $\langle k_t \rangle$ and does not depend on ${P_t}^{\gamma}$(or $\hat{p}_{\perp}^{\ min}$). In fact, the values of $\langle P_t56 \rangle$ are proportional to the values of $\langle k_t \rangle$ in this case.

The picture changes when ISR is taken into accound. In this case the variable $\langle P_t56 \rangle$ initially gets large value at $\langle k_t \rangle = 0$: $\langle P_t56 \rangle = 6.4\ GeV/c$ and $\langle P_t56 \rangle = 7.2\ GeV/c$ for $\hat{p}_{\perp}^{\ min} = 40\ GeV/c$ and $\hat{p}_{\perp}^{\ min} = 100\ GeV/c$, respectively. But at the same time, in contrast to the case "ISR is OFF", the values of $\langle P_t56 \rangle$ grow more slowly with $\langle k_t \rangle$ when "ISR is ON". Indeed, they grow up from $6.4\ (7.2)$ at $\langle k_t \rangle = 0.0$ to $9.0\ (10.3)$ at $\langle k_t \rangle = 5\ GeV/c$ for $\hat{p}_{\perp}^{\ min}\!=\!40\ GeV/c$ $(100\ GeV/c)$.

The most remarkable thing, as it follows from Tables 19 and 20, that $\langle P_t56 \rangle$ depends weakly on $\langle k_t \rangle$ in the range of its reasonable values $\langle k_t \rangle \leq 1\ GeV/c$.

The variations of the fractional disbalance $F\equiv({P_t}^{\gamma}-{P_t}^{Jet})/{P_t}^{\gamma}$ and its standard deviation $\sigma(F)$ with $\langle k_t \rangle$ are also shown in Tables 19 and 20 and in plots of Fig. 28. One can see that for

reasonable values $\langle k_t \rangle \leq 1\ GeV/c$ and for the case "ISR is ON" the changes in the fractional disbalance F with k_t variation are very small. They are of order of 0.2% for $\hat{p}_{\perp}^{min} = 40\ GeV/c$ and of order of 0.1% for $\hat{p}_{\perp}^{min} = 100\ GeV/c$ [43].

10. "$\gamma + Jet$" EVENT RATE ESTIMATION FOR GLUON DISTRIBUTION DETERMINATION AT THE TEVATRON RUN II.

The number of "$\gamma + Jet$" events suitable for measurement of gluon distribution in different x and Q^2 intervals at Run II is estimated. It is shown that with $L_{int} = 3\ fb^{-1}$ it would be possible to collect about one million of these events. This number would allow to cover a new kinematical area not studied in any previous experiment ($10^{-3} < x < 1.0$ with $1.6 \cdot 10^3 \leq Q^2 \leq 2 \cdot 10^4\ (GeV/c)^2$). This area in the region of small $x \geq 10^{-3}$ has Q^2 by about one order of magnitude higher than reached at HERA now.

As many of theoretical predictions for production of new particles (Higgs, SUSY) at the Tevatron are based on model estimations of the gluon density behavior at low x and high Q^2, the measurement of the proton gluon density for this kinematic region directly in Tevatron experiments would be obviously useful. One of the promising channels for this measurement, as was shown in [31], is a high P_t direct photon production $p\bar{p}(p) \to \gamma^{dir} + X$. The region of high P_t, reached by UA1 [32], UA2 [33], CDF [34] and D0 [35] extends up to $P_t \approx 80\ GeV/c$ and recently up to $P_t = 105\ GeV/c$ [36]. These data together with the later ones (see references in [38]–[46] and recent E706 [47] and UA6 [48] results) give an opportunity for tuning the form of gluon distribution (see [39], [43], [49]). The rates and estimated cross sections of inclusive direct photon production at the LHC were given in [31] (see also [50]).

Here for the same aim we shall consider the process $p\bar{p} \to \gamma^{dir} + 1\ Jet + X$ defined in the leading order by two QCD subprocesses (1a) and (1b) (for experimental results see [51], [52]).

Apart from the advantages, discussed in Section 8 in connection with the background suppression (see also [53]–[59]), the "$\gamma^{dir} + 1\ Jet$" final state may be easier for physical analysis than inclusive photon production process "$\gamma^{dir} + X$" if we shall look at this problem from the viewpoint of extraction of information on the gluon distribution in a proton. Indeed, in the case of inclusive direct photon production the cross section is given as an integral over the products of a fundamental $2 \to 2$ parton subprocess cross sections and the corresponding parton distribution functions $f_a(x_a, Q^2)$ (a = quark or gluon), while in the case of $p\bar{p} \to \gamma^{dir} + 1\ Jet + X$ for ${P_t}^{Jet} \geq 30\, GeV/c$ (i.e. in the region where "k_t smearing effects" [44] are not important, see [44]) the cross section is expressed directly in terms of these distributions (see, for example, [42]):

$$\frac{d\sigma}{d\eta_1 d\eta_2 d{P_t}^2} = \sum_{a,b} x_a\, f_a(x_a, Q^2)\, x_b\, f_b(x_b, Q^2) \frac{d\sigma}{d\hat{t}}(a\, b \to c\, d), \tag{33}$$

where

$$x_{a,b} \;=\; P_t/\sqrt{s} \cdot\ (exp(\pm\eta_1) \;+\; exp(\pm\eta_2)). \tag{34}$$

The designation used above are as the following: $\eta_1 = \eta^{\gamma}$, $\eta_2 = \eta^{Jet}$; $P_t = {P_t}^{\gamma}$; $a, b = q, \bar{q}, g$; $c, d = q, \bar{q}, g, \gamma$. Formula (33) and the knowledge of $q,\ \bar{q}$ distributions allow the gluon distribution $f_g(x, Q^2)$ to be determined after account of selection efficiencies for jets and $\gamma^{dir}-$candidates

[43] Recall that the numbers in Tables 19 and 20 may be compared with those in the tables of Appendix 6, where the same $\hat{p}_{\perp}^{min}$ cuts are used, rather than with the results of the tables of Appendices 2 – 5, where $\hat{p}_{\perp}^{min}$ cuts were taken to be two times smaller (see for explanation the beginning of Section 7).

[44] This terminology is different from ours, used in Sections 2 and 9, as we denote by "k_t" only the value of parton intrinsic transverse momentum.

as well as after subtraction of the background contribution, left after the used selection cuts 1–13 of Table 13 (as it was discussed in Section 8 keeping in hand this physical application).

In the previous sections a lot of details connected with the structure and topology of these events and the features of objects appearing in them were discussed. Now with this information in mind we are in position to discuss an application of the "$\gamma + Jet$" event samples, selected with the previously proposed cuts, for estimating the rates of gluon-based subprocess (1a) in different x and Q^2 intervals.

Table 21 shows percentage of "Compton-like" subprocess (1a) (amounting to 100% together with (1b)) in the samples of events selected with cuts (17) – (23) of Section 3.2 for $P_{tCUT}^{clust} = 10\ GeV/c$ for different P_t^{γ} and η^{Jet} intervals: Central (CC) ($|\eta^{Jet}| < 0.7$) [45], Intercryostat (IC) $0.7 < |\eta^{Jet}| < 1.8$ and End (EC) $1.8 < |\eta^{Jet}| < 2.5$ parts of calorimeter. We see that the contribution of Compton-like subprocess grows by about $5-6\%$ with $|\eta^{Jet}|$ enlarging and drops with growing $P_t^{Jet} (\approx P_t^{\gamma}$ in the sample of the events collected with the cuts $1-13$ of Table 13).

Table 21: The percentage of Compton-like process $q\,g \to \gamma + q$.

Calorimeter part	P_t^{Jet} interval (GeV/c)			
	40–50	50–70	70–90	90–140
CC	84	80	74	68
IC	85	82	76	70
EC	89	85	82	73

In Table 22 we present the $Q^2 (\equiv (P_t^{\gamma})^2)$ [46] and x (defined according to (34)) distribution of the number of events that are caused by the $q\,g \to \gamma + q$ subprocess, and passed the following cuts (P_t^{out} was not limited):

$$P_t^{\gamma} > 40\ GeV/c, \quad |\eta^{\gamma}| < 2.5, \quad P_t^{Jet} > 30\ GeV/c, \quad |\eta^{Jet}| < 4.2, \quad P_t^{hadr} > 7\ GeV/c,$$
$$P_{tCUT}^{isol} = 4\ GeV/c,\ \epsilon_{CUT}^{\gamma} = 7\%,\ \Delta\phi < 17^\circ,\ P_{tCUT}^{clust} = 10\ GeV/c. \qquad (35)$$

Table 22: Number of $g\,q \to \gamma^{dir} + q$ events at different Q^2 and x intervals for $L_{int} = 3\ fb^{-1}$.

Q^2 $(GeV/c)^2$	x values of a parton						All x
	$.001-.005$	$.005-.01$	$.01-.05$	$.05-.1$	$.1-.5$	$.5-1.$	$.001-1.$
1600-2500	8582	56288	245157	115870	203018	3647	632563
2500-4900	371	13514	119305	64412	119889	3196	320688
4900-8100	0	204	17865	13514	26364	1059	59007
8100-19600	0	0	3838	5623	11539	548	21549
							1 033 807

The analogous information for events with the charmed quarks in the initial state $g\,c \to \gamma^{dir} + c$ is presented in Table 23 (see also tables of Appendix 1). The simulation of the process $g\,b \to \gamma^{dir} + b$ has shown that the rates for the b-quark are 8 – 10 times smaller than for the c-quark (these event rates are also given in tables of Appendix 1 for different P_t^{γ} intervals) [47].

[45] see also tables of Appendix 1

[46] see [9]

[47] Analogous estimation for LHC energy was done in [18] and [60].

Table 23: Number of $g\,c \rightarrow \gamma^{dir} + c$ events at different Q^2 and x intervals for $L_{int} = 3\ fb^{-1}$.

Q^2 $(GeV/c)^2$	x values of a parton						All x
	$.001 - .005$	$.005 - .01$	$.01 - .05$	$.05 - .1$	$.1 - .5$	$.5 - 1.$	$.001 - 1.$
1600-2500	264	2318	21236	11758	14172	58	49805
2500-4900	13	332	9522	6193	7785	40	23885
4900-8100	0	4	914	1055	1648	16	3637
8100-19600	0	0	142	329	612	8	1092
							78 419

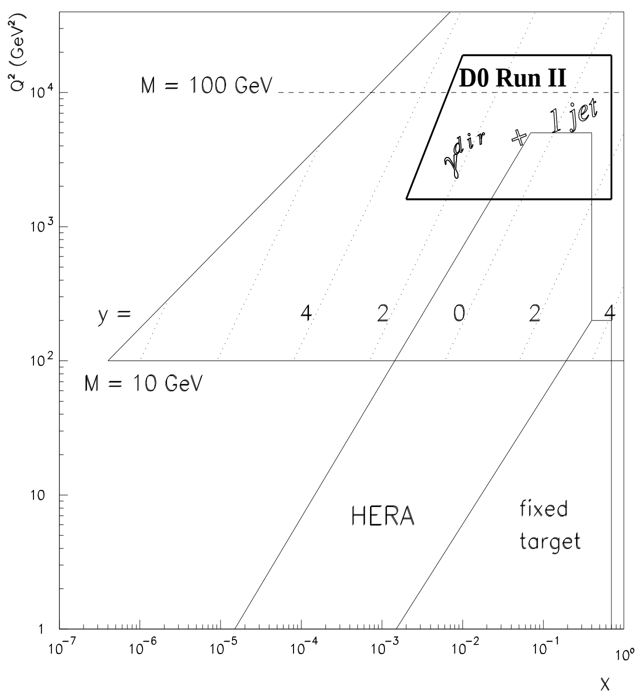

Figure 29: The (x, Q^2) kinematic region for studying $p\bar{p} \rightarrow \gamma + Jet$ process at Tevatron Run II.

Fig. 29 shows in the widely used (x, Q^2) kinematic plot (see [61] and also in [44]) what area can be covered by studying the process $q\ g\ \rightarrow\ \gamma + q$ at Tevatron. The distribution of number of events in this area is given by Table 22. From this figure and Table 22 it becomes clear that with integrated luminosity $L_{int} = 3\ fb^{-1}$ it would be possible to study the gluon distribution with a good statistics of "$\gamma + Jet$" events in the region of $10^{-3} < x < 1.0$ with Q^2 by about one order of magnitude higher than reached at HERA now. It is worth emphasizing that extension of the experimentally reachable region at the Tevatron to the region of lower Q^2 overlapping with the area covered by HERA would also be of great interest.

11. SUMMARY.

We have done an attempt here to consider, following [10]–[18], the physics of high P_t direct photon and jet associative production in proton-antiproton collisions basing on the predictions of PYTHIA generator and the models implemented there. This work may be useful for two practical goals: for absolute jet energy scale determination and for gluon distribution measurement at Tevatron energy.

The detailed information provided in the PYTHIA event listings allows to track the origin of different particles (like photons) and of objects (like clusters and jets) that appear in the final state. So, the aims of this work was to explore at the particle level as much as possible this information for finding out what effect may be produced by new variables, proposed in [10]–[17] for describing "$\gamma + Jet$" events, and the cuts on them for solution of the mentioned above practical tasks.

For the first problem of the jet energy determination an important task is to select the events that may be caused (with a high probability) by the $q\bar{q} \to g + \gamma$ and $qg \to q + \gamma$ fundamental parton subprocesses of direct photon production. To take into account a possible effect of initial state radiation (its spectra are presented in different ${P_t}^{\gamma}$ intervals in Tables 2–7 of Section 5) we used here the P_t-balance equation (see (16)) written for an event as a whole. It allows to express ${P_t}^{\gamma} - {P_t}^{Jet}$ fractional disbalance (see (28)) through new variables [10]–[17] that describe the P_t activity *out* of "$\gamma + Jet$" system. They are ${P_t}^{out}$ and ${P_t}^{clust}$, i.e. P_t of mini-jets or clusters that are additional to the main jet in event. The latter is the most "visible" part of ${P_t}^{out}$.

These two sources of the ${P_t}^{\gamma} - {P_t}^{Jet}$ disbalance are investigated. It is shown that the limitation of P_t of clusters, i.e. ${P_t}^{clust}$, can help to decrease this disbalance (see Figs. 12–18 and Tables 4–12 of Appendices 2–5).

Analogously, the limitation of P_t activity of all detectable particles ($|\eta_i| < 4.2$) beyond the "$\gamma + Jet$" system, i.e. ${P_t}^{out}$, also leads to a noticeable ${P_t}^{\gamma} - {P_t}^{Jet}$ disbalance reduction (see Figs. 19 and 20).

It is demonstrated that in the events selected by means of simultaneous restriction from above of the ${P_t}^{clust}$ and ${P_t}^{out}$ activity the values of ${P_t}^{\gamma}$ and ${P_t}^{Jet}$ are well baalnced with each other while considering the PYTHIA particle level of simulation. The samples of these "$\gamma + Jet$" events gained in this way are of a large enough volume for jet energy scale determination in the interval $40 < {P_t}^{\gamma} < 140\ GeV/c$ (see Tables 1–12 of Appendix 6).

It is worth mentioning that the most effect for improvement of ${P_t}^{\gamma}$ and ${P_t}^{Jet}$ balance can be reached by applying additionally the jet isolation criterion defined in [10]–[17]. As it can be seen from Figs. 15, 16 (Selection 2) as well as from Figs. 17, 18 (Selection 3) and also from Tables 13–18 of Appendices 2–5 and Tables 13–24 of Appendix 6, the application of this criterion allows to select the events having the ${P_t}^{\gamma} - {P_t}^{Jet}$ disbalance at the particle level less than 1% [48]. Definitely, the detector effects may worsen the balance determination due to the limited accuracy of the experimental measurement. We are planning to present the results of full GEANT simulation with the following digitization and reconstruction of signals by using the corresponding D0 packages (like D0GSTAR) in the forthcoming papers.

We present also PYTHIA predictions for the dependence of the distributions of the number of selected "$\gamma + Jet$" events on ${P_t}^{\gamma}$ and η^{Jet} (see Tables 8–12 of Section 5 and also tables of Appendices 2–5 with account of ${P_t}^{clust}$ variation). The features of "$\gamma + Jet$" events in the central region of the D0 detector ($|\eta^{Jet}| < 0.7$) are exposed (see Figs. 8, 9). The P_t structure of the region in the $\eta - \phi$ space inside and beyond a jet is established (see Figs. 10, 11).

The corrections to the measurable values of ${P_t}^{jet}$ that have take into account the contribution from neutrinos belonging to a jet are presented for different ${P_t}^{Jet} (\approx {P_t}^{\gamma}$ for the selected events) intervals in the tables of Appendix 1. It is shown in Section 4 that a cut on ${P_t}^{miss} < 10\ GeV/c$ allows to reduce this contribution down to the value of $\Delta_\nu = \langle P_{t(\nu)}^{Jet} \rangle_{all\ events} = 0.1\ GeV/c$. At the same time, as it is shown in [26], and discussed in Sections 4, 8 (see also [17]), this cut noticeably decreases the number of the background $e^{\pm}$-events in which $e^{\pm}$ (produced in the $W^{\pm} \to e^{\pm}\nu$ weak decay) may be registered as direct photon.

The study of the fractional disbalance $({P_t}^{\gamma} - {P_t}^{Jet})/{P_t}^{\gamma}$ dependence on an intrinsic parton transverse momentum $\langle k_t \rangle$, performed in Section 9, has shown its weak impact on the disbalance in the case of initial state radiation account.

The possibility of the background events (caused by QCD subprocesses of qg, gg, qq scat-

[48] The achieved disbalance value at the particle level of simulation shows the most optimistic value of $({P_t}^{\gamma} - {P_t}^{Jet})/{P_t}^{\gamma}$.

tering) suppression was studied in Section 8. Basing on the introduced selection criteria that include 17 cuts (see Table 13 of Section 8), the background suppression relative factors and the values of signal event selection efficiencies are estimated (see Table 14).

It is shown that after applying the first 6 "photonic" cuts (that may be used, for example, for selecting events with inclusive photon production and lead to signal-to-background ratio $S/B = 3.2$ in the interval ${P_t}^{\gamma} > 70\ GeV/c$, see Table 14) the use of the next 11 "hadronic" cuts of Table 13 may lead to further essential improvement of S/B ratio (by factor of 3.5 for the same ${P_t}^{\gamma} > 70\ GeV/c$ where S/B becomes 11.4, see Table 14).

It is important to underline that this improvement is achieved by applying "hadronic" cuts that select the events having clear "$\gamma + Jet$" topology at the particle level and also having rather "clean" area (in a sense of limited P_t activity) beyond a "$\gamma + Jet$" system. The consideration of the cuts, connected with detector effects (e.g., based on an electromagnetic shower profile [35], [36]), may lead to further improvement of S/B ratio. In this sense and taking into account the fact that these "hadronic" cuts lead to an essential improvement of ${P_t}^{\gamma} - {P_t}^{Jet}$ balance, one may say that the cuts on ${P_t}^{clust}$ and ${P_t}^{out}$, considered here, do act quite effectively to select the events caused by leading order diagrams (see Fig. 1) and do suppress the contribution of NLO diagrams, presented in Figs. 2, 4.

Another interesting predictions of PYTHIA is about the dominant contribution of "γ-brem" events into the total background at Tevatron energy, as in was already mentioned in Section 8 (see also [17] and [26]). As the "γ-brem" background has irreducible nature its careful estimation is an important task and we plan to make the analogous estimation with HERWIG generator.

To finish the discussion of the jet calibration study let us mention that the main results on this subject are summed up in Tables 1–12 (Selection 1) and 13–24 (Selection 2 with jet isolation criterion) of Appendix 6 and Fig. 27.

It should be emphasized that numbers presented in all mentioned tables and figures were found within the PYTHIA particle level of simulation. They may depend on the used generator and on the particular choice of a long set of its parameters [49] as well as they may change after account of the results of the full GEANT-based simulation.

The preliminary D0 Run II data taken during January 2002 were used to demonstrate how do the cuts (1–16) of Table 13 work to select γ-candidate and γ-candidate + 1 jet events (see the slides of already mentioned our talk at QCD group [27]). It is interesting to note that the final number of selected events with ${P_t}^{\gamma} > 40\ GeV/c$ approximately agrees (after correction to the values of photon purity and selection efficiency taken from [36]) with the results of our estimation presented in Table 8 and Table 4 of Appendix 2.

It is shown that the samples of the "$\gamma + Jet$" events, gained with the cuts used for the jet energy calibration, can provide an information suitable also for determining the gluon distribution inside a proton in the kinematic region (see Fig. 29) that includes x values as small as accessible at HERA [62], [63], but at much higher Q^2 values (by about one order of magnitude): $10^{-3} \leq x \leq 1.0$ with $1.6 \cdot 10^3 \leq Q^2 \leq 2 \cdot 10^4\ (GeV/c)^2$. The number of events, based on the gluonic process (1a), that may be collected with $L_{int} = 3\ fb^{-1}$ in different x- and Q^2- intervals of this new kinematic region for this goal are presented in Table 22 (all quarks included) and in Table 23 (only for charm quarks) [50].

[49] We have already mentioned that we are planning to perform analogous analysis by help of another generator like HERWIG, for example. The comparison of predictions of different generators (PYTHIA, HERWIG, etc.) with the experimental results is a part of a work in any experiment.

[50] see also tables of Appendix 1

12. ACKNOWLEDGMENTS.

We are greatly thankful to D. Denegri who initiated our interest to study the physics of "$\gamma + Jet$" processes, for his permanent support and fruitful suggestions. It is a pleasure for us to express our deep recognition for helpful discussions to P. Aurenche, M. Dittmar, M. Fontannaz, J.Ph. Guillet, M.L. Mangano, E. Pilon, H. Rohringer, S. Tapprogge, H. Weerts and J. Womersley. Our special gratitude is to J. Womersley also for supplying us with the preliminary version of paper [1], interest in the work and encouragements.

References

[1] D0 Collaboration, F. Abachi *et al.*, NIM **A424** (1999)352 (Its ealier prototype: B. Abbot *et al.*, "Jet Energy Scale at D0"; D0 Note #3287, D0, FNAL, 1997 contains some more detailed discussions of different physical aspects of the calibration).

[2] CDF Collaboration. F. Abe *et al.*, Phys.Rev. **D50** (1994)2966; F. Abe *et al.*, Phys.Rev.Lett. **73** (1994)225.

[3] D. Denegri, R. Kinnunen, A. Nikitenko, CMS Note 1997/039 "Study of calorimeter calibration with τ's in CMS".

[4] R. Kinnunen, A. Nikitenko, CMS Note 1997/097 "Study of calorimeter calibration with pions from jets in CMS".

[5] J. Womersley. A talk at CMS Week meeting, Aachen, 1997.

[6] J. Freeman, W. Wu, **draft** "In situ calibration of CMS HCAL calorimeter".

[7] R. Mehdiyev, I. Vichou, ATLAS Note ATL-COM-PHYS-99-054 (1999) "Hadronic jet energy scale calibration using Z+jet events".

[8] ATLAS Detector and Physics Performance, Technical Design Report, Volumes **1, 2**, 1999. CERN/LHCC 99-14.

[9] T. Sjostrand, Comp.Phys.Comm. **82** (1994)74.

[10] N.B. Skachkov, V.F. Konoplyanikov, D.V. Bandourin, "Photon – jet events for calibration of HCAL". Second Annual RDMS CMS Collaboration Meeting. CMS-Document, 1996–213. CERN, December 16-17, 1996, p.7-23.

[11] N.B. Skachkov, V.F. Konoplyanikov, D.V. Bandourin, "γ-direct + 1 jet events for HCAL calibration". Third Annual RDMS CMS Collaboration Meeting. CMS-Document, 1997–168. CERN, December 16-17, 1997, p.139-153.

[12] D.V. Bandurin, V.F. Konoplyanikov, N.B. Skachkov, ”Jet energy scale setting with ”gamma+jet” events for a hadronic calorimeter of CMS.” Fifth Annual RDMS CMS Collaboration Meeting. CMS Document 2000-058. Conference. ”Physics Program with the CMS Detector”, ITEP, Moscow, Russia. November 22-24, 2000. p. 422-427.

[13] D.V. Bandourin, V.F. Konoplyanikov, N.B. Skachkov. “Jet energy scale setting with “$\gamma + Jet$” events at LHC energies. Generalities, selection rules.” JINR Preprint E2-2000-251, JINR, Dubna, hep-ex/0011012.

[14] D.V. Bandourin, V.F. Konoplyanikov, N.B. Skachkov. “Jet energy scale setting with “$\gamma + Jet$” events at LHC energies. Event rates, P_t structure of jet.” JINR Preprint E2-2000-252, JINR, Dubna, hep-ex/0011013.

[15] D.V. Bandourin, V.F. Konoplyanikov, N.B. Skachkov. “Jet energy scale setting with “$\gamma + Jet$” events at LHC energies. Minijets and cluster suppression and ${P_t}^{\gamma} - {P_t}^{Jet}$ disbalance.” JINR Preprint E2-2000-253, JINR, Dubna, hep-ex/0011084.

[16] D.V. Bandourin, V.F. Konoplyanikov, N.B. Skachkov. “Jet energy scale setting with “$\gamma + Jet$” events at LHC energies. Selection of events with a clean “$\gamma + Jet$” topology and ${P_t}^{\gamma} - {P_t}^{Jet}$ disbalance.” JINR Preprint E2-2000-254, JINR, Dubna, hep-ex/0011014.

[17] D.V. Bandourin, V.F. Konoplyanikov, N.B. Skachkov. “Jet energy scale setting with “$\gamma + Jet$” events at LHC energies. Detailed study of the background suppression.” JINR Preprint E2-2000-255, JINR, Dubna, hep-ex/0011017.

[18] D.V. Bandourin, V.F. Konoplyanikov, N.B. Skachkov, “ “$\gamma + Jet$” events rate estimation for gluon distribution determination at LHC”, Part.Nucl.Lett.103:34-43,2000, hep-ex/0011015.

[19] M. Dittmar, K.Mazumdar, N. Skachkov, Proc. of “CERN Workshop on Standard Model Physics (and more) at the LHC”, QCD, Section 2.7 “Measuring parton Luminosities ...”, Yellow Report CERN-2000-004, 9 May 2000, CERN, Geneva.

[20] D.V. Bandourin, V.F. Konoplyanikov, N.B. Skachkov. “On the possibility of $\pi^0, \eta, \omega, K_s^0$ mesons and a photon discrimination basing on the calorimeter information in the CMS detector”, JINR Communication E1-2001-261, JINR, Dubna, hep-ex/0108050.

[21] D.V. Bandourin, N.B. Skachkov. “Separation of a signle photon and products of the π^0, η, K_s^0 mesons neutral decay channels in the CMS electromagnetic calorimeter using neural network”, JINR Communication E2-2001-259, JINR, Dubna, hep-ex/0108051.

[22] GEANT3 - Detector Description and Simulation Tool, R. Brun *et al*, GEANT3 CERN DD/EE/84-1, revised 1987.

[23] GEANT-3 based simulation package of D0 detector D0GSTAR. Yuri Fisyak, John Womersley, “D0 GEANT Simulation of the Total Apparatus Response.”, D0GSTAR User’s Guide at WWW: http://www-d0.fnal.gov/d0dist/dist/packages/d0gstar/devel/docs/tex/manual/manual.html.

[24] S. Abdullin, A. Khanov, N. Stepanov, CMS Note CMS TN/94–180 “CMSJET”.

[25] D.V. Bandourin, V.F. Konoplyanikov, N.B. Skachkov. “On the application of “$\gamma + Jet$” events for setting the absolute scale of the jet energy at the LHC and determining the gluon distribution”. CMS Note in preparation.

[26] Talk at QCD group meeting, see http://www-d0.fnal.gov/Run2Physics/qcd/, link to "Meeting June 21, 2001".

[27] Talk at QCD group meeting, see http://www-d0.fnal.gov/Run2Physics/qcd/, link to "Meeting February 25, 2002".

[28] I.A. Bertram *et al.*, "Single jet energy resolutions at D0 for Run I", D0 Note 3414, 1998.

[29] S. Frixione, Phys.Lett. **B429** (1998)369.

[30] S. Catani, M. Fontannaz and E. Pilon, Phys.Rev. **D58** (1998)094025.

[31] P. Aurenche *et al.* Proc. of "ECFA LHC Workshop", Aachen, Germany, 4-9 Oktob. 1990, edited by G. Jarlskog and D. Rein (CERN-Report No 90-10; Geneva, Switzerland 1990), Vol. **II**.

[32] UA1 Collaboration, C. Albajar *et al.*, Phys.Lett, **209B** (1998)385.

[33] UA2 Collaboration, R. Ansari *et al.*, Phys.Lett. **176B** (1986)239.

[34] CDF Collaboration. F. Abe *et al.*, Phys.Rev.Lett. **68** (1992)2734; F. Abe *et al.*,Phys.Rev. **D48** (1993)2998; F. Abe *et al.*,Phys.Rev.Lett., **73** (1994)2662.

[35] D0 Collaboration, F. Abachi *et al.*, Phys.Rev.Lett, **77** (1996)5011.

[36] D0 Collaboration, B. Abbott *et al.* , Phys.Rev.Lett. **84** 2786-2791,2000.

[37] L3 Collaboration, D. Kirkby, CALT-69-1992, hep-ex/9505012.

[38] T. Ferbel and W.R. Molzon, Rev.Mod.Phys. **56** (1984)181.

[39] P. Aurenche, *et al.* Phys.Lett. **169B** (1986)441.

[40] E.N. Argyres, A.P. Contogouris, N. Mebarki and S.D.P. Vlassopulos, Phys.Rev, **D35** (1987)1534–1589.

[41] P. Aurenche, *et al.* Phys.Rev. **D39** (1989)3275.

[42] J.F. Owens, Rev.Mod.Phys. **59** (1987)465.

[43] W. Vogelsang and A. Vogt, Nucl.Phys. **B453** (1995)334.

[44] J. Huston ATLAS Note ATL-Phys-99-008, CERN,1999.

[45] W. Vogelsang and M. Whally, J.Phys. **G23** (1997)A1.

[46] S. Frixione and W. Vogelsang, CERN-TH/99-247, hep-ph/9908387.

[47] E706 Collaboration, L. Apanasevich *et al.*, Phys.Rev.Lett., **81** (1997)2642.

[48] UA6 Collaboration, G. Ballocchi *et al.*, Phys.Lett.,**B436** (1998)222.

[49] A.D. Martin *et al.*, Eur.Phys.J. **C4** (1998)463.

[50] P. Aurenche, M. Fontannaz, S. Frixione Proc. of “CERN Workshop on Standard Model Physics (and more) at the LHC”, QCD, Section 6.1 “General features of photon production”, Yellow Report CERN-2000-004, 9 May 2000, CERN, Geneva.

[51] ISR–AFS Collaboration, T.Akesson *et al.*, Zeit.Phys. **C34** (1987)293.

[52] CDF Collaboration, F. Abe *et al.*, Phys.Rev. **D57** (1998)67.

[53] E.L. Berger and J. Qiu, Phys.Rev. **D44** (1991)2002.

[54] M. Fontannaz, S. Frixione, S. Tapprogge Proc. of “CERN Workshop on Standard Model Physics (and more) at the LHC”, QCD, Section 6 “Prompt photon production”, Yellow Report CERN-2000-004, 9 May 2000, CERN, Geneva.

[55] G.P. Skoro, M.V. Tokarev, “Asymmetry of jet production in polarized pp collisions and sign of ΔG”, Proc. of the XIV International Seminar on High Energy Physics Problems “Relativistic Nuclear Physics and QCD”, Vol.II, p.120., hep-ph/0009028.

[56] G.P. Skoro, M.V. Tokarev, “Asymmetry of jet production in polarized pp collisions at RHIC and sign of ΔG”, Nuov. Cim. **A111** (1998) 353.

[57] G.P. Skoro, M. Zupan, M.V. Tokarev, ”Asymmetry of Prompt Photon Production in $\vec{p}-\vec{p}$ Collisions at RHIC” Nuov. Cim. **A112** (1999) 809.

[58] P. Chiapetta, G.J. Gounaris, J. Layssac and F.M. Renard “Glue constraining asymmetries in W, γ or Z production at CERN LHC”, hep-ph/9807563.

[59] J. Huston *et al.* “Study of the uncertainty of the gluon distribution”, hep-ph/9801444.

[60] M. Dittmar, F. Pauss, D. Zurcher, Phys.Rev.D56:7284-7290,1997; hep-ex/9705004.

[61] R. Ball, M. Dittmar, W.J. Stirling, Proc. of “CERN Workshop on Standard Model Physics (and more) at the LHC”, QCD, Section 2 “Parton distribution functons”, Yellow Report CERN-2000-004, 9 May 2000, CERN, Geneva.

[62] H1 Collaboration, S. Aid *et al.*, Nucl.Phys. **B470** (1996)3; C. Adloff *et al.* Nucl.Phys. **B497** (1997)3.

[63] ZEUS Collaboration, M. Derrick *et al.*, Zeit.Phys. **C69** (1996)607; M. Derrick *et al.*, Zeit.Phys. **C72** (1996)399.

[64] Particle Data Group, D.E. Groom *et al.*, The European Physical Journal C15 (2000) 1.